TERRESTRIAL LIDAR-BASED BRIDGE EVALUATION

by

Wanqiu Liu

A dissertation submitted to the faculty of
The University of North Carolina at Charlotte
in partial fulfillment of the requirements
for the degree of Doctor of Philosophy in
Infrastructure and Environmental Systems

Charlotte

2010

Approved by:

_____
Dr. Shen-en Chen

_____
Dr. Edd Hauser

_____
Dr. S. Gary Teng

_____
Dr. Srinivas S. Pulugurtha

_____
Dr. Jing Zhou

ABSTRACT

WANQIU LIU. Terrestrial LiDAR-based bridge evaluation. (Under the direction of DR. SHEN-EN CHEN)

Considering the over half million bridges in the US state highway system, more than 70% of which were built before 1935, it is of little wonder that bridge maintenance and management is facing severe challenges and the significant funding scarcity rapidly escalates the problem. Commercial remote sensing techniques have the capability of covering large areas and are suggested to be cost effective methods for bridge inspection. This dissertation introduces several applications of the remote bridge inspection technologies using ground-based LiDAR systems. In particular, the application of terrestrial LiDAR for bridge health monitoring is studied. An automatic bridge condition evaluation system based on terrestrial LiDAR data, LiBE (LiDAR-based Bridge Evaluation), is developed. The research works completed thus far have shown that LiDAR technology has the capability for bridge surface defect detection and quantification, clearance measurement, and displacement measurement during bridge static load testing. Several bridges in Mecklenburg County, NC, and other areas have been evaluated using LiBE and quantitative bridge rating mechanisms are proposed. A cost-benefit analysis has been conducted that demonstrates the relevancy of the technique to current nation-wide bridge management problem, as well as, the potential of reducing the bridge maintenance costs to the stack holders. The results generated from these technologies are valuable for bridge maintenance decision making.

ACKNOWLEDGMENTS

TABLE OF CONTENTS

LIST OF TABLES

LIST OF FIGURES

LIST OF ABBREVIATIONS

AADT   Annual Average Daily Traffic

AASHO   American Association of State Highway Officials

AASHTO   American Association of State Highway and Transportation Officials

ADT   Average Daily Traffic

ASCE   American Society of Civil Engineers

BMS   Bridge Management System

CBA   Cost-Benefit Analysis

CBR   Cost-Benefit Ratio

CDOT   Charlotte Department of Transportation

CRS   Commercial Remote Sensing

DEM   Digital Elevation Model

FHWA   Federal Highway Administration

GIS   Geographic Information System

GPR   Ground Penetrating Radar

GPS   Global Positioning System

GSM   Global System for Mobile communications

HBRRP   Highway Bridge Replacement and Rehabilitation Program

HPS   High Performance Steel

HTF   Highway Trust Fund

IRSV   Integrated Remote Sensing and Visualization

ISTEA   Intermodal Surface Transportation Efficiency Act

LaDAR   Laser Detection and Ranging

LiBE   LiDAR-based Bridge Evaluation

LiDAR   Light Detection and Ranging

NBI   National Bridge Inventory

NBIP   National Bridge Inventory Program

NBIS   National Bridge Inspection Standards

NCDOT   North Carolina Department of Transportation

NCHRP   National Cooperative Highway Research Program

NDE   Non-Destructive Evaluation

NDI   Non-Destructive Inspection

NPV   Net Present Value

NSTIFC   National Surface Transportation Infrastructure Financing Commission

PC   Prestressed Concrete

RC   Reinforced Concrete

RITA   Research Innovative Technology Administration

SBRP   Special Bridge Replacement Program

SHM   Structure Health Monitoring

STIP   State Transportation Improvement Program

SAR   Synthetic Aperture Radar

SI   Spatial Information

TIP   Transportation Improvement Program

TRB   Transportation Research Board

UNCC   University of North Carolina at Charlotte

USDOT   U.S. Department of Transportation

CHAPTER 1: INTRODUCTION

A nation's transportation infrastructure performance is crucial to its economic growth and public safety. The function and condition of roads, rails and ports determine the efficiency of goods exchange. State highway bridges are part of the critical transportation infrastructure that can be considered as the backbone of this nation (Merkle and Myers 2006). The well being of these bridges are essential to the sustained operations of our society.

The importance of bridge safety was brought to the nation's attention again when the I-35W Bridge in Minnesota suddenly collapsed in August 2007. Bridges in the U.S. are facing the crisis of high deterioration rates, and scarcity of maintenance and new construction funding. More than 70% of in-service bridges in the United States were built before 1935 (Abudayyeh et al. 2004). For the most heavily used bridges, which are on the interstate highway system, 17% were constructed during 1950s, 44% were built during 1960s and 20% were built during 1970s (NSTPRSC 2007). American Society of Civil Engineers (ASCE) report card for America's infrastructure showed that more than 26% of the nation's bridges are either classified as structurally deficient or functionally obsolete (ASCE 2009).

Federal aid funds are issued for public bridge maintenance and rehabilitation. Federal funding for surface transportation is mainly coming from the Highway Trust Fund (HTF). With the increasing investment needs for national infrastructure improvement, HTF is facing the problem of financial deficit. The cumulative gap between federal transportation revenues and investment roughly needs $400 billion in 2010-2015, which may increase to about $2.3 trillion through 2035 (NSTIFC 2009). An annual funding need of $17 billion for bridge condition improvement was estimated by ASCE with only $10.5 billion can be allocated (ASCE 2009). Therefore, how to effectively use the limited funding source becomes extremely important.

1.1 Bridge inspection and management history

Before the 1960s, there was no nation-wide bridge safety inspection and maintenance regulation in the U.S. Bridge safety issues, although previously discussed and researched among state and local government agencies responsible for bridges, first attracted a broad public interest after the collapse of the Silver Bridge at Point Pleasant, West Virginia (46 people were killed) in 1967 (Brinckerhoff 1993). In 1968, a national bridge inspection standard was required to be established by action taken by the U.S. Congress. Bridge inspection authorization was added to the "Federal Highway Act of 1968" (FHWA 2002). The National Bridge Inventory (NBI) system was reauthorized in the "Federal Highway Act of 1970" as the basis for funding for the Special Bridge Replacement Program (SBRP) (Czepiel 1995).

In 1971, the Federal Highway Administration (FHWA) Bridge Inspector's Training Manual, the American Association of State Highway Officials (AASHO) Manual for Maintenance Inspection of Bridges, and the FHWA Recording and Coding

Guide for the Structure Inventory and Appraisal of the Nation's Bridges were developed to form the National Bridge Inspection Standards (NBIS). It is the minimum standard for the inspection of the nation's highway bridges. The Surface Transportation Assistance Act of 1978 changed the basis for eligibility of bridges for federal funding. Under this act, the National Bridge Inventory Program (NBIP) was expanded to include bridges on all public roads, not just principal highways. The SBRP was replaced by the Highway Bridge Replacement and Rehabilitation Program (HBRRP), in which funding for bridge rehabilitation was added in addition to replacement projects (Czepiel 1995).

Before the 1980's, there were no existing bridge management systems, nor were there national "management systems" specified for Transit, Safety, Pavements, and other components of our highway system. The AASHTO Guide for Bridge Maintenance Management (AASHTO 1980) and Manual for Bridge Maintenance (AASHTO 1987) were used as guides for bridge maintenance tasks. Later in 1995, the Intermodal Surface Transportation Efficiency Act (ISTEA) legislation required each state implement a comprehensive Bridge Management System (BMS), which represented "a remarkable challenge" since few states had previously implemented a system that could be considered to meet the definition of a comprehensive BMS (FHWA 2002). North Carolina was one state that developed its own version of a comprehensive BMS prior to the federal dictate. Figure 1-1 shows a schematic history of the development of the Nation Bridge inspection and management practice that is accomplished by various Federal-State-Local partnerships.
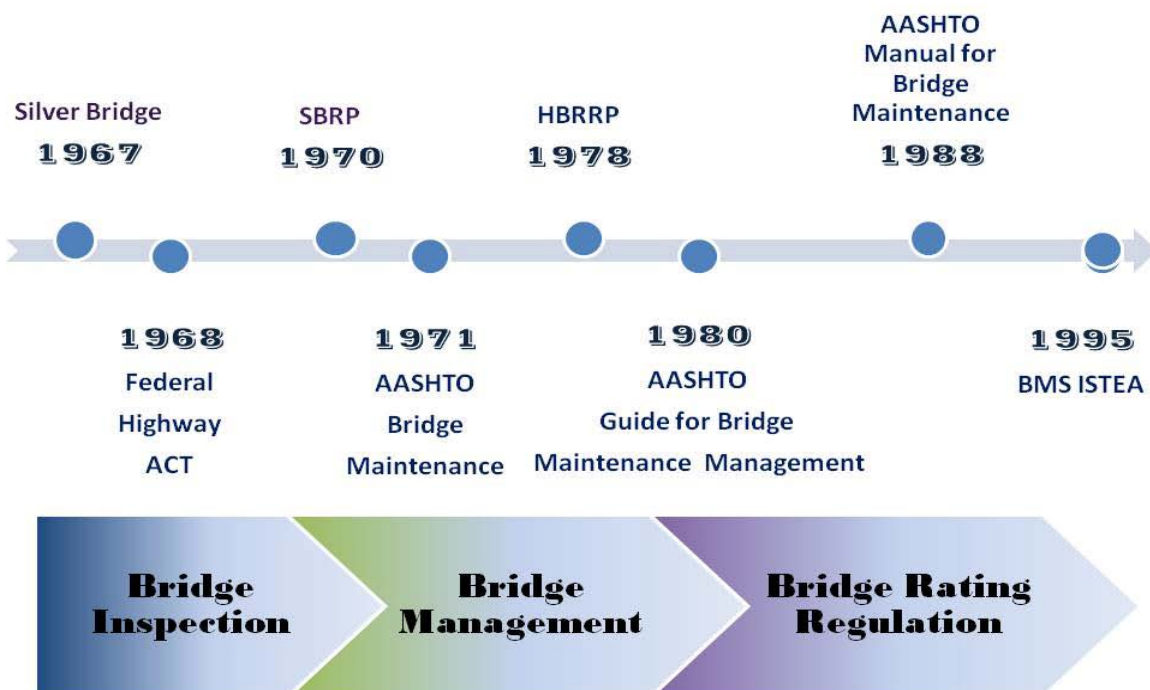
Figure 1-1 History of bridge management system

1.2 Bridge funding

There are around 590,750 public bridges in the U.S. Between 2000 and 2003, the percentage of U.S. bridges rated structurally deficient or functionally obsolete decreased from 28.5% to 27.1%. However, it still may cost $9.4 billion annually for the period of 20 years to eliminate all bridge deficiencies (ASCE 2005). Establishing a long-term development and maintenance plan must become a national priority.

Federal aid funds are provided for public bridge maintenance and rehabilitation, and systematic preventive maintenance is eligible for these funds. Although many steps are taken to supervise and manage deficient bridges, most funds are used for building new infrastructure rather than rehabilitating the existing deteriorating structures (Biswas 2004). In fact, funds required for repairing highways, transit systems and bridges have

reached several billions of dollars annually. Funding for bridge rehabilitation was first added in the HBRRP, in addition to replacement projects, since 1978. The Surface Transportation Assistance Act of 1982 countered this problem. Highway, safety and transit programs were extended for a period of four years from 1983 to 1986. More focus was then given to the bridge replacement and rehabilitation program. The Transportation Equity Act for the 21st Century (TEA-21) authorized the set-aside of $100 million for each fiscal year from 1999 to 2003 for major bridges to continue under the HBRRP (Lwin 2006).

1.3 Issues in current bridge inspection and management system

The latest version of NBIS became effective in January 2005. The policies and procedures in NBIS have been evaluated by the American Society of Civil Engineering/ Structures Engineering Institute (ASCE/SEI), and American Association of State Highway and Transportation Officials (AASHTO). These three organizations formed an Ad-hoc group with the purpose of ensuring that bridge management would be adequate to ensure public safety (ASCE/SEI-AASHTO 2009). It was recognized, however, that improvements in particular areas were still needed as identified by this Ad-hoc group. The main debates were focused on bridge inspection interval, inspection and rating quality and consistency, new inspection methodologies and data management.

Some state DOTs, such as Illinois, Kansas, New Mexico and California suggested to expand the inspection cycle, or reduce the cycle restriction range to only critical bridges (FHWA 2005). The Ad-hoc group presented a rational inspection interval concept, in which the inspection interval is determined by critical bridge factors, such as design, details, material, age and so on. Liu (2008; Appendix B) studied 69 collapsed

bridges in the U.S. after 1967. Seventeen of them collapsed during or just after construction. Sixteen of them were caused by structural defects and the remaining 36 were due to collisions and natural disasters. The data showed that new bridges have a relatively higher failure rate since the number of collapsed new bridges is higher than those in long time service. Therefore the inspection frequency for new bridges should be higher for bridges already in service. In Europe, an Interim Memorandum on Bridges (# IM13) requires bridges in England to be inspected at least once a year (Jandu 2008). Bridge evaluation studies elsewhere in Europe have found that long interval, in depth bridge inspection may lead to better inspection quality (ASCE/SEI-AASHTO 2009). Therefore, the inspection cycle should be allowed to vary for different conditions. However, it is recognized that this would be difficult to set such variable regulations.

Currently, visual-based inspection is the primary method for bridge inspection in the U.S. Errors caused by visual-based inspection are high and ratings generated by different inspectors for the same bridge can be different. The process, however, can be improved through the development of robust inspection manuals (Parekh 1986), qualified inspector training, and utilization of advanced non-destructive equipment. A 2001 bridge inspection survey among the states indicated the increase in the utilization of nondestructive evaluations and the number of Nondestructive Testing Level III-certified personnel since 1993 (Rolander et al. 2001).

Intelligent bridge maintenance and management systems are important to bridge owners, especially for monitoring bridges in critical condition. They can help bridge owners make maintenance decisions effectively and hence improve bridge safety (Neves 2006). The documented bridge data will also benefit the estimation of bridge

deterioration rates, which are currently lacking in the U.S. (ASCE/SEI-AASHTO 2009).

PONTIS, BRIDGIT, and Bridgeware are three bridge management systems currently

used by the state DOTs. More than 40 states use PONTIS to manage their bridge

(Jivacate and Najafi 2003). However, these systems are still mainly used for inspection

data collection and they appear to be underutilized to provide cost analysis, and structural

maintenance related decision making.

1.4 Role of remote sensing in bridge inspection and management

Successful bridge maintenance should be based on reliable bridge inspection data,

accurate bridge performance prediction and effective maintenance planning. All public

bridges in the U.S. are required to be inspected once every two years (FHWA 2002). The

inspections are mainly visual-based. Quantitative data for bridge condition evaluation can

rarely be found in current bridge inspection records.

For the past fifty years, several Commercial Remote Sensing (CRS) and Spatial

Information (SI) technologies for wide-bandwidth spectral information sensing and

imaging have been developed integrally with satellite/airborne/ground-based surveillance

platforms such as IKONOS, Quickbird, OrbView-3, orthotropic and small-format aerial

photography and LiDAR (Light Detection and Ranging) scans. However, CRS-SI

applications to bridge health monitoring have been extremely limited. Issues associated

with the application of CRS-SI technology to bridge monitoring have been identified

through discussion with individual bridge managers from several states (Ribarsky et al.

2009), including:

1)   **Limitations in current bridge inspection.** Current bridge maintenance is a generalized visual inspection process established by the federal government. There is no guideline in the use of CRS-SI technologies for bridge management.

2)   **Misunderstanding of CRS-SI capabilities.** The national survey shows a gap in between CRS technologies and their availabilities to bridge managers. As a result, bridge managers generally have limited experiences with CRS-SI technologies.

3)   **Complexity in multivariate data integration and presentation.** Because CRS data typically exists in image format and bridge data in PDF or text-file formats, integration of the data so that the bridge managers can "fused" data into manageable knowledge can be a challenge.

Comparing to traditional nondestructive structural inspection methods, remote sensing technologies, such as the Scanning LiDAR technique, have the advantage of large coverage area, large amount of information, cheap and up-to-date data collection, ease of manipulating with computer, and providing repeatable evaluation and inspection with high accuracy. The utilization of remote sensing technologies for bridge monitoring and management can alter the way we understand bridges and they have the potential to be cost effective tools for monitoring a large amount of bridges simultaneously. The development of automatic bridge inspection and management system based on remote sensing data also standardize the inspection procedure and save investigation and inspection time.

Laser radar system, also called LiDAR, is an optical remote sensing technology developed for range measurement. Terrestrial LiDAR scanners have the advantage of high speed data collection and large area coverage. Comparing to photogrammetry,

LiDAR technology provide data directly in 3D instead of 2D imagery. LiDAR scanners are often simple to use and unaffected by lighting condition. With the help of LiDAR scanner, bridge inspectors can obtain bridge structure dimension data without the restriction of the accessibility to the structure. The measurement resolution is in millimeters. The quantitative bridge structure surface shape measurements also have strong potential for bridge service status evaluation and prediction.

1.5 Current research work and dissertation organization

1.5.1 Research objectives

The research work introduced in this dissertation is part of the project entitled "Integrated Remote Sensing and Visualization (IRSV) System for Transportation Infrastructure Operations and Management" supported by the U.S. Department of Transportation (USDOT) - Research and Innovative Technology Administration (RITA). The intent of this multi-year project is to develop and validate CRS applications that can enhance current BMS. This dissertation will focus on exploiting the applications of LiDAR technology for bridge health monitoring. The goal of this study in relation to ground-based LiDAR application is to investigate the viability of applying LiDAR for bridge condition evaluation. This viability study addresses the questions of 1) how LiDAR can be applied? and 2) how costly is the technology to state DOTs? Specifically, the research objectives include:

1. Establish a cost-benefit analysis for possible adoption of 3-D LiDAR scanner or similar remote sensing technologies for bridge monitoring under current North Carolina bridge management operations.

2. Develop an automatic bridge damage detection and quantification system based on LiDAR data and establish bridge evaluation procedure using the quantification results.

3. Develop an automatic bridge displacement measurement system for briddge static load testing based on LiDAR data.

4. Develop bridge clearance measurement system based on LiDAR data to evaluate bridge service status.

5. Investigate the resolution requirements of 3-D LiDAR scanner for the proposed bridge evaluation applications.

6. Developed bridge rating criteria based on the quantitative bridge evaluation data from LiDAR data and the developed bridge evaluation system.

1.5.2 Scope of work

This dissertation will focus on the applications of remote sensing technology, in particular terrestrial LiDAR technology, for bridge health monitoring and evaluation. An automatic bridge evaluation system based on LiDAR data have been developed and will be introduced. Around twenty bridges in Charlotte-Mecklenburg area, NC, were selected for study and have been scanned using the LiDAR scanner. Most of these bridges have low condition ratings. Several bridges in good condition were also scanned for comparison. Eight of them are steel bridges and thirteen of them are concrete bridges. The detailed bridge information is listed in Table 1-1. Also, a newly constructed bridge over highway I-77, near Charlotte, and Bridge # 640024 on US-74 in Wilmington, NC, has been scanned during this study. Since the study in this research is only based on the selected bridges, not all the bridge types have been covered. Table 1-1 also referenced sections in this dissertation where a particular bridge has been studied in greater detail.

Table 1-1 Twenty selected bridges

Bridge Number	System	Condition	Sufficiency Rating	Status	Type	Referenced Section & Application
590084	NCDOT	Poor	82.1	Obsolete	PPC Cored Slab	6.1-AC
590140	NCDOT	Fair	77.5	Obsolete	RC Girder	
590147	NCDOT	Fair	47.5	Deficient	RC Girder	4.2-DE, 6.2-AC
590179	NCDOT	Fair	72.3		Concrete	2.2-AP, 3.1-AP, 6.2-AC
590239	NCDOT	Fair	78.2		Steel	
590296	NCDOT	Fair	94.7		PC	
590511	NCDOT	Good	80.4		RC Deck	4.3-CM
590512	NCDOT	Good	80.4		RC Deck	4.3-CM
590038	NCDOT	Fair	30.4	Deficient	RC Deck	
590049	NCDOT	Fair	48.4	Deficient	RC Deck	2.4-DD
590059	NCDOT	Poor	11.8	Deficient	Steel Plank	
590108	NCDOT	Fair	100	Deficient	RC Deck	
590161	NCDOT	Fair	63.7	Obsolete	Steel	
590165	NCDOT	Poor	48.2	Deficient	Steel	
590355	NCDOT	Fair	70.3	Obsolete	RC Deck	
590177	NCDOT	Fair	29.1	Deficient	Steel	
590255	CDOT	Fair	77.7	Obsolete	Steel	6.2-AC
590376	CDOT	Fair	84.83	Deficient	Steel	
590379	CDOT	Fair	29.3	Deficient	PC	
590700	CDOT	Poor			Steel	4.3-CM
590702	CDOT	Good			Steel	4.3-CM, 6.2-AC
590704	CDOT	Fair			Concrete	4.3-CM, 6.2-AC
640024	NCDOT	Poor	30.1	Deficient	Concrete	4.2-DE, 6.2-AC
I-77						Chapter 5-LT

*AC-Accuracy Check (LiDAR); AP-Aerial Photo; CM-Clearance Measurement (LiDAR); DD-Damage Detection (Thermography); DE-Damage Evaluation (LiDAR); LT-Load Testing

1.5.3 Dissertation organization

In Chapter 2, a literature review of remote sensing technologies in bridge health monitoring is first presented. A discussion of the role of high resolution remote sensing imagery in structure monitoring is given in Chapter 3. A cost benefit analysis has also been implemented for the evaluation of bridge inspection and maintenance investments in Chapter 3. The result indicated that appropriate increase for funding of bridge inspection and maintenance will result in significant monetary savings in agencies' bridge replacement program. Chapter 4 introduces terrestrial LiDAR scan technology and the automatic bridge evaluation system LiBE (LiDAR-based Bridge Evaluation) developed by the author. The LiDAR scanner has also been used for displacement measurement in bridge static load testing. The developed methodologies and programs are introduced in Chapter 5. The LiDAR scan and LiBE system evaluation accuracy have been validated in Chapter 6. Bridges are also rated by the LiBE system based on the quantitative evaluation of bridge status from LiDAR data. Rating criteria are described in Chapter 6. Chapter 7 is the summary and conclusion.

CHAPTER 2: BACKGROUND AND LITERATURE REVIEW

2.1 Introduction

Advanced structural health monitoring (SHM) techniques provide accurate assessment to infrastructure condition and can reduce the cost for unnecessary structure replacement through proper maintenance. Sensors, such as electromagnetic acoustic transducers, magnetic sensing, laser ultrasonics, infrared or thermal camera, guided waves, field measurement probes and strain gages, have been adopted to measure structure information including static and dynamic displacement, strain and stress, acceleration, surface and interior damage and corrosion (Papaelias et al. 2008). Structural condition rating, as well as the remaining life of a structure, can then be determined based on the collected information.

Due to the sheer size of most bridge structures, health monitoring techniques may become cost prohibitive: Considering the number of sensors, level of details for monitoring, and the long term engagement for meaningful applications for very large structures, existing SHM technologies are still not cost effective. The advancements in commercial remote sensing technologies show the potential as cost-effective methods for long-term monitoring of infrastructure.

For the past fifty years, several CRS-SI technologies for wide-bandwidth spectral information sensing and imaging have been developed integrally with satellite/airborne/ground-based surveillance platforms such as IKONOS, Quickbird and OrbView-3. Additional airborne sensors include ADAR 5500, Intermap STARS-3i, TerraPoint; powerful LiDARs including LandSat, SPOT and AVHRR, are technically-proven and available commercially (Birk et al. 2003). Several of these CRS-SI technologies have been implemented for traffic planning and environmental studies (NCRST 2000). Conferences, including the "Remote Sensing for Transportation" organized by Transportation Research Board, discussed the application of remote sensing in transportation engineering (TRB 2000). Annual Transportation Research Board (TRB) meetings also support specialty panels such as "Geospatial Data Acquisition Technologies in Design and Construction" and "Exploration and Classification of Earth Materials" to explore potential applications of remote sensing. The 4th National Transportation Asset Management Workshop in Madison WI, sponsored by AASHTO, FHWA, and Midwest Regional University, placed emphasis on applying remote sensing techniques in asset management (UTC 2001). This conference identified the advantages and opportunities of utilizing remote sensing techniques in transportation infrastructure asset management.

The focus of this chapter is on commercial remote sensing techniques and their applications in civil infrastructure health monitoring, in particular for bridges. Resolution requirements of remote sensors for structure monitoring are given and spatial resolutions of various remote sensors are also summarized in Section 2.2. Section 2.3 describes the

applications of satellite or airborne remote sensing for infrastructure health-related analysis. Section 2.4 reviews the ground-based remote sensing applications for SHM.

2.2 Overview of remote sensing resolution requirements

Remote sensing in this dissertation is defined as the sensing technique that collects information of an object, area, or phenomenon from a distance without physically contacting it. Typically, remote sensing refers to imagery and image information taken by airborne and satellite systems (ACE 2003). In this chapter, both space borne/airborne and ground-based remote sensing systems are discussed.

Based on spatial resolution, satellite data is classified as coarse resolution data and high resolution data. Ranging from dozens of meters to several hundred kilometers, coarse resolution satellite data are mainly used for large scale problems, such as weather prediction (Glantz et al. 2009) or marine observation (Ahn et al. 2006). High resolution wide-bandwidth sensing and imaging also make infrastructure monitoring and management possible (Pieraccini, 2004; Lee and Shinozuka 2006; Pieraccini, et al. 2008).

It is well recognized that spatial resolution, which refers to the ability to distinguish between two closely spaced objects (Sabins 1997) is more important than spectral resolution, which reflects the ability of differentiating image spectrum for structure monitoring (Jensen and Cowen 1999). Hence, the resolution discussed in this chapter only refers to spatial resolution. Welch (1982) estimated that the spatial resolution requirement for unban scene monitoring to be 0.5-10 m.

To address resolution issues for bridge monitoring, we first explore the tolerance of bridge displacements. Moulton et al. (1985) collected data from 314 bridges in 39 U.S. states, the District of Columbia, and four Canadian provinces, and generated bridge

movement tolerance criteria. According to their study, differential settlements of 25 mm

would be considered intolerable for span lengths less than 18 m. The tolerable differential

settlements typically increase with the increase in span lengths. Bridge horizontal

movements were thought to be more critical than its vertical movements. The study

suggested that horizontal movements less than 51 mm were tolerable in 88 percent of the

cases. Therefore, the resolution required for bridge movement measurement should be

better than 25 mm.

Table 2-1 Sensing and measurement attributes for bridges (Chase 2005)

Damage	Deterioration	Operation	Service
Impact	Corrosion	*Traffic Counts*	*Congestion*
Overload	Fatigue	Maximum Stress	*Accidents*
Fire	Loss of Prestress Force	Stress Cycles	Reduced Traffic Capacity
Scour	Unintended Structural behavior	*Deflection*	Reduced Load Capacity
Seismic	Chemical Changes	*Displacement*	*Increasing Traffic*
Cracking	*Transportation Property Loss*	*Clearance*	*Delay*
Settlement	Water absorption	*Bridge Geometrics*	Unreliable travel time
Movement			
Lack of Movement			

In another study, the FHWA defined cracks with widths larger than 4.08 mm for

reinforced concrete, and 0.76 mm for prestressed concrete as wide cracks (FHWA 2002).

Wide cracks were required to be monitored and recorded. Therefore the resolution

requirement for monitoring bridge cracks can be defined to be or better than 5 mm. Table

2-1 lists the attributes associated with bridge performance monitoring. The italic items are the ones that can be collected by remote sensing devices. Table 2-2 summarizes the resolution requirements for infrastructure, especially bridge, attributes detection.

Table 2-2 Resolution requirements for infrastructure attribute detection

Attributes	Resolution requirements
Urban scene	0.5-10 m
Bridge geometry information	0.5 m
Traffic counting	1 m
Clearance	0.3 m
Bridge intolerable abutment movement	25 mm
Bridge structure surface defects	13 mm
Bridge structure surface cracks	5 mm
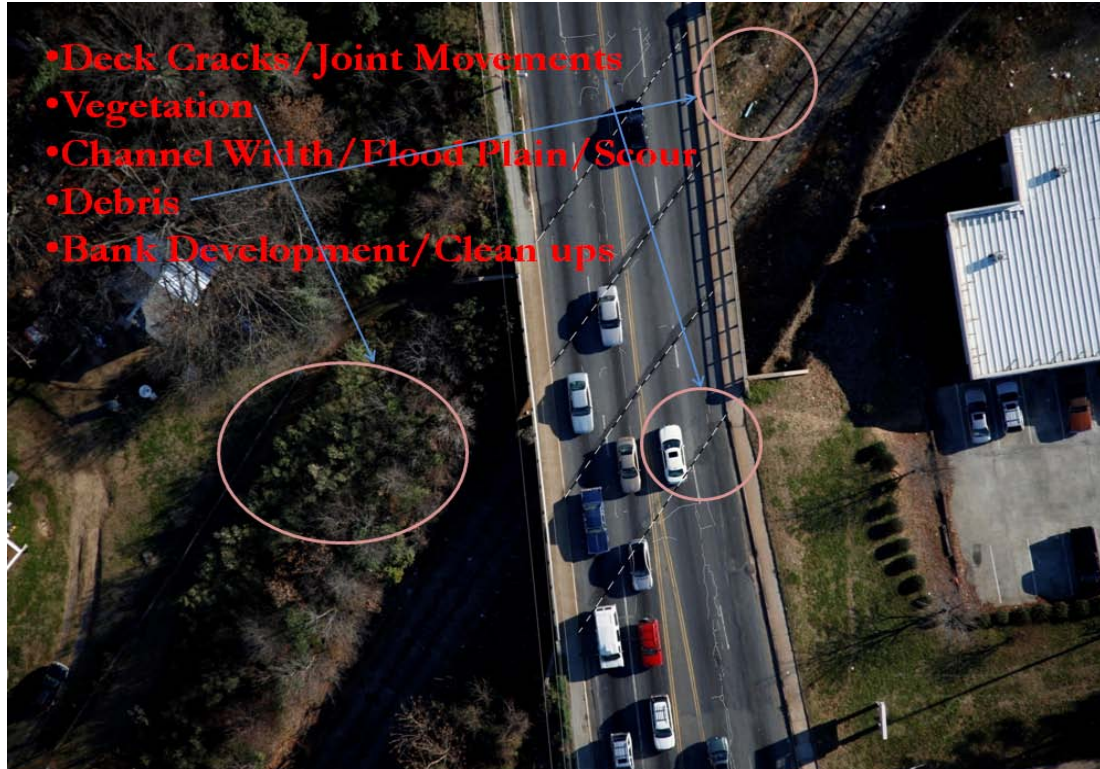
Figure 2-1 Aerial photo of NCDOT Bridge # 590179 provided by InSiteful Imagery

Currently, many commercial satellite sensors can provide earth images with a resolution near or better than 0.5 m. GeoEye launched the world's first one-meter commercial remote sensing satellite IKONOS in 1999. The latest launched GeoEye-1 (September 2008) has a ground resolution of 0.41 m (GeoEye 2009). DigitalGlobe now offers commercial panchromatic satellite data reaching the resolution of 0.46 m from Worldview-2 satellite (DigitalGlobe 2009).

Table 2-3 Summary of resolution comparison for different data acquisition approaches
(Welch 1974; Welch 1976; InSiteful Imagery 2007; CCRS 2009)

Provider	Technology	Resolution
DMSP satellites	Operational Linescan System (OLS) sensor	2.7 km
Meteosat satellites	Imaging radiometer sensitive to visible band	2.5 km
GMS satellites	Visible and infrared spin scan radiometer	1.25 km
GOES satellites	Multispectral channels imaging radiometer	1 km
HCMM satellite	Visible and thermal infrared radiometer	500 m
Skylab space station	Multispectral camera (S-190A)	60 m
MOS-1 satellites	Multispectral electronic self-scanning radiometer	50 m
Landsat satellites	Thematic mapper (TM) sensor	30 m
SPOT satellite	Scanning HRV sensor	10 m
IRS satellites	Panchromatic (PAN) high resolution camera	5.8 m
Worldview-2	star trackers	0.46 m
GeoEye-1		0.41 m
STAR	Spaceborne Radar Systems	5 m
Digital imaging systems	Digital camera	0.3 m
InSiteful Imagery	Small-format aerial photography	0.013 m

Note: values are taken from the sensor with the highest resolution in corresponding satellite

Compared to satellite imagery, airborne sensors have the potential of providing images with higher resolutions. In particular, the Small Format Aerial Photography (SFAP) technique that equips low flying small airplanes with professional grade photogrammetry equipment can provide extremely high-resolution photos. InSiteful

imagery (2007) provides aerial photography with a resolution of 13 mm, which is higher than most ortho-photography. Figure 2-1 is a SFAP airborne image (0.013 m resolution) of a bridge in Charlotte, North Carolina. The image was taken by a Canon 5D camera on a C210L aircraft at 300 m above ground level. The picture shows railing geometry, traffic lines, traveling vehicles and wearing surface conditions clearly. The rutting of the bridge deck can be detected (circled in Figure 2-1). Table 2-3 compares the resolution between different airborne/satellite acquisition approaches.

Table 2-4 Ground-based remote sensing techniques: resolution comparison

Remote Sensing Techniques	Function Description	Resolution or Limitation
Digital and video camera	Surface images for defect detection and displacement measurement	Depending on equipment character and distance to the object
Interferometric radar	Static and dynamic displacement measurement	0.5 mm
3D laser scanner	Static and dynamic displacement measurement and defect detection	0.5 mm with the distance of 30 m
Infrared camera	Structure interior defect detection	0.25 mm and maximum measure depth is 12.7 mm for composite reinforcement
Ground penetrating radar	Structure defect detection and material thickness measurement	2.6% material thickness measurement error; for concrete and polystyrene maximum measure depth is 700 mm

Ground-based sensors provide detailed object information with better resolution than satellite and airborne-based sensors. Most ground-based remote sensing devices can measure structure with accuracy in millimeters. A number of research projects have discussed the applications of using ground-based remote sensing techniques for infrastructure monitoring (Tarchi 2000; Sakagami 2002; Fuch et al. 2004a&b). The

techniques include, among others, ground-based interferometric SAR, digital and video camera, infrared camera, and ground penetrating radar. Table 2-4 lists several popular ground-based remote sensing techniques and corresponding resolutions. Notable is a recent review on short-range photogrammtry applied to bridge deformation measurements that identified the technique with resolutions about 3 mm to 14 mm (Jiang 2008).

2.3 General application of remote sensing techniques for infrastructure

Due to the natural geospatial representation and unique data acquisition features of remote sensing, many researchers (Welch 1982; Park et al. 1999; Benson 2000) have shown interest in the potential applications of remote sensing for infrastructure evaluation.

Current application areas of remote sensing for infrastructure can be roughly classified into three categories: construction planning and management, transportation, and SHM, which will be discussed in Sections 2.3.1, 2.3.2 and 2.3.3, respectively. Ground-based remote sensing techniques measure structural information with high accuracy and record a diversity of information; their applications in SHM are reviewed in Section 2.4.

2.3.1 Construction planning and management

Satellite imagery provides a large area perspective of the landscape features such as forests, lakes and grasslands. Digital Elevation Models (DEM) generated from interferometric Synthetic Aperture Radar (SAR) collects topology features of the earth surfaces. The image processing and Geographic Information System (GIS) offers great opportunities of using satellite data for infrastructure planning and management. Present

researches for infrastructure planning and management are largely based on the visual interpretation of satellite imagery combining with digital elevation model of the object area.

Han (2007) developed an integrated algorithm that detects over river bridge features from satellite imagery. The algorithm detected the rivers and then extracted the bridge features from the river occupied area. Satellite and airborne optical imagery and SAR have also been investigated for the identification of other bridge types (Lomenie 2003; Wu 2005; Yang et al. 2006; Chaudhuri and Samal 2008; Schulz 2007; Soergel et al. 2007). Similar methods have been applied to disaster management and damage assessment (Simonetto and Oriot 1999; Eguchi et al. 2005; Tralli et al. 2005; Stramondo et al. 2006). Combinations of optical data have been shown to improve the results: Satellite images and digital elevation models combined with other historical cartography and site survey data were utilized in selecting optimal site and planning fieldwork for the dam installations (Forzieri et al. 2008). The selected sites were identified from the visual interpretation of satellite images in GIS environment based on several fathomable parameters. A DEM was analyzed to measure one of the key parameter: catchment areas.

Other GIS and remote sensing applications include landfill sites selection (Eihoz 2006; Ghose et. al, 2006), urban infrastructure physical and environmental planning (Saxena 2001; Amekudzi and Baffour 2002), infrastructure protection from terrorist attacks (Morain 2002), highway corridor planning (Uddin 2002) and infrastructure type classification (Caceres and Slatton 2007). Digital images (Quinones-Rozo et al. 2008) and 3-D laser scans (Filho 2005) have been found practical in tracking excavation.

Throughout these studies, remote sensing data were recognized as being efficient in assisting infrastructure planning and management.

2.3.2 Transportation planning and management

Satellite imagery has been widely used for roadway identification and mapping (Hinz and Baumgartner 2000; Butenuth et al. 2003; Hinz and Baumgartner 2003; Herold, et al. 2004; Luo et al. 2005; Keskinen 2007; Cai and Rasdorf 2008). Keskinen (2007) mapped road infrastructure in Taita Hills, Kenya, using both visual and digital processing methods to analyze remote sensing data. Combined uses of remote sensing, image processing and GIS techniques for environmental studies in transportation infrastructure asset management was investigated by Amekudzi and Baffour (2002). They discussed several important considerations for developing remote sensing, GIS databases, and analytical methods to integrate infrastructure and environmental asset management. The impacts of civil infrastructure development on environment can be monitored and analyzed. A conceptual computerized image processing system was provided by Grivas that integrates various satellite data for transportation infrastructure assessment (Grivas et al. 1997). Gafy and Abdelrazig (2004) reported transportation environment assessment using remote sensing data. Abdalla (2004), on the other hand, integrated GIS, Global Positioning System (GPS), Global System for Mobile communications (GSM), and Remote Sensing in road safety studies. Finally, Kim et al. (1997) measured traffic congestion using scanned high resolution satellite panchromatic imagery.

2.3.3 Structural health monitoring

SHM aims to insure operational safety and provide early warning before costly repair or failure (Ko and Ni 2005). Non-destructive inspection (NDI) technologies are the

basic tools for SHM (Achenbach 2009). The evaluation of a health monitoring system is

based on the desired sensing type and accuracy of the collected information, capital and

operating budgets, and technical personnel resources (Shrive 2005). Remote sensing is

expected to be a cost-effective SHM tool, if structural performance data (displacement,

strain, acceleration) as well as environmental information (temperature, etc.) can be

identified. Figure 2-2 compares the system design of conventional SHM sensing system

in general and that of remote sensing system for health monitoring. Figure 2-3

summarizes the issues of bridge and its components which can be monitored using

remote sensing techniques.
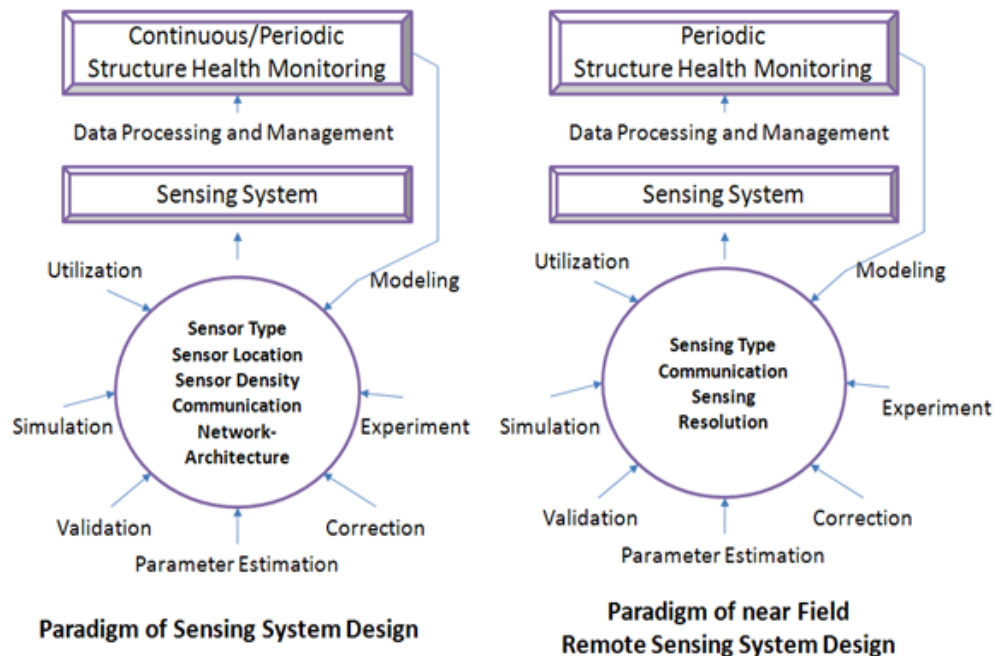
Figure 2-2 Sensing system design for structure health monitoring (modified from Zhang and Aktan 2005)

Due to the resolution requirements, the literature review at this point is devoid of citations that relate to using satellite data for SHM. However, with the advances in high resolution CRS, it is anticipated that health monitoring and related applications will be much more widespread in the near future. The obvious advantage of using remote sensor for SHM is the ease of data collection, since no physical contact or surface treatment is needed. With innovative testing technique design and use of the off-the-shelf GIS-application software, very low cost technologies can be developed.
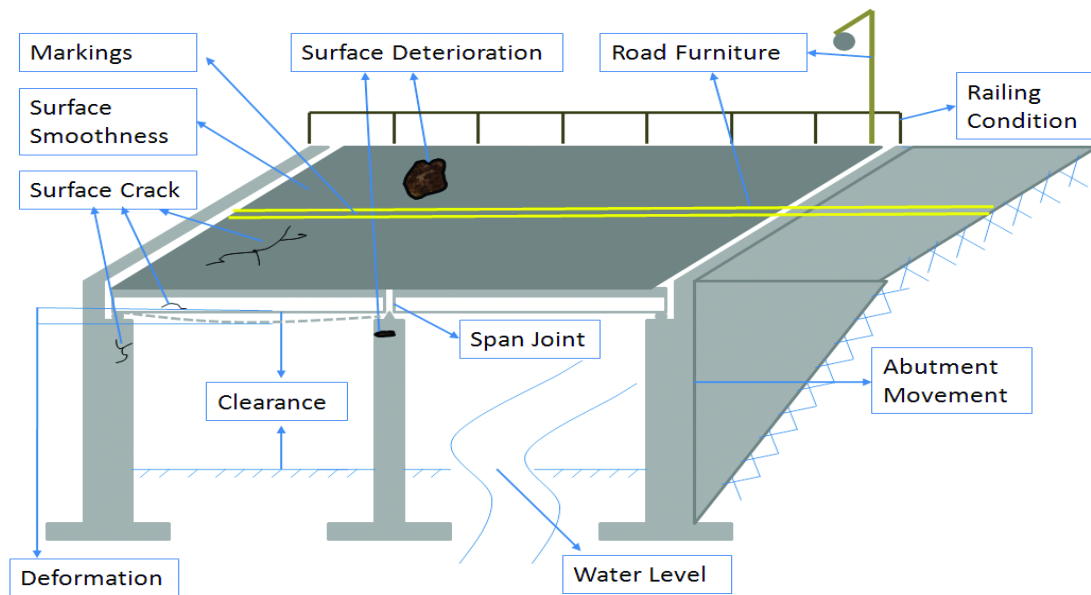
Figure 2-3 Summarizations of bridge issues which can reflect bridge heath condition and can be monitored by remote sensing

To date, most research in SHM using satellite data is concentrated on using GPS for structural static and dynamic displacement data collection (Wong et al. 2001; Jiang et al. 2002; Roberts et al. 2003; Roberts et al. 2007; Brown and Roberts 2008; Yao et al. 2008). GPS provides absolute 3D position of receivers fixed on structures with accuracy

in millimeters. The number of monitoring points is determined by the installed receiver number. Since GPS satellites collect earth surface point position and elevation information periodically, with proper data processing system developed, GPS can provide real time monitoring of structures.

Remote sensing in surveying transportation infrastructure was explored by Herold et al. (2006), with a main focus is on the understanding of spectral properties of road surfaces and urban surfaces of different types, ages and conditions. It was found that pavement age and some surface defects, such as raveling, can be described at spatial resolutions of four meters; but other pavement quality information such as rutting and cracking cannot easily be detected.

Stoeckeler (1970) presented a technique to compare what is discernible on different aerial photos. Herold and Roberts (2005) identified road condition through spectral analysis of satellite data and prove the potential of using multiband satellite data in road way mapping. Chung and Shinozuka (2004) developed an automated pavement inspection and management system based on remote sensing data and geographic information. Satellite imaging systems combined with information systems provided a solution to address safety issues related to pipelines and oil facilities (Roper and Dutta 2006). The technology is also effective in helping plan oil spill cleanups. Huertas and Nevatia (2000) presented an airborne image-based change detection methodology for 3D structures especially buildings. Due to resolution restriction, only relatively large dimension changes and missing of buildings can be detected (Perera 1995). ERS SAR data (Parcharidis et al. 2008) was used to continuously measure the ground deformation of western Greece for structure stability risk assessment.

2.4 Ground-based remote sensing technique for SHM

Ground base remote sensing as a type of SHM tool can obtain more detailed structure information than satellite and airborne sensors. Figure 2-4 illustrates how ground-based remote sensing techniques can be used to extract structure displacement, strain, distress, surface crack, corrosion and collision damage, and critical structural factors, such as bridge clearance, degree of curve and skew distance (Birge 1985).These data can be extracted directly from surface data provided by remote sensing devices in the forms of multi-spectral photography, radar images or 3D geometry data. With proper signal processing and analysis methods and structure computer model, surface information acquired can be used for subsurface defect identification. Some remote sensing techniques such as infrared camera are able to provide subsurface information directly (Figure 2-4).
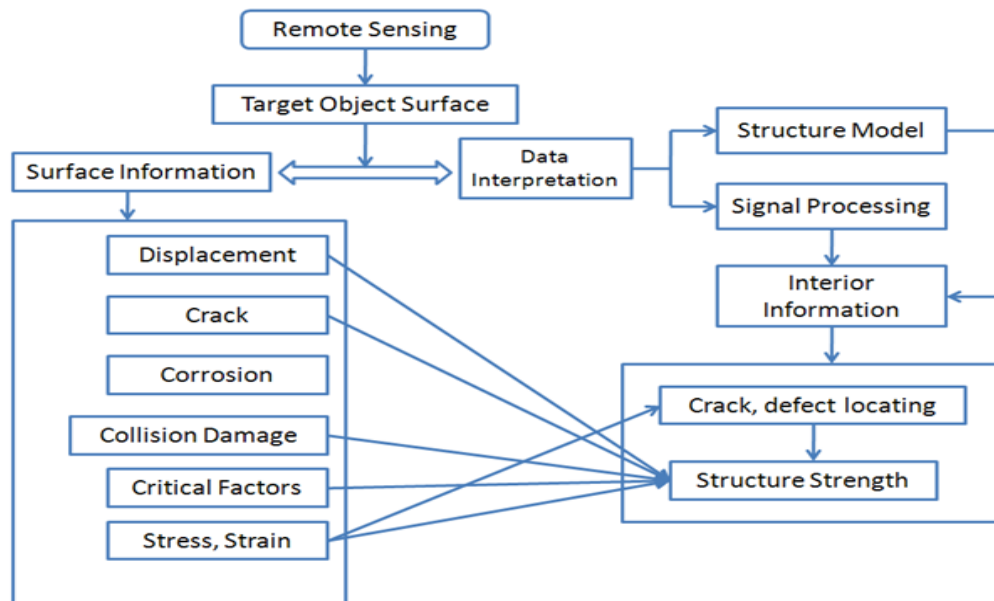
Figure 2-4 Role of ground-based remote sensors in structure health monitoring

2.4.1 Structure surface monitoring and data acquisition techniques

Image-based structure inspection system has gained interest during the past decades due to the high resolution it provides and its relatively low capital and operating cost. Birge reported measurements of stations, offsets and elevations of objects based on two photos taken from moving vehicles (Birge 1985). This method has also been used to measure bridge critical features such as clearance, degree of curve and skew distances with an accuracy of 0.15 m. Computer base image analysis has been used for the measurement of wooden, concrete, bitumen and coated plastic structure surface (Abdel-Qader et al. 2006; Patricio and Maravall 2007; Rosati et al. 2009; Rodriguez-Valverde et al. 2008). The resolution of these inspections is determined by the character of the imaging system and the capture distance to the objects. Lee and Shinozuka (2006) processed digital images for bridges taken from commercial digital video for real time dynamic displacement measurement.

Aircraft or satellite SARs collect earth surface elevations based on quantitative comparison of radar images of the same scenes that are taken at different times (Tarchi 2000). Ground-based differential interferometric SAR was used by Pieraccini for displacement measurement of large civil structures, such as bridges, dam and buildings with an accuracy of sub millimeter (Tarchi et al. 2000; Pieraccini et al. 2004). SAR has also been studied for structure damage and change detection (Shinozuka and Loh 2004). Interferometric radar and accelerometer have been used for structural dynamic monitoring through measuring structure displacement data (Fratini et al. 2007; Pieraccini et al. 2008).

Laser radar system, also called LiDAR (Light Detection and Ranging), is an optical remote sensing technology developed for range detection. 3D laser scanners have the advantage of high speed data collection and large coverage area. They are often simple to use and unaffected by lighting condition. A set of points on the object surface in three-dimensional a coordinate system, often called point clouds, will be recorded in each scan. Currently few works have been found using 3D laser scanner in bridge inspection: Fuchs et al. (2004 a&b) introduced a laser system for bridge testing. The system has been shown to be useful tool in measuring unprepared surface movements for load testing without targets and can reach accuracy in sub millimeters over a 30 m range. Pieraccini et al. (2006) used laser scanning to quantify urban site built displacement induced by a landslide. A kinematic terrestrial-based laser scanning system that can be deployed on moving vehicles or watercrafts was introduced by Glennie (2007). The system acquired 360 degrees of coverage and a 3D point cloud was georeferenced using high accuracy GPS/INS system. Mobile 3D laser scan systems can reach accuracy in centimeters, although less accurate than fixed location scanners. Drawback of the kinematic terrestrial-based laser scanning system is that their 3D scan accuracy is directly affected by the accuracy of recorded GPS data. Teza et al. (2009) have developed a computation-based method for mass loss recognition of concrete bridges. The curvature distributions of undamaged reference area information were needed for the detection of curvature distributions change in order to identify damage area.

Moire techniques, such as moiré interferometry and geometric moire, have been recognized as high accuracy surface strain, stress and displacement measuring tools (Guralnick and Suen 1991) for engineering materials. Guralnick indicated that, for larger

surface coarse measurement, shadow Moiré method was the most appropriated one and had applied the method for pavement surface inspection. The displacement resolution of geometric Moire used by Chona et al. (1995) for fracture parameters determination is 0.0125 mm. Shadow Moire has also been applied in out-of-plane deformation measuring during heating and cooling of plastic ball grid array with a resolution around 29.2 µm (Tsai et al. 2008). Moiré related technology has not been widely used in civil structure health monitoring, since it needs structure surface treatment and corresponding data processing system in order to obtain desired information. Hence, although Moiré image can be detected remotely, it is not a true remote sensing technique in the strict sense.

2.4.2 The integrating of surface monitoring data with structure numerical model

Surface damage detection is thought to be the first level of general damage identification. Modal analysis method can help locate damage and estimate the severity of structural damage. Dutta and Talukdar (2004) developed a method to detect the bridge deck cracks by comparing the natural frequencies of the intact and damaged condition: a simply supported single span bridge and a two span bridge Finite Element model were discussed. The location of cracks can be acquired from the changes in element curvature. Internal and non visible cracks can also be detected using this method. Park et al. (2007) presented structural vibration approaches to predict prestressed concrete girder bridge prestress-loss and detect flexural cracks. A prestress-loss prediction model and a mode shape-based damage detection method were utilized in each approach, respectively. Righiniotis (2004) studied the relationship between the maximum load and the fracture toughness, target failure and the cracks of the bridge. After obtaining crack information

using a non-destructive inspection technique, the maximum affordable load can be calculated from the derived relationship model.

2.4.3 Structural subsurface defect detection techniques

Thermography detects thermal patterns and associated changes by converting them to visible images formed by temperature differences. Therefore, thermographic investigation is not restricted by lighting condition. Figure 2-5 is an example of using thermography to detect bridge defect. The thermography is captured by infrared camera. The measured temperature is not only depending on the object surface temperature, but also its emissivity and atmosphere absorption (Clark et al. 2003). Therefore, accuracy of defect inspection varies for different material types and environmental conditions. Standards need to be established for different materials and environmental factors in order to utilize infrared camera as an independent defect detection tool. According to ASTM standard (ASTM 1997), the defect should have temperature differences of at least 0.5 degrees Celsius in order to be detected. Avdelidis et al. (2004) classified infrared thermography into two approaches: passive and active. The active approach requires external stimulus source, such as hot air guns, quartz lamps, Xenon flash lamps, hot or cold water, vortex tubes, sprayed liquid nitrogen and so on (Burleigh and Bohner 1999). Most regular applications for infrastructure are based on passive approach, which measures material temperature difference than ambient.

Thermal images have been used for detecting the disbonding in structure materials (Burleigh et al. 1999; Sakagami et al. 2002; Miceli et al. 2003). Burleigh showed the thickness limitation of 12 mm for composite reinforcement measurement (Burleigh and Bohner 1999). The minimum detectable defect identified was about 0.25

mm wide. With an increase in material thickness, the detection ability decreases. For example, for 12 mm fiberglass, the minimum defect dimension was 6.3 to 25.4 mm. Washer et al. (2008) researched the thermal performance of concrete with the influence of environmental factors to test the application of infrared cameras for bridge defect detection. The initial analysis results indicated the influence of solar radiation on the contrast of recorded thermal images. Weil (1998) reviewed and provided a case study for the application of thermography and ground penetrating radar etc. in structure void detection, but the work was mainly visual-based.
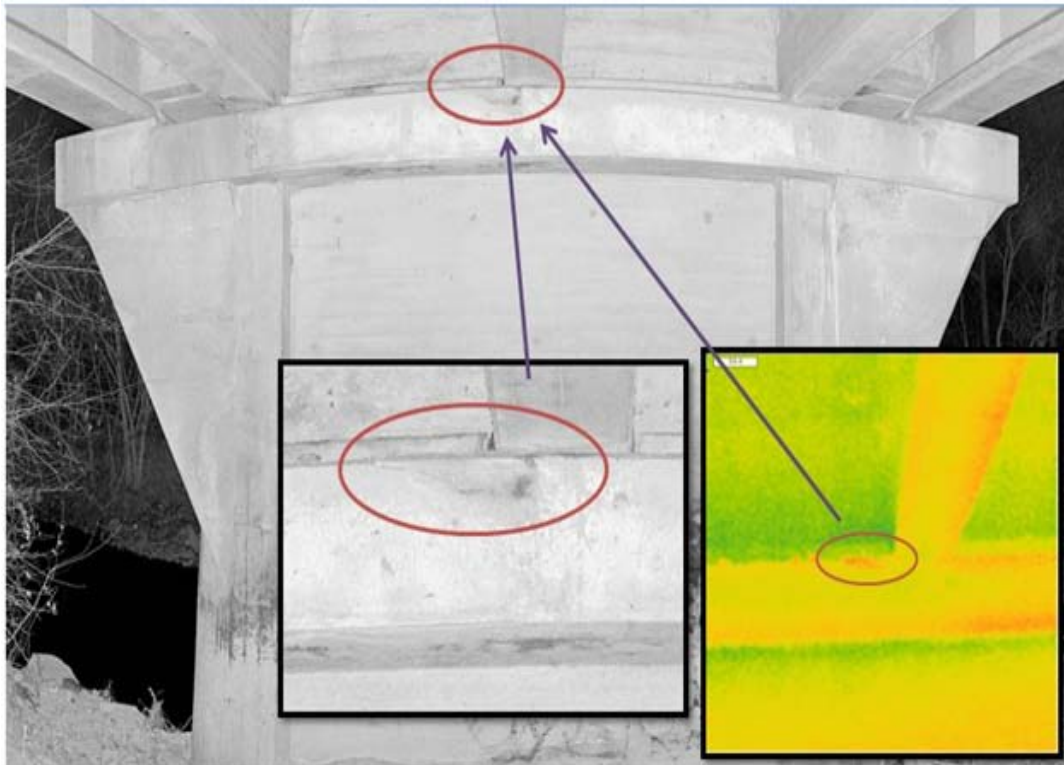
Figure 2-5 Bridge abutment defect detection from thermography (Bridge # 590049, NCDOT)

Ground penetrating radar (GPR) often uses an air-coupled horn antenna to generate radar pause with a distance from 0.3 to 0.5 m to target structure. Reflected energy is determined by the target structure material properties. By recording and analyzing the GPR return signals, structure subsurface defects can be detected. GPR has been used in pavement and structure assessment for more than 30 years (Maser 1995; Yelf and Carse 2000; Moropoulou 2002; Yehia et al. 2008). Shin and Grivas (2003) compared ground truth with GPR measured bridge deck condition and their statistic result indicated a 75% true detection rate and a 15% false detection rate. Al-Qadi and Lahouar showed that the average error of GPR for concrete slab reinforcing bar location was about 2.6% (Al-Qadi and Lahouar 2005). Huston (1999) indicated that the GPR system they used was able to detect concrete feature at 360 mm depth. Yelf and Caser (2000) suggested a depth limitation of 700 mm for concrete and polystyrene. The restrictions of GPR for pervasive structure inspection application are caused by the uncertainty of structure material properties and the difficulty in locating individual reflected pulses (Al-Qadi and Lahouar 2004).

Although various remote sensing technologies such as infrared and radar imaging systems, portable ultrasonic systems, telemetry systems, laser deflection measurement systems and so on (Washer 1998), have been proved to have the ability for SHM, evaluation of these tools is still critical before general application. FHWA has created the NDE validation center in 1998 especially for NDE methods evaluation.

2.5 Summary

This chapter reviewed the applications of remote sensing technologies for infrastructure monitoring, especially SHM for bridges. The development of remote

sensing techniques attracts researchers to apply them into different fields other than traditional uses, such as land observation and weather monitoring. The high resolution satellite and ground-based remote sensing data make SHM possible. Most of the remote sensing technologies can provide real time monitoring of the targets. Since they offer structure information from an incomparable large scale, appropriate investigation on SHM can make it cost efficient.

Compared to contact testing methods, ground-based testing techniques are more sensitive to noise (Rizzo et al. 2005). Improvement of the resolution and reliability of available remote sensing data are required for further application. Although remote sensing cannot totally substitute for visual inspection, it alters the way to understand structure condition and it provides indepth and accurate structure assessment that visual inspection can never achieve. There are huge development opportunities for high resolution and efficient structure monitoring systems based on remote sensing. Validation of remote sensing techniques is also crucial for general application in SHM.

CHAPTER 3: REMOTE SENSING IMAGERY IN STRUCTURAL EVALUATION
AND A COST BENEFIT ANALYSIS FOR BRIDGE INSPECTION INVESTMENT

3.1 Introduction

Bridge health monitoring as a method of protecting aging infrastructure potentially can produce significant highway safety and economic benefits. Current challenges to improve and augment existing health monitoring methods include decreasing the cost and operational logistics involved in these techniques. Due to the sheer size of many bridge structures, the number of sensors required and the level of details, monitoring techniques become expensive, and the long-term search for meaningful applications may not be cost effective. Advancements in CRS technology make it a very attractive method for long-term monitoring of bridge infrastructure.

According to NBIS, all public bridges in the U.S. are required to be inspected at least once every two years. There are several recent or current studies on whether this interval is reasonable (ASCE/SEI-AASHTO 2009). However, considering the costs required for the 2-year inspection cycle, there would appear to be only a small prospect of increasing the frequency of inspections. Advanced sensing technologies may be helpful and represent the focus of this chapter. Unfortunately, most current bridge inspections are still visual-based due to the high costs of instrumentation for the majority of bridges in this country. It is widely recognized that visual inspections are subjective and the inspection results lack accuracy (Chase and Washer 1997).

Spatial resolution can be reflected by the number of independent pixel values per unit length in an image. For infrastructure monitoring, spatial resolution is recognized to be more important than spectral resolution, which reflects the ability of differentiating image spectrum. Therefore in this chapter, only spatial resolution of remote sensing is discussed. "Remote" refers to any CRS device or methodology that does not actually touch, or be embedded in the bridge members. It is suggested in this chapter that remote sensing can be a low cost supplement to on-the-ground visual bridge inspection. Data produced through these technologies can be relatively easy to be managed comparing to the profuse number of conventional digital photographs.

This chapter investigates the potential applications of high resolution remote sensing photography for bridge monitoring. Both satellite and airborne sensors provide a large field of view for bridge components. The technology primarily produces two dimensional views of the bridge deck and parapets. Possible detectable bridge issues are summarized and simulative ratings are given to reflect the severity of detectable bridge problems and as a reference for visual-based bridge inspection standard creation, or for automatic detection method generation. In Section 3.3, a cost benefit analysis (CBA) has been introduced for bridge inspection and maintenance investment. A sample of bridges in three counties in North Carolina - Mecklenburg, Beaufort, and Rutherford - were chosen as representing metropolitan areas of the Piedmont, coastal, and mountain areas respectively. This CBA analysis indicates that appropriate increase for funding of bridge inspection with the adoption of advanced bridge inspection technologies will result in significant monetary savings in agencies' bridge replacement program.

Table 3-1 Summarized bridge issues reflected from remote sensing photography

Cause	Observations	Required resolution	Cause	Observations	Required resolution
					Bridge deck
Sun shadow	Shading	1 m	Abutment	Relative displacement	0.025 m
Rain	Shading	0.5 m	Pier		0.025 m
Car accident		1 m	Bridge deck displacement		
Section loss		0.5 m	Deck punch-through	Large openings	0.5 m
Deterioration		0.1 m	Deck		0.5 m
Chemical spill	Discoloring	0.1 m	Wear at joint	Gap at expansion	0.1 m
Collision	Deformation	0.1m			
					Wearing surface
New wear surface	Discoloring	1.0 m	Cracking	Shading	0.005 m
Raveling	Local	0.5 m	Potholing		0.1 m
			Rutting		0.1 m
		Railing			**Curb**
Missing		0.5 m	Cracking	Shading	0.005 m
Cracking	Shading	0.005 m	Spalling		0.1 m
Section loss		0.1 m	Alignment	Curb edge	0.5 m
Spalling		0.1 m	Collision damage	Shading, edge detection	0.1 m
	River bank (1 miles)				**Sidewalk**
Pollution	De-vegetation	1m	Deterioration	Shading	0.1m
Smaller flow	River channel widening	0.5 m			**Drainage device**
		Traffic	Scaling potion		0.1 m
Increase in		1 m			**Land use**
Increase in trucking			Surrounding land use	Changes in image	1 m
Rush hour traffic					**Geometry of bridge**
Loading condition			Edge detection	Horizontal misalignment	0.5 m
					Utilities
Light shape, cables		0.1 m	Traffic line		1 m

*ADT-Average Daily Traffic

3.2 Visual interpretation of satellite and airborne imagery for bridge health monitoring

Table 3-1 gives the possible bridge issues that can be detected from the high-resolution airborne images to enhance visual inspection that can be developed into further automatic detection methods. Note that the *italic* attributes identified in Table 3-1 do not directly reveal or cause bridge structural problems. Some of these attributes like sun shadows and rain dampness can act as noise for feature extractions for structure-related attributes identification. Some attributes may reflect bridge conditions indirectly. For example, the definition of the traffic line can indicate the pavement maintenance condition and the irregularity of traffic line may be caused by structural component movements or surface defects.

Table 3-2 Bridge Deck Surface Deterioration Identification

Type of Deterioration	Discernible?	Rating	Type of Deterioration	Discernible?	Rating
Through Deck	Yes	0	Worn-out wearing	Yes	6
Large relative	Yes	3	Debris	Yes	6
Overload Damage	Yes	3	Brand new deck or	Yes	9
Scaling	Yes	3	Delaminations	No	
Spalling	Yes	4	Pop-outs	No	
Slight Collision	Yes	4	Chloride	No	
Cracking	Yes	4	Efflorescence	No	
Wears (Abrasion)	Yes	5	Ettringite Formation	No	
Damaged Repair	Yes	5	Honeycombs	No	
Grease or chemical	Yes	6			

*Notes: 8, 9 Effective system nearly new condition; 6, 7 No structure service required; 4, 5 Questionable structure; 2, 3 certain structural problem, immediate service required; 0, 1 No traffic allowed

Resolution limitation of remote sensing technologies restricts their damage assessment capability. Only wide structural cracks (width≥ 0.0048 m) (FHWA 2002) are able to be detected from satellite or airborne images. Small pop-out holes and internal defects, such as ettringite formations and honeycombs may be identified in surface satellite or airborne images. As a result, detectable bridge defects may represent serious damages to the bridge structure.

Figure 3-1 Sample remote sensing images for bridge deterioration detection (Insiteful Imagery 2007; Owen; Google Earth)

Table 3-2 also provides cumulative ratings for possible bridge deck problems that reflect the severity and their influence that affects the whole structure. The detectable cracking at the mid-span of simple span structures and at the supports of continuous span structures is one of the visual signs of overload damage. This affects the level of posting of the structure. Large amounts of scaling and spalling can represent stiffness loss of concrete. Wear and abrasion can be detected by the relative brightness, since wear area may be smoother than remaining area of the deck. This kind of deterioration can be a traffic safety hazard, especially in wet weather. Figure 3-1 illustrates four sample images for bridge deterioration from either satellite or airborne sensors. The upper left of Figure 3-1 shows a collapsed bridge in Laval, Montreal, Canada. Span displacement can be detected from satellite images as in the upper right image in Figure 3-1. Pavement spalling and damage repair can be found in the lower two images of Figure 3-1, respectively. Pavement spalling may or may not pose serious structural problems, but can be a nuisance to traffic and bridge users.

3.3 Bridge inspection cost-benefit analysis

3.3.1 Study Area Description and Status of Bridges

Mecklenburg County, Beaufort County and Rutherford County are selected in this project as typical representatives of the State's Piedmont metropolitan, the coastal, and mountain areas, respectively. All three counties are among those counties with the largest number of bridges in their regions. Table 3-3 lists the general information of the study area and State of North Carolina. Mecklenburg County has the largest population density and Beaufort County has the least, ranging from 1321 to 54 persons per square mile. The Annual Average Daily Traffic (AADT) of the three selected counties is calculated by

summing the AADT data for all routes in the corresponding county and dividing the result by the total number of routes using North Carolina Department of Transportation (NCDOT) traffic survey data (NCDOT 2007). The data in Table 3-3 shows that the AADT is almost proportional to the county population.

Table 3-3 Study Area Description Data (U.S. Census Bureau 2000; NCDOT 2007)

Region	Population	Area (Square miles)	Population Density (per square mile)	Average Annual Daily Traffic
Mecklenburg County	659,454	546.22	1,321.5	21,249.27
Beaufort County	44,958	958.69	54.3	2,854.54
Rutherford County	62,899	565.90	111.5	2,669.495
NC Statewide	8,049,313	53,818.51	165.2	
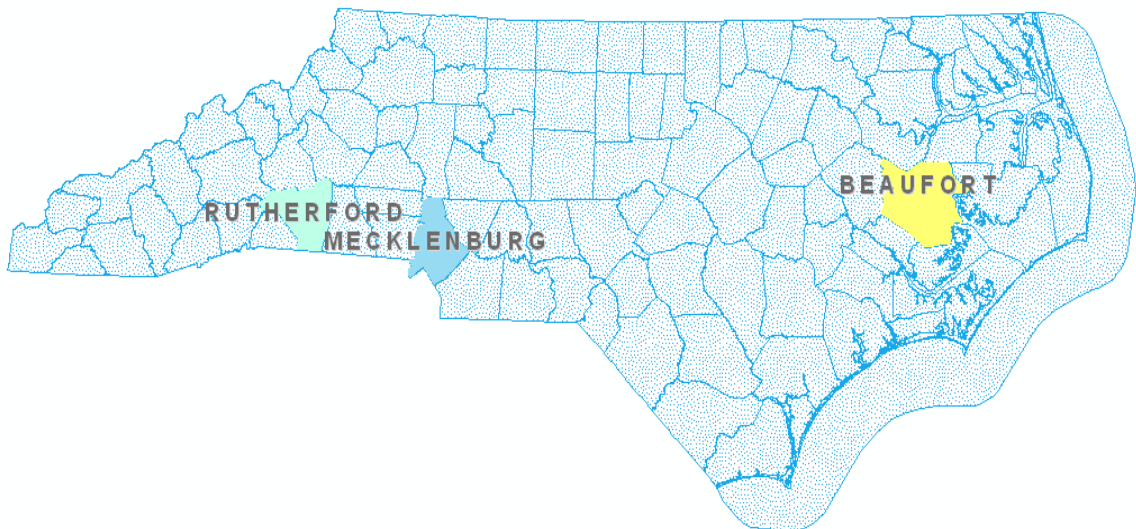
Figure 3-2 NC County map and study counties
(Created using Arc Map, data from NCDOT webpage)

Mecklenburg County has the largest population in North Carolina. NC's largest city, Charlotte, is located in this county. Charlotte is in the top ten fastest growing metro areas in the U.S. Interstate highways I-77, I-85, I-277 and I-485, state highways NC-16, NC-24, NC-27, NC-49, NC-51, NC-73 and NC-115 are passing through this county. The total number of bridges in this county is around 589, and 88 of them are over water (Table 3-4).

Table 3-4 Bridge Statistics of the Study Area (Brent 1996)

Region		Mecklenburg County	Beaufort County	Rutherford County	NC Statewide
Total	Num.	589	150	309	1809
	%				
Bridge	Num.	401	119	255	13102
	%	68.08	79.3	82.5	72.40
Culverts	Num.	188	31	54	4995
	%	31.92	20.7	17.5	27.60
SD	Num.	26	37	57	2515
	%	4.41	24.7	18.4	13.90
FO	Num.	107	13	66	3138
	%	18.17	9.7	21.4	17.34
SD+FO	Num.	133	50	123	5653
	%	22.58	34.4	39.8	31.24
Posted	Num.	38	63	136	4580
	%	6.45	42	44	25.31
Over Water	Num.	88	114	292	
	%	14.9	89.3	94.5	

Definitions: SD - Structural Deficient; FO - Functional Obsolete

Beaufort County is located on the North Carolina coast. Agriculture is the one of the most important economic sectors in this county. The county also has an industrial park which offers jobs to the residents. The total number of bridges in that county is 150

and 114 of them are over water bridges. Rutherford County, like Mecklenburg, is located on the North Carolina/South Carolina border (Figure 3-2). It is famous for the natural wonders, including Chimney Rock and the Bottomless Pools. Many places in this county have been listed on the National Register of Historic Places. The total number of bridges in this county is around 309 and 292 of them are over water bridges.

Appendix A summarizes the bridge replacement plans of the three counties from NCDOT 2007-2013 State Transportation Improvement Program (STIP). Although Mecklenburg has the largest number of bridges, the planned to be replaced bridges are fewer than that of the other counties. The data in Table 3-4 indicated that Mecklenburg County's bridge deficiency rate is lower than Beaufort County and Rutherford County. One of the reasons may be that the percentage of bridges over water in Beaufort County and Rutherford County are greater than that of Mecklenburg County. Bridge structures over water are typically more vulnerable to corrosion than bridges over highways. Almost all the bridges listed in the 2007-2013 STIP are over water bridges. Therefore in the analysis of this section, only bridges over water are considered. The average costs for bridge replacement are higher in Rutherford County than the others. The possible reasons could be the scale differences of the bridges and the inconvenience of construction material and labor transport in Rutherford County.

3.3.2 Cost-Benefit Analysis

This project focuses on proposing and evaluating bridge maintenance investment strategy of state-maintained bridges for these three counties. For the cost-benefit analysis, the basic assumption is that the increase in bridge inspection and maintenance investment will result in the increase of bridge service life.

Investment in bridge inspection and maintenance includes support for new inspection technology development and validation, real time problem identification and resolution, and systematized bridge maintenance plan development and implementation. Global visualization and traffic analysis will help the bridge manager in predicting the performance of a bridge. Advanced bridge health monitoring methods can improve the inspection accuracy and reduce unnecessary bridge repair or reconstruction. An example for showing the importance of in-time maintenance can be found for Bridge # 590177 in Mecklenburg County. The original wooden bridge piers have been hollowed by insects based on our inspection in 2009. The new piers have been coated with epoxy which curtailed the problem. If the bridge piers were pre-coated or the damage was discovered earlier, the costs for the installation of new piers would have been saved.

Another assumption is that the bridge service life will increase in each county and will be reflected in the reduction of the deficiency rate with proper inspection and maintenance. The NCDOT has adopted a pre-requirement for bridge replacement which states that bridge should have the sufficiency rating lower than 50 to be put on the STIP. The bridge with the sufficiency rating lower than 50 is also considered to be deficient in this dissertation. The deficiency rate herein is defined as the total number of deficient bridges divided by the total number of bridges. Hence, if a county has a deficiency rate decrease of 5 percent, the county will have 5 percent saving from bridge replacement costs.

Generally, a bridge service life is expected to be 50 years with the maximum of 80 years. In this thesis, all the bridges are assumed to be designed with a service life of 50

years if no maintenance actions are applied during their service lives. With the best

maintenance before replacement, a bridge is assumed to serve for 80 years.

Table 3-5 Benefits and Costs for Bridge Inspection and Maintenance Improvement for each County

2007	2017	2027	2037	2047	2057	2067	2077	2087
Mecklenburg County								
Coating Cost								
$17,600	$23,890	$32,430	$44,023	$59,758	$81,117	$110,112	$149,471	$202,898
Inspection Improvement Cost								
$68,921	$93,556	$126,996	$172,390	$234,009	$317,653	$431,195	$585,321	$794,538
Cost Reduction from Replacement								
$123,922	$166,055	$222,514	$298,168	$399,546	$535,391	$717,424	$961,348	$1,288,206
Beaufort County								
Coating Cost								
$22,800	$30,950	$42,012	$57,029	$77,413	$105,084	$142,646	$193,633	$262,845
Inspection Improvement cost								
$89,284	$121,197	$164,518	$223,323	$303,148	$411,505	$558,594	$758,257	$1,029,289
Cost reduction from Replacement								
$177,813	$238,269	$319,280	$427,836	$573,300	$768,222	$1029,417	$1,379,419	$1,848,422
Rutherford County								
Coating Cost								
$58,400	$79,275	$107,610	$146,075	$198,288	$269,163	$365,373	$495,972	$673,253
Inspection Improvement Cost								
$228,691	$310,435	$421,397	$572,021	$776,484	$1,054,031	$1,430,783	$1,942,202	$2,636,423
Cost Reduction from Replacement								
$640,706	$858,547	$1,150,452	$1,541,606	$2,065,752	$2,768,108	$3,709,265	$4,970,415	$6,660,356

Corrosion protection coating will help to prevent bridge damage from corrosion

damage. Assume that if 100% of the bridge surface is repainted every ten years, there

will be no major bridge structure damage caused by corrosion. Therefore, the maximum service life increase is set to be 60%. Following this logic, with 1% recoating of bridge surface every 10 years, the bridge deficiency rate of the county will decrease by 0.6%. Based on the 50 years bridge service life prediction, 20% of the bridge will depreciate every 10 years assuming no recoating maintenance as well as ignoring the differences in geometry changes and aging. All the deficient bridges in each county are assumed to be eliminated within 10 years with bridge replacement. The new bridge construction increase rate in each county is assumed to be 1% every 10 years.

This cost-benefit analysis is projected for an 80-year period, starting with FY 2007. The average coating cost per square ft is estimated as $2.5 (AGA 2007). The average surface area of a bridge is chosen as 8000 square ft (Better Road 2009). In this dissertation, FY 2007 is taken as the base year, since the bridge replacement costs are taken from the STIP 2007 data and 7% discount rate is selected for the analysis. The budget for research on developing an integrated advanced bridge monitoring system is $ 922,595 for two years (Chen 2007). The Mecklenburg County land area is 546.22 square miles. The research assumes that Geoeye and Quickbird can provide high resolution commercial satellite images that are suitable for bridge health monitoring. The price is around $26-$78 per square kilometers (Chen 2007). The total cost on satellite images of Mecklenburg County could be around $30,000. The NCDOT has planned to spend $92,800 for GIS system development in the 2007-2013 STIP.

Since the IRSV project covers the satellite and GIS part, and the budget for purchasing satellite image and GIS development is small comparing to the total cost of IRSV project, therefore the IRSV budget is used as an estimate to cover all similar

research. Therefore, the corresponding cost on this project is $783.19 per bridge. The achievement of the IRSV project not only benefits Mecklenburg County, but also the whole State and Nation. Hence, this dissertation estimates that this kind of project will be issued once every 10 years in each county to ensure the timely identification of bridge problems and efficient bridge maintenance plans. Subsequently the cost will be $783.19 per bridge per 10 years.

Table 3-5 lists the benefits and costs for the improvement of bridge inspection and maintenance. For the simplicity of the analysis and analytical exercise, the main costs are coming from the adoption of advanced inspection techniques and bridge repainting program. The benefits are the money savings from the reduction of bridge replacement in each county. The nominal net present value and cost benefit ratio and the ones with discount rate 7% and 10% are given in Table 3-6 for comparison following Eq. (3-1) and Eq. (3-2).

$$NPV = \frac{\sum(B-C)_t}{(1+r)^t} \tag{3-1}$$

$$CBR = \frac{\sum B}{\sum C} \tag{3-2}$$

in which B and C are the total benefit and cost of FY t. r is the discount rate (*OMB 2009*).

Table 3-6 Net Present Value (NPV) and Cost-Benefit Ratio (CBR)

	Nominal		**7% Discount Rate**		**10% Discount Rate (Optional)**	
	NPV	CBR	NPV	CBR	NPV	CBR
Mecklenburg	$1,166,692.4	1.329	$112,063.6	1.397	$78,443.6	1.411
Beaufort	$2,168,450.1	1.472	$274,442.7	1.548	$139,108.1	1.564
Rutherford	$12,599,332.1	2.071	$1,150,992.0	2.177	$758,265.4	2.200

3.3.3 Solution and conclusion

The Cost-Benefit analysis shows that in this simple scheme, the investment strategies are viable options as they produce large NPV and the benefits are generally larger than cost. Mountainous areas may receive more savings from bridge inspection and maintenance investment. The analysis in this dissertation is based on bridge statistical data in the three counties only. It does not rely on a particular bridge, but included a general study of all state-maintained bridges in the three counties. The work of this section has demonstrated the importance of efficient bridge inspection and maintenance programs, and provides a reference for bridge managers when considering adopting advanced technologies such as an IRSV system for bridge monitoring.

CHAPTER 4: TERRESTERIAL LIDAR-BASED TECHNOLOGY AND ITS
APPLICATION IN BRIDGE EVALUATION

4.1 Introduction to terrestrial LiDAR scanner

Terrestrial 3D laser scanners operate on the same basic principles as microwave Radars (Radio Detection and Ranging), but at a much shorter wavelength. They often operate in the ultraviolet, visible, near infrared, mid infrared and far infrared regions. Laser scanners can also be considered as LiDAR or LaDAR (Laser Detection And Ranging) systems (Jelalian 1992).

A basic LiDAR system consists of a transmitter, a receiver and a signal processing unit. A pulse or a series of light is emitted from the transmitter and part of the scattered energy is reflected back to the receiver after reaching the object area (Figure 4-1). The time the light traveled between the scanner and the object, can be measured. By multiplying the speed of light with its travel time, the two way distance between the scanner and the object can be calculated.

Currently, there are mainly two range measuring techniques for laser scanners: One is time-of-flight technology and the other is phase shift technology. The time-of-flight scanner follows the classic method of measuring the traveling time of emitted light pulses between the scanner and the object. With known speed of the laser light, the time that the light travels between the emitted light and the returned signal will yield the

-distance to the object. For time of flight technology, the range measuring ability is determined by the scanner's time delay measurement accuracy (Carrara et al. 1995). The latter type of scanner emits constant waves with different modulation wavelengths. The distance between the scanner and object is then measured by detecting the phase shift of the reflected waves. The ability of range determination of phase shift technology can be improved by using multiple waves with various modulation lengths. The measured distance based on phase shift technology is limited by the maximum modulation length of the selected waves. Theoretically, time-of-flight technology has no range measuring limitations unless the emitted energy is not strong enough to get a response. Phase-based scanners typically have higher speed of acquisition, data density and resolution as compared to the time of flight technique (Sgrenzaroli 2005).
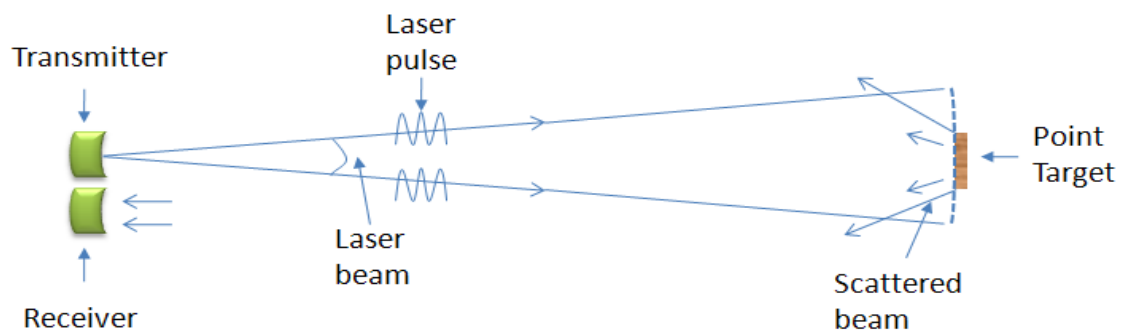
Figure 4-1 The operation of a LiDAR system

The laser scanner used in this bridge monitoring study is a Faro LS 880HE (Faro Technology 2007), which is a phase-based laser system. It operates at a wavelength of 785nm. Detailed specifications of the Laser scanner system are given in Table 4-1. The scanner used in this dissertation is capable of capturing 120,000 points per second.

Table 4-1 Specifications of the Laser scanner (adopted from Faro Technology 2007)

Item	Specification	Item	Specification
Range	76m	Measurement speed	120,000 points/sec
Wavelength	785nm	Beam diameter	3mm, circular
Vertical view	320 °	Horizontal view	360 °
Vertical resolution	0.009 °	Horizontal resolution	0.00076 °
Distance error	±3mm at 25m	Power consumption	~60W
Size	400mm×160mm×280mm	Weight	14.5kg
Temperature	5 ° ~40 ° C	Humidity	Non considering
Georeferencing	yes	Control panel	External PC

A laser scanner can only collect the range information of object points along its direction of view. To obtain the surrounding surface information instead of a single point, a reflection mirror is placed opposite to the scanner transmitter that allows 360 degree vertical rotation and the laser head itself also rotates 360 degree horizontally (Figure 4-2). After the scanner head rotates 360 degree horizontally, a full scan is finished. The point cloud of the object surrounding surface information that is along the scanner's field of view can be measured and recorded in a single scan. For a typical scan in current study, around 9,000×4,000 points are measured with 360 ° horizontally and 320 ° vertically (due to the blocking of the scanner underpan). Each scanned physical position point is assigned a 3D coordinate value according to its relative position to the scanner with the origin located at the position of the scanner head. Comparing to traditional photographic image-based defect detection techniques, the laser scan can display the position of the

defect over the entire structure without extraneous works to register pixels in single images and extrapolate defect information in 3D.
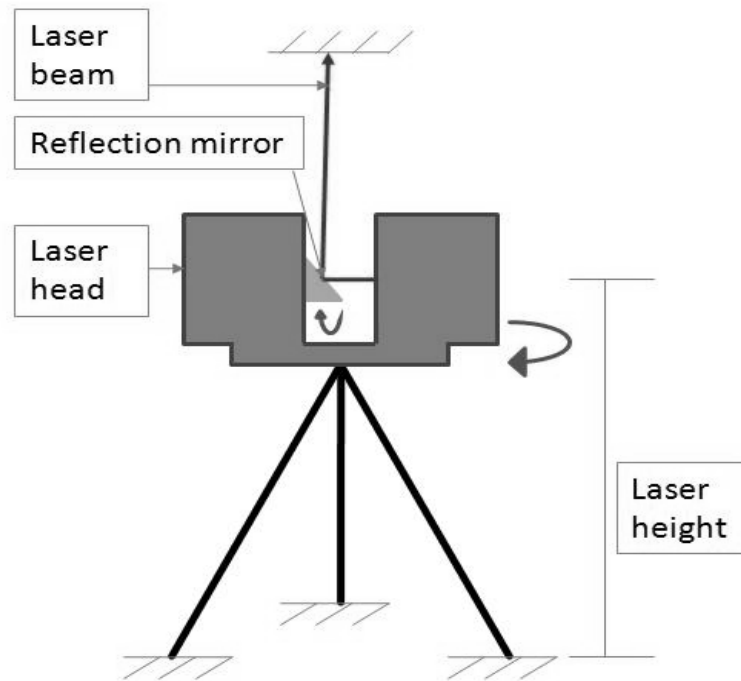
Figure 4-2 Schematic of laser scanner operation

To date, the application of laser scanner has been limited to mainly considering documentation and data restoration for as-built structures (Lichti and Gordon 2004; Kayen et al. 2006). Girardeau-Montaut et al. (2005) presented a method to detect changes by comparing point clouds acquired by laser scanner for changes in physical structure damage detection. Pieraccini (2007) reported using interferometric radar to measure the static and dynamic movements of bridges. Table 4-2 summarized the specific areas that LiDAR scan can be used in related to bridges. In this research, the laser scanner has been studied for the application in bridge health monitoring. When scanning a bridge, the laser

scanner is put underneath the bridge. A LiDAR-based automated bridge structure evaluation system, called LiBE, has also been developed with the functions of defect detection and quantification, clearance measurement and displacement measurement for bridge static load testing. The following parts will introduce the potentials of LiBE for bridge health monitoring. Section 4.2 will introduce the methodology that has been used for bridge surface automatic defect detection and quantification. Section 4.3 discusses the bridge low clearance issues and the application of LiDAR scan for bridge clearance measurement. The load testing part will be introduced separately in Chapter 5.

Table 4-2 Possible applications of LiDAR scan in bridge engineering

LiDAR scan applications	
Construction delivery	Image Documentation
Geometry Estimation	Bridge Clearance Determination
Structural Damage Measurement (impact)	Structure Defect Quantification (mass loss)
Bridge Displacement Measurement During Static Load Tests	

4.2 Defect detection

4.2.1 Introduction

There has been in place a federal (FHWA) mandate that all bridges built and/or maintained with public funds are to be inspected at least every other year since 1968 (FHWA 2005). These inspections are commonly done visually by trained inspectors. However, there appears to be a growing consensus among bridge engineers that there is a

need for additional rapid and non-intrusive methods for bridge damage evaluation that would add valuable information to the nation's BMS.

Previous attempts of using LiDAR scan to quantify damage involve Gaussian curvature computation where damaged surface curvature information was compared with an undamaged reference surface (Teza et al. 2009). Since, most of the critical bridge components have flat surfaces, such as girders, decks and some of the bridge abutments, the LiBE methodology focuses on the defect detection and quantification of bridge components with flat surfaces. First, the flat bridge surface plane is identified based on the coordinate values of automatic selected boundaries. Second, all the surface points are rotated to make the flat plane vertical to Z (out of plane) coordinate. The points on the damaged area are identified as irregularity points based on the distances between the points to the flat surface and their gradients, and the distance between each point to the flat plane can then be calculated based only on the point's Z value. The interested surface is then divided into smaller grids, where if more than half of the points in the grid are irregularity points, the grid is classified as irregularity grid. Each defective area on the selected surface can be detected by searching the connectivity of the irregularity grids. The defective area and volume are quantified by adding up the area and volume of each defective grid within the defective area. Defective volume of each grid can be calculated as:

$$V = A \times \bar{D} \times \gamma \qquad (4\text{-}1)$$

where $\bar{D}$ is the average depth of the irregularity grid and γ is the defective ratio of the grid. x_i and y_i $(i = 1, ..., 4)$ are the coordinate values of the ith point of the four

boundary points, which are numbered counter clockwise. The defective area is then defined as:

$$A = (x1 \times y2 - x2 \times y1 + x2 \times y3 - x3 \times y2 + x3 \times y4 - x4 \times y3 + x4 \times y1 - x1 \times y4)/2$$

Most of the bridge surface defects that can be detected by LiDAR scanner are visible to human eyes, and sometimes, the defects are documented as digital images. However, it is hard for bridge inspectors to quantify the defects especially when the bridge components are inaccessible. One LiDAR scan can record surface information of a bridge 360 degree horizontally and vertically. The obtained visual information of the bridge is organized in the scan. It is easy to get the relative position of a defective area on the bridge from the scan, which is difficult to be achieved using local digital images. The proposed defect detection technique can also quantify the defects with a minimum detectable area of 0.01 m × 0.01 m. The analysis based on LiDAR data is repeatable. If the defects of a bridge are studied periodically, the mass loss rate can be determined. The data can then be used to generate or update the deterioration rate prediction model. Detail introduction to this methodology will be given in Section 4.2.2. The FORTRAN source code for defect detection and quantification is given in APPENDIX E.

4.2.2 Detailed Methodology

This part explores a surface damage detection algorithm, as part of LiBE, for material mass loss quantification. LiDAR has the potential for providing high-density, full-field surface static imaging, hence, can be used to generate volumetric quantification of concrete corrosion or steel erosion. By recording the surface topology of the object, the laser radar can detect different damages on the bridge structure and differentiate damage types according to the surface flatness and smoothness. The LiBE algorithm differentiates information departed from original surface through surface gradient and

displacement calculation. The technique is applied to the extended pile cap of a concrete bridge (NC county Bridge # 590147, Figure 4-3), which quantifies the mass loss. The aging bridge is built in 1938 and has been listed in the North Carolina 2009 TIP list for possible replacement. The bridge is a reinforced concrete girder bridge with three 40 ft spans. The bridge is supported on timber piles with reinforced concrete caps. Large spalls are found underneath three of the four girders (Figure 4-3).
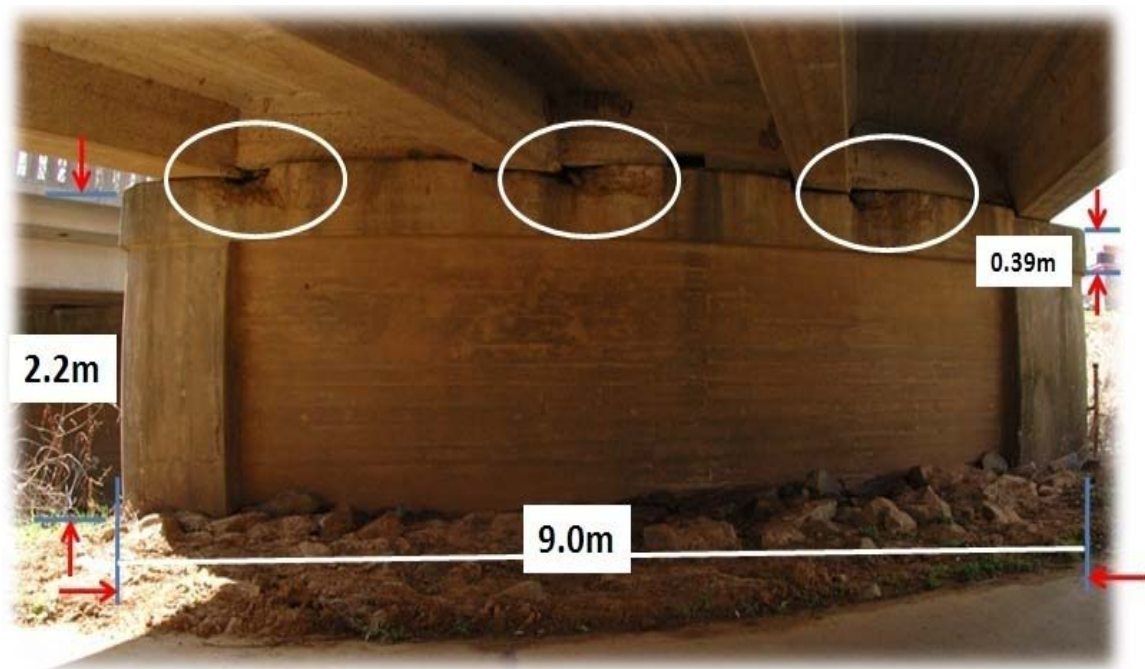
Figure 4-3 Substructure of Bridge # 590147 showing distress in pile cap

4.2.2.1 LiBE Damage Detection

Deteriorations of concrete bridge structure may come in several forms: cracking, scaling, spalling, efflorescence and collision damage, etc. (FHWA 2002; Abdel-Qader et al. 2006). Cracking in concrete members, in particular, is most common as a result of either excessive loading or environmentally-induced internal stressing (such as erosion or

corrosion of rebars). Significant research efforts have been spent in the detection of cracking in concrete (Dutta and Talukdar 2004; Righiniotis 2004; Abdel-Qader 2006; Park et al. 2007). Scaling, spalling and efflorescence are largely due to environmental effects and typically result in material mass loss.

Program Start

Read First Point Information as Start

Read Each Column of Scanned Point Data

Record Filtered Points according to Discontinuity of Row Numbers → Points Coordinates are Stored in New Matrix with Start Column and Row (1,1)

No

End of Data?

Yes

Define Reference Plane

Rotate Coordinates to Make Reference Plane Parallel to z=0 Plane

Divide Study Area into n*m Grid

Calculate Average Distance and Average Gradient Using Sample Points

For each point

Calculate Surface Gradient and distance to reference plane

Distance Check

Gradient Check

For each Grid

Gradient Irregular Rate >0.5 and Distance Irregular Rate >0.5 — Yes → Defect k is located in Grid

Yes

Omnidirectional Grid Irregularity Check — Yes → Defect k is located in Grid

Mass Loss Quantification

Program End

Figure 4-4 Flow chart of LiBE damage detection program

Using a LiDAR scan to detect surface defects of a bridge, a reference plane is necessary to simulate the intact condition of the bridge surface. The scanner records 3D positions of the bridge component, the information is limited to the surface points. Figure 4-4 shows the flow chart of the LiBE system in its current stage of development for bridge structure surface analysis.

For a single flat surface, the analysis is actually in 2D, which requires rotating the surface-of-interest to make the reference plane parallel to X-Y plane (Figure 4-5). To reduce the error induced by surface roughness in creating the reference plane, the plane should go through at least two points on a diagonal line near the boundary of the study area and one point on the upper center of the selected area (black points in Figure 4-6). The distance between a selected point (gray point in Figure 4-6) on the lower center and the reference plane is used to check the accuracy of the reference plane. For each of the four selected points, coordinate values are compared with the corresponding average coordinate values of the eight surrounding points. If there is a significant difference between the points (often 0.05 m larger than the average), which may be caused by environmental noise (such as trees or other non-bridge objects), other neighboring points will be used to replace the point. Since a scan point is arranged with column and row numbers according to the horizontal and vertical scan angle of the point, the neighboring point can be selected by increasing column or row numbers at least three for each corresponding selected point. After rotating the bridge surface-of-interest, the point coordinate values in Z-direction will be used to determine the deviation from the simulated reference plane and can be used to calculate surface gradient at that point.
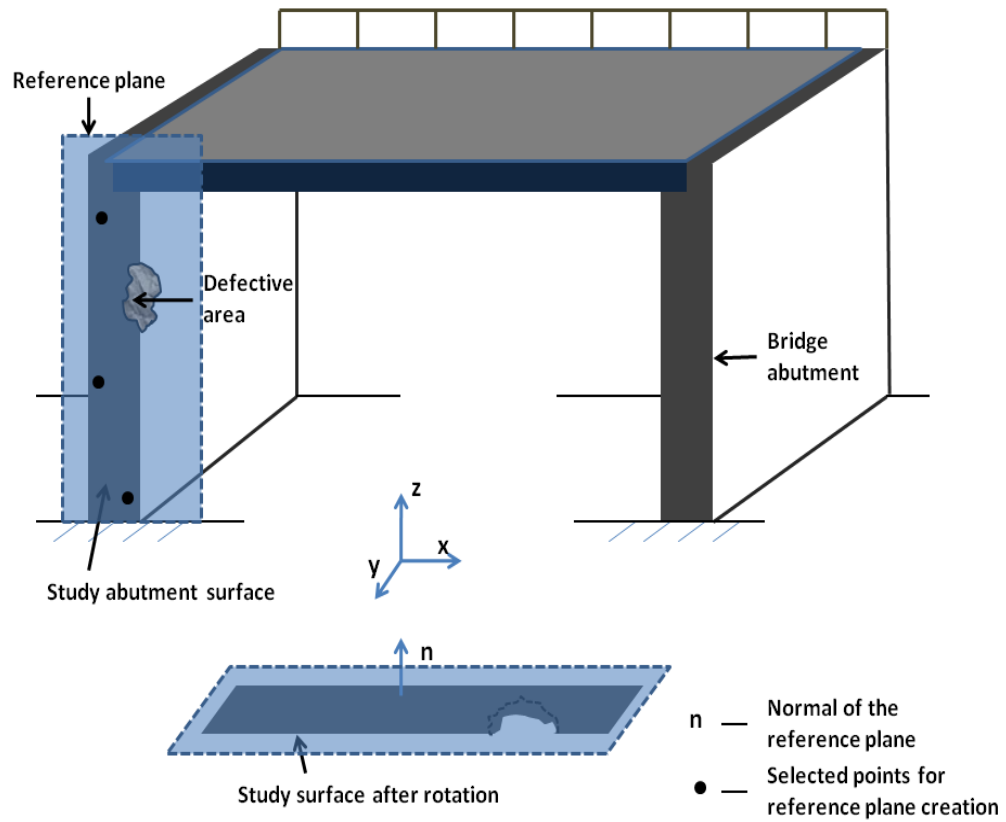
Figure 4-5 The creation of the reference plane and rotation of study bridge surface
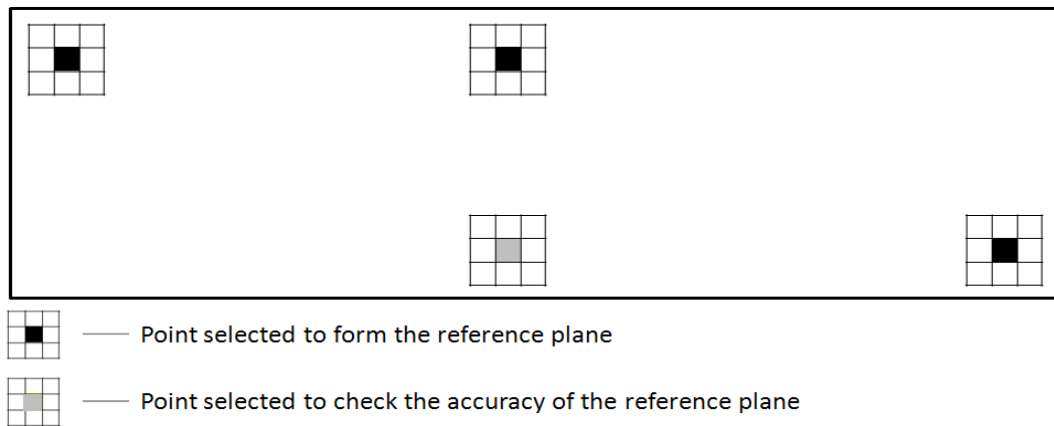
Figure 4-6 Location of points for reference plane determination

4.2.2.2 Gradient Calculation

Since the surrounding surface information is recorded point by point with the rotation of laser head and oblique mirror, the scanned points are represented in curves instead of straight lines, hence, conjugate graticular (latitude and longitude) coordinate system is used (Figure 4-7). Gradients in both latitude and longitude directions are calculated and the corresponding absolute value is added together to reflect the surface irregularity. Eq. (4-2) shows the approximate method to get the irregularity $G(C,R)$ for a particular point in column C and row R.

$$G(C,R) = \left| \frac{z(C+\alpha,R) - z(C-\alpha,R)}{\sqrt{(x(C+\alpha,R) - x(C-\alpha,R))^2 + (y(C+\alpha,R) - y(C-\alpha,R))^2}} \right|$$
$$+ \left| \frac{z(C,R+\alpha) - z(C,R-\alpha)}{\sqrt{(x(C,R+\alpha) - x(C,R-\alpha))^2 + (y(C,R+\alpha) - y(C,R-\alpha))^2}} \right|$$

(4-2)

where α is the number of points in each interval (interval size), which can be selected by the user, and z(C, R), x(C, R) and y(C, R) are position coordinates in Cartesian. The origin of the Cartesian would be defaulted to the position of the laser scanner.
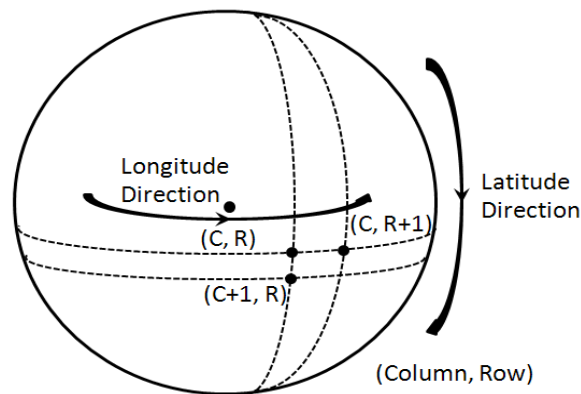
Figure 4-7 Point cloud position reference coordinate system

4.2.2.3 Defect Area Identification and Mass Loss Calculation

Surface of bridge components are often rough due to the material (wood, concrete and steel) used. Therefore, the surface gradient calculated may not be continuous. Dirt spots and paints also influence the smoothness of the surface. By increasing the interval size for the gradient calculation can help reduce gradient sensitivity-to-noise ratio. Detection of defective area can either by comparing gradient or displacement information. For relatively large defects (Figure 4-3), it is not efficient to determine the defective area point by point. Hence, each selected area for analysis is divided into smaller search grids. In the current case, 10×10 point grids are selected and can result in a 0.01 m $\times$ 0.01 m resolution. For cracks or span joint detection, the interval size needs to be minimized to increase its sensitivity and $\alpha = 1\,or\,2$ can be chosen in these cases. For relatively large defective area (larger than 0.1 m $\times$ 0.1 m), larger interval size $\alpha = 5 \sim 10$ should be used. For gradient-based damage detection method, each position point is considered to be irregular if it satisfies the following criterion:

$$G(C,R) > \beta_1 \times G_{ave} \tag{4-3}$$

For distance-based detection method, the following criterion can be used

$$D(C,R) > \beta_2 \times D_{ave} \tag{4-4}$$

where $D(C,R)$ is the distance between the point in column C and row R to the reference plane. G_{ave} and D_{ave} are the average of surface gradient and average point distance to the reference plane. β_1 and β_2 are the adjusting parameters. They are selected based on the proportion of the total defective area to the total study area. Larger defective ratio in the study area needs larger β_1 and β_2 and often $1.0 \le \beta_1, \beta_2 \le 2.0$.

Distance $D(C,R)$ can be simply defined as:

$$D(C,R) = |z(C,R) - z'(C,R)| \qquad (4\text{-}5)$$

Since after plane rotation, the distance from scan point to the reference plane is equal to the distance from scan point to x-y plane minus the distance from the reference plane to x-y plane, $z'(C,R)$. The distance from the reference plane to x-y plane is a fix number. In the scan point irregularity identification, Equation (4-4), the value $z'(C,R)$ could be added to both sides and the equation remains invariant. Therefore,

$$D(C,R) = |z(C,R)| \qquad (4\text{-}6)$$

After point irregularity check, grids are then searched for defects. The percentage of irregularity points within each grid is computed as its irregularity rates $\gamma_G(i)$ and $\gamma_D(i)$ (Eqs. (4-7) and (4-8)).

$$\gamma_G(i) = \frac{NG(i)}{CN*RN}, i = 1, \dots, M \qquad (4\text{-}7)$$

$$\gamma_D(i) = \frac{ND(i)}{CN*RN}, i = 1, \dots, M \qquad (4\text{-}8)$$

where $\gamma_G(i)$ and $\gamma_D(i)$ are the gradient irregular rate and distance irregular rate of the ith grid, respectively. $NG(i)$ and $ND(i)$ are the total number of irregularity points in grid i based on gradient check and distance check, respectively. CN and RN are the number of columns and rows selected for the grids, respectively, and M represents the total number of grids. If both the distance irregular and gradient irregular rates in a grid are larger than a predefined threshold, the grid is considered to contain defect. When high threshold for gradient irregularity rate is used, it means that almost all the points in a grid should have high gradients in order to be considered to contain a defect. Sometimes, a

defective area may have small areas with relatively flat surface. In this case, high threshold for gradient irregular rate will exclude the grids which contain small flat areas from one defective area. Hence, the selected threshold should be small enough to keep the integrity of the detective area in the detection and large enough to differentiate defects from intact area. Based on numerical experiment, threshold within the range of 0.3~0.8 is suitable for use and the value will only influence the selection of the grids on the defect boundary. In the example of this dissertation, the thresholds of both distance irregular and gradient irregular rates are chosen as 0.5. If only less than 1/16 of the grid area has scan points, the grid is ignored in defect detection.
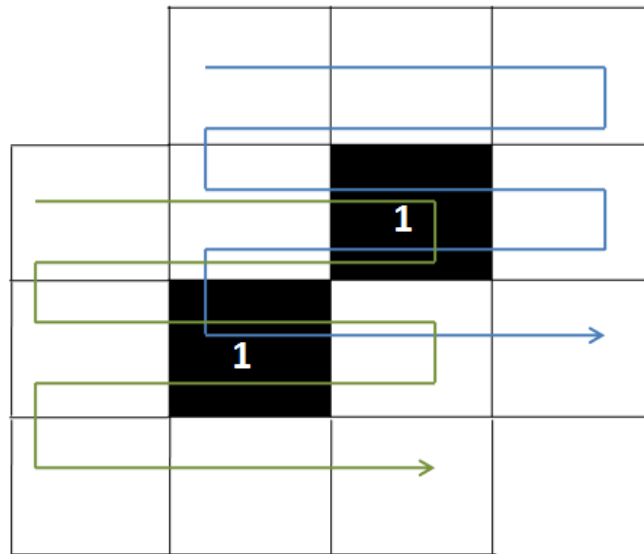
Figure 4-8 Omnidirectional grid search concept

Omni-directional search concept is introduced to detect and quantify the defective area (Figure 4-8). When one grid is classified as containing defect, a defect number is assigned to the grid and eight surrounding grids will be searched for defect, unless the

grid has already been assigned a defect number. If one of the eight grids is classified as containing defect, the same defect number is assigned to it and another omni-directional search is followed. This process is repeating until all the ramifications of all the surrounding grid of the original grid have been checked.

Grids with the same defect number are considered to belong to the same defective area. The volume loss of each defect area can then be computed as:

$$V_i = \sum_{j=1}^{M} (A_{ij} * \overline{D}_{ij} * r_{ij}), \ i = 1,..., N$$

(4-9)

where V_i represents the volume of i th defect area. A_{ij} is the area of the j th grid. $\overline{D}_{ij}$ and r_{ij} are the average point distance to reference plane and irregularity ratio of the j th grid. N is the total number of defects.

4.2.2.4 Damage detection for Bridge # 590147

As shown in Figure 4-3, the pile cap has three damaged locations. Since the three damaged parts are relatively large, the number of points in each gradient calculating interval used is $\alpha = 5$. Adjusting parameters $\beta_1 = 1.0$ and $\beta_2 = 1.8$ are also used. Two damage quantification techniques can be established either based on gradient (Eq. (4-3)) or distance (Eq. (4-4)) determinations. Figures 4-9 and 4-10 display the structure surface data based on distance and gradient calculations, separately. It is clear that both of these two methods can be used to identify the three defective parts. In the first case, distance change from the individual points to the reference plane is continuous. Hence, it is hard to define the threshold value to separate the defective areas from the rest of the surfaces. In the case that the select surface is not smooth enough, like the example in this section,

the upper part of the selected area will extrude a little bit. If a smaller adjusting parameter for distance ($\beta_2 = 1.7$) is used, the calculated defect area will contain part of the extruded area. Likewise a higher threshold value will result in smaller calculated defective area (Figure 4-11). Using gradient calculation, on the other hand, the surface gradient values at the edge of the defect would increase abruptly. Therefore, for damage identification, using gradient information is more efficient to detect the edge of defective area. The drawback using gradient calculation is that there may be flat areas inside the defects, whose gradient value is low, which will be assumed by the algorithm as undamaged area. Therefore, it is better to combine both two methods for the calculation. The point irregularity criterion is then changed to

$$G(C,R) > \beta_1 \times G_{ave}.or.D(C,R) > \beta_2 \times D_{ave}$$

(4-10)
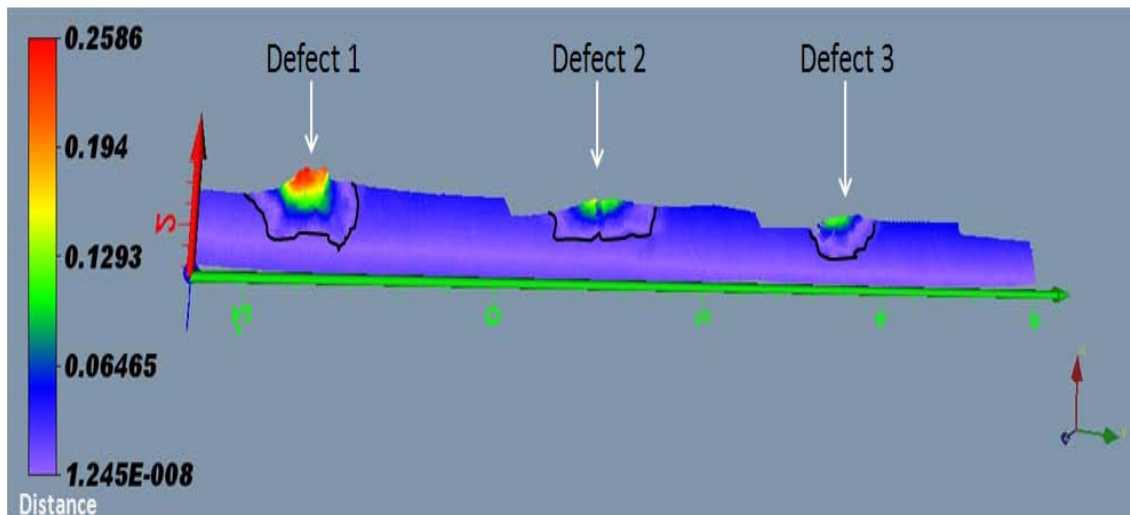
Figure 4-9 Defect position identification using distance data rendering
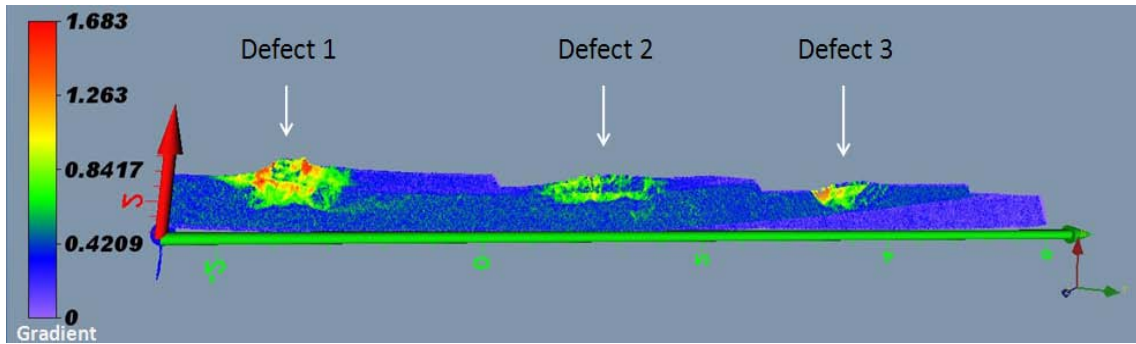
Figure 4-10 Defect position identification using gradient data rendering

In this dissertation, adjusting parameters are chosen as $\beta_1 = 1.0$ and $\beta_2 = 1.8$. Mass loss of defect area is then calculated based on distance information. Figure 4-12 shows the computed defective area based on the combination of both methods. The quantifications of the defects are given in Table 4-3. Due to symmetry, the second and third (from left to right) defective areas have almost the same sizes.
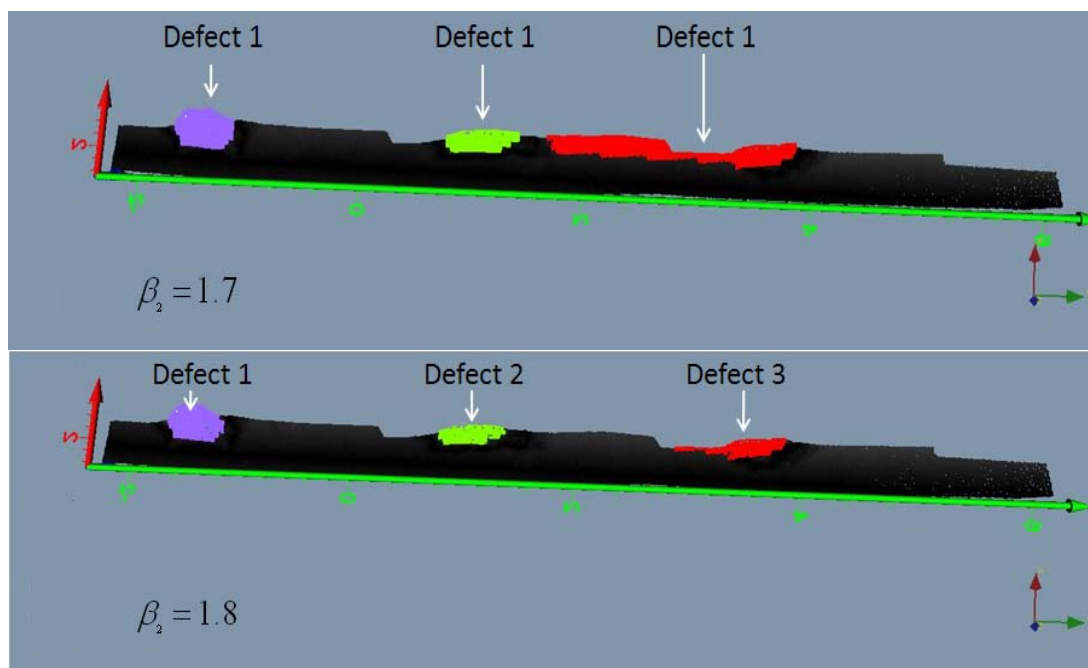
Figure 4-11 Defect calculations using distance value only ($\beta_2 = 1.7$ and 1.8 respectively)
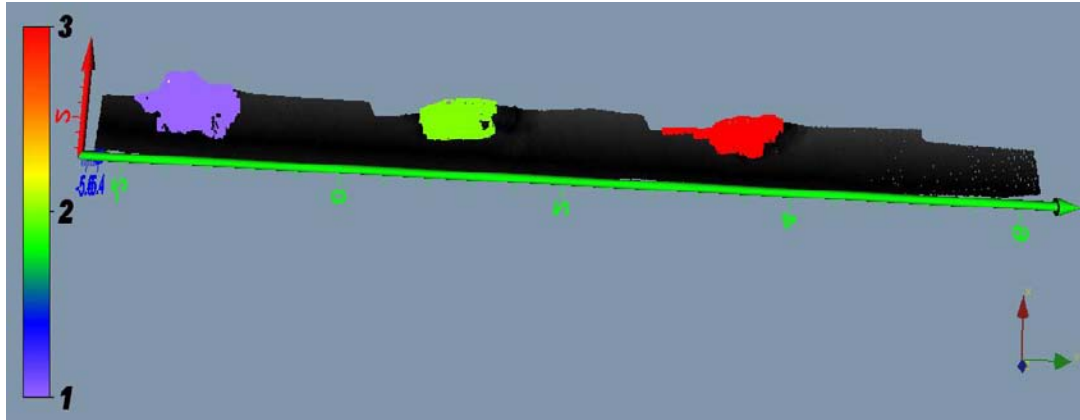
Figure 4-12 Defect calculation using both distance and gradient information

Table 4-3 Defect quantification

| Defect Number | Use Distance Only | | | | Use Distance & Gradient | |
| | $\beta_2 = 1.7$ | | $\beta_2 = 1.8$ | | | |
	Volume (m3)	Area (m2)	Volume (m3)	Area (m2)	Volume (m3)	Area (m2)
1	1.138E-2	9.716E-2	1.132E-2	9.547E-2	1.231E-2	1.191E-1
2	3.882E-3	5.985E-2	3.783E-3	5.696E-2	4.322E-3	7.042E-2
3	9.509E-3	2.021E-1	3.464E-3	5.600E-2	4.667E-3	8.589E-2

4.2.3 Failure Analysis for Bridge # 590147

From the image of the bridge substructure, it is obvious that there are considerable mass losses on the extended pile cap under three of the four bridge girders. Further study indicates that all three damages were observed on the right side of the girders. This is because the girders are settled in an angle about 60 degrees to the substructure, which brings larger shear stresses to the right side than the left side.

Table 4-4 Actual height of points on the girders

Girder Number	1	2	3	4
Left Side Height (m)	2.361	2.359	2.359	2.352
Right Side Height (m)	2.356	2.355	2.354	2.358
Difference (Left-right) (m)	0.005	0.004	0.005	-0.006

By exporting the coordinate values of the points from both sides of the girders (Figure 4-13), the average relative height for each side of the girders to the scanner can be obtained. The data in Table 4-4 shows that except for girder 4, all three girders with damages have settled with left side higher than the right side.
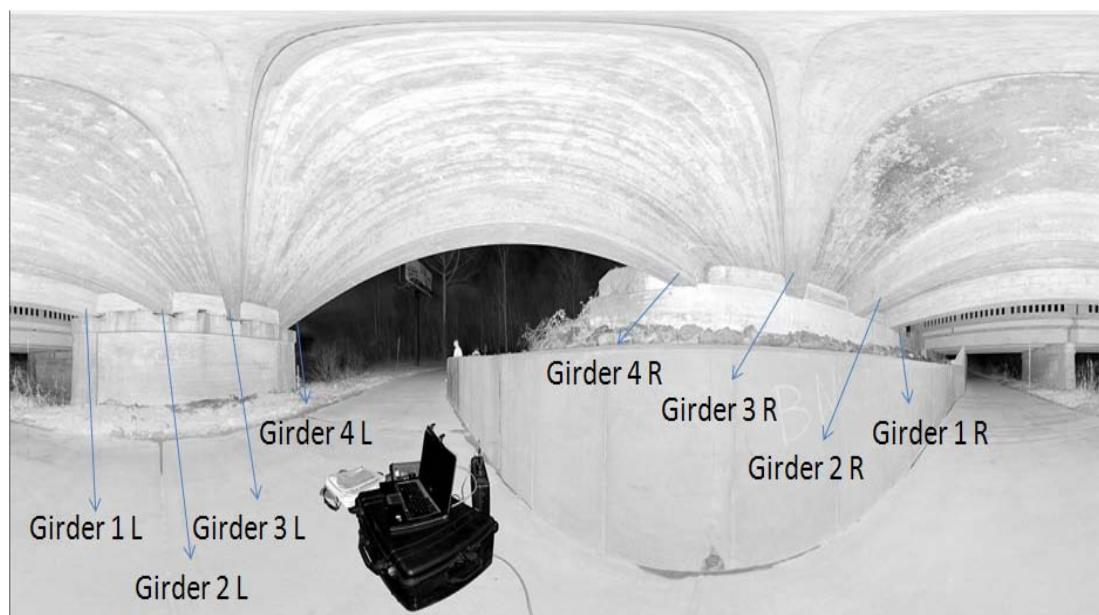
Figure 4-13 Point samples from both sides of the four girders

Figure 4-14 attempts to demonstrate three likely scenarios of damage causes. In the ideal case, if both sides of a girder are of the same height (Figure 4-14, case 1), the

weight of the bridge superstructure and traffic load will be distributed evenly at the contact area between the floor beam and the pier. However, if the pier is not even, the contact area will be reduced and results in concrete overstress at the contact points. The worst condition is case 3, where the height difference and bending effect will be added to increase the pressure on the edge of the pier. It is obvious that, girder 1, 2 and 3 have mass loss as a result of the elevation differential. Further analysis of the cause of the elevation differential is needed, which may be due to differential settlements. However, it is confident to conclude that even the slightest elevation differential can result in early distress of the concrete material, such as the presented bridge pile cap failures.
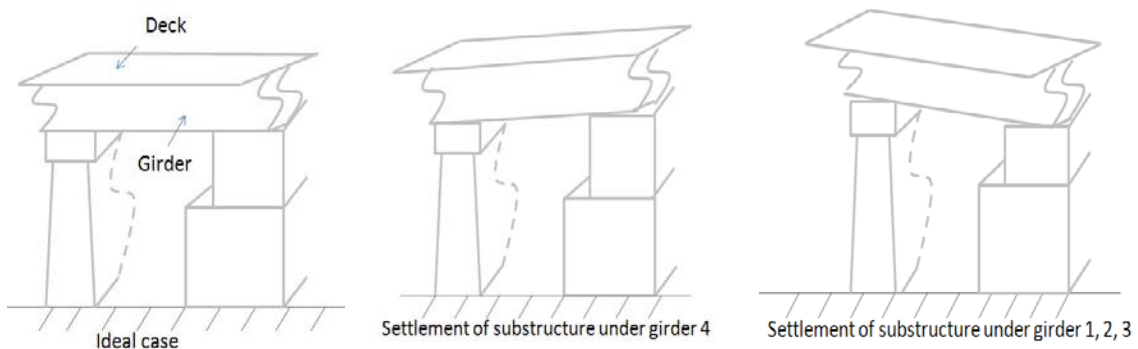
Figure 4-14 Three hypotheses of the different girder sitting scenarios causing pile cap distress

4.2.4 Defect detection for bridge # 640024

Reinforced concrete girder bridges are typical state highway bridges that are vulnerable to water and chloride attacks. These attacks will result in the corrosion of the inner reinforcement. The corrosion, if not detected, can gradually reduce the strength of the girder and volumetric expansions due to oxide formation will result in concrete delamination (Liu and Frangopol 2004). If the surface concrete cover of the bridge girder

is damaged, the steel reinforcement corrosion will be speed up. Many works have focused on predicting the deterioration rate of concrete bridges in order to schedule maintenance. Almost all the presented methods are based on the visual inspection results of bridge components combining with bridge inventory data (Stewart 2001; Zhao and Chen 2001; Sasmal and Ramanjaneyulu 2008). High accuracy quantitative records of damages are generally lack in these data sources. LiDAR data can provide quantifications to surface defects with high accuracy. Periodical measurements of the corrosion induced damage can help to update the deterioration rate prediction model and improve the prediction accuracy.

Figure 4-15 Bridge # 640024 in Wilmington, NC

One of the most difficult challenges in conducting a LiDAR scan of bridge superstructure is where bridges traverse a waterway. Bridge # 640024 on US-74 over Banks Channel was selected for testing using the laser scanner (Figure 4-15). The research team worked with the Division Bridge Engineer in the Wilmington area (New Hanover County) to test out the capability of providing a steady platform and keep it level in order to run a LiDAR scan. In this particular case, a boat that is used by NCDOT personnel for inspection and light maintenance work was provided to provide a platform on a bridge span. The experiment worked better than anticipated, with little unsteadiness in the 22 ft height. "The Boston Whaler" boat was secured to bridge piers on both ends of the boat. However, one of the factors that made this test successful was a relatively moderate current on the inland waterway on the day the test was run.

1	
Area (m²)	0.507
Volume (m³)	0.0285
2	
Area (m²)	6.62E-4
Volume (m³)	2.63E-5
3	
Area (m²)	2.13E-4
Volume (m³)	7.11E-6
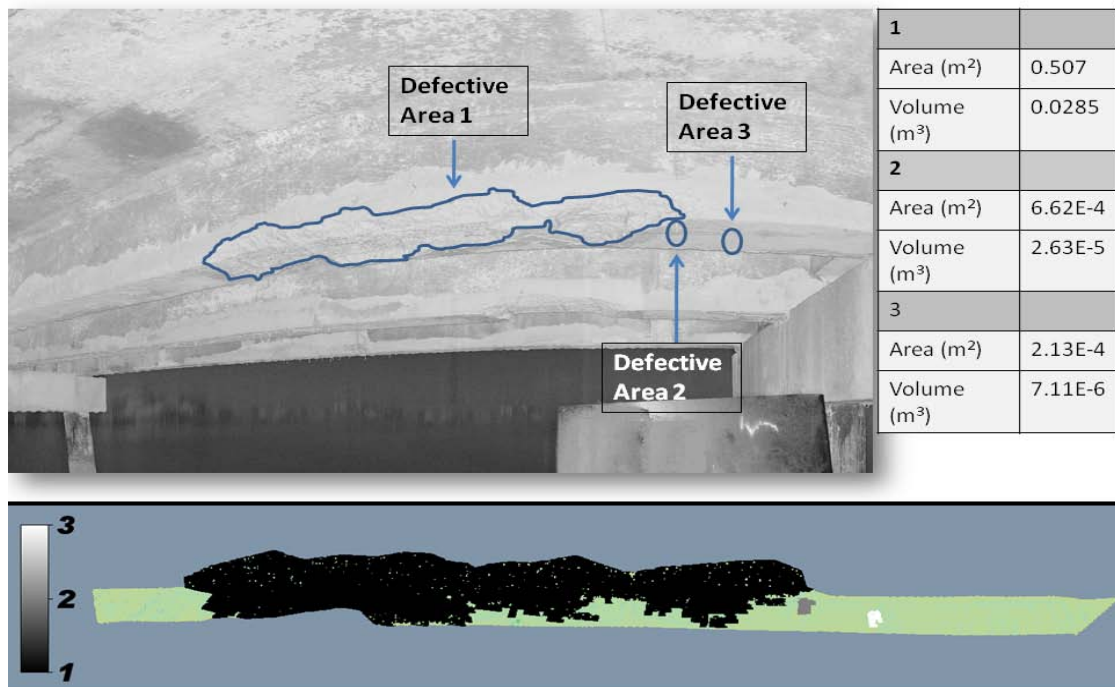
Figure 4-16 Detected defective areas of a girder under Bridge # 640024

Built in 1957, this concrete bridge has sixteen spans. Chipping and cracking can be found at the lower part of the piles. The pile caps also have cracks and spalls. The most damaged parts of the bridge are the reinforced concrete girders, many of which have cracks and spall areas. Exposed rebars can also be seen. Analysis using LiBE on part of a girder shows concrete spall damages with significant defective areas detected. Defective areas 2 and 3 are two minor irregularities resulted from the exposed ends of stirrups. The areas and volumes of the three defective areas are provided in the table on the top right corner of Figure 4-16. If this girder can be studied periodically, the mass loss rate, corrosion area and depth increasing rate can be determined. The data can then be used to update the deterioration rate prediction model or evaluate the efficiency of maintenance coatings.

4.3 Clearance measurement

4.3.1 Introduction

Collision damage to bridge superstructure is a common problem especially for bridges with low vertical clearance. Collision between vehicle and bridge can be life threatening for drivers and passengers. For example, the collapse of a pedestrian bridge over the Baltimore Beltway, Maryland, due to truck impact had killed one person and injured three others (Fu et al. 2004). Comparing to ships, which may weigh 5,000 tons (small ships) to over 70,000 tons (large ships), trucks with 36 tons weight limit in most states, are much lighter in comparison (Sivakumar 2007). From kinetic energy transfer, ship impact induced bridge damages should be much more severe than truck impact induced damages, even though ships may travel several times slower than trucks. Hence, most of the past researches about bridge collision damages were focused on ship impacts

(Pedersen et al. 1993; Consolazio and Cowan 2003; Wang et al. 2008). However, roadway vehicle collisions with bridges are more common than ship collisions and the impacts to roadway user safety and bridge structural deterioration cannot be ignored.

Study by Fu et al. (2004) showed that the recorded overheight accidents in Maryland have increased by 81% between 1995 and 2000, whereupon only 19% of the struck bridges have been repaired. Repair of truck-struck bridges can be costly: Structural damage of the 10th Street Bridge in Wilmington, DE, induced by a tractor trailer hitting, costs about $100,000 for repair (Dawson and Shenton 2005). Harik (1990) analyzed 114 bridge failures in the U.S. between 1951 and 1988 and found 15% of them were due to truck collisions.

While complete failure may occur, bridge strikes can result in damages with less severity including superstructure damage, exposure of rebar of the reinforced concrete component, spall on concrete component, deformation and tear of steel girder and nick under bridge deck (Horberry 2002). Exposure of rebar to the atmosphere can speed up the corrosion rate of the steel reinforcements. The generated rusts will affect the bond behavior between steel and concrete, and, with the expansion force induced by rusted rebar volume increase, further concrete cracking and spalling may occur. Spalls and nicks on concrete surface will increase the possibility of exposed rebar to moisture. Nicks on steel component may damage its coating and result in the development of corrosion pits (FHWA 2002). Another related issue is severe plastic deformation of steel component can increase the risk of fracture failures.

Vertical clearance has been recognized as an important bridge design parameter to reduce the possibility of collision damage (Baba and Ono 1987; Anon 1989; Dunker and

Rabbat 1990; Ramey et al. 1997; Thompson and Sobanjo 2003). Various strategies have been presented to reduce vehicle-bridge collisions or to reduce the damage level of vehicle collision to bridges. Horberry (2002) recommended revising bridge markings in order to urge driver vigilance before passing under a low clearance bridge. Energy dissipation systems such as different kind of bumpers, and other protection systems have been recommended and evaluated to reduce bridge collision damage (Qiao et al. 2004; Sharma et al. 2008; Wang et al. 2008). Georgia has elevated over 50 bridges to increase their clearance height in order to reduce the possibility of vehicle collision (Hite et al. 2006).

Clearance measurement is critical to the assessment of bridge clearance problems. To measure bridge clearance, Lefevre (2000) presented a prototype radar system that monitors water level under a bridge. Field tests indicated the accuracy of this method reaching 0.009m. Fuchs et al. (2004 a&b) described several applications of laser scan on bridges, notably the use in bridge static load tests. This section introduces an automatic bridge clearance measurement method based on terrestrial Lidar, which is part of a LiBE system. The algorithm for bridge clearance calculation includes a search-and-match procedure. The system outcome can provide bridge vertical clearance information at multiple points under a bridge with accuracy in the order of millimeters. The display of clearance change over the entire bridge coverage area can be useful to assess damages and help engineers to device bridge improvement planning. Temporal analysis of clearance changes can also be performed for monitoring bridge abutment settlement or the increase in road pavement thickness. Three low clearance bridges with different collision damage level and a non low clearance bridge, in Mecklenburg County, North

Carolina, are selected for analysis using the presented methods as application examples at the end of the section. The FORTRAN source code for clearance measurement is given in APPENDIX F.

4.3.2 LiBE Clearance Measurement

For the selected bridges described in this section, a typical full scan collects about 8000 points per vertical cycle (320 degree) and 9000 points per horizontal cycle (360 degree). Due to the scanner underpan blocking out part of the light path, only data from a 320 degree vertical scan are recorded. The coordinate values of each point are stored with a column number and a row number assigned to indicate which horizontal and vertical cycles, the point belongs to. The origin of the coordinate system for all the points is often located at the center of the scanner head.

A search-and-match procedure is implemented in the proposed bridge clearance measurement program, where a point on the surface under a bridge structure is assumed to share vertical cycle number with the corresponding point on the ground in the same vertical line. However, such assumption can be difficult to measure accurately when geometrical mismatch occurs. Figure 4-17 demonstrates the possible error calculation that may result based on this assumption. Point 2 is the assumed corresponding point on the ground sharing the same vertical line with Point 1; hence, Point 1 and Point 2 are in the same vertical scan cycle. Since there are totally 9000 vertical cycles for a full scan, the maximum azimuth angle, a, between the two vertical planes, which Point 1 and Point 2 belong to, is equal to $2 * \pi/9000$. Hence the maximum horizontal deviation between Point 1 and Point 2 is

$$D1 = 2 * D * \tan(a/2) \tag{4-11}$$

where D is the horizontal distance between the scanner and the point of interest on the deck. Therefore for a distance of 25 m ($D=25$ m), the maximum horizontal difference between Point 1 and Point 2 is 0.0087 m. The accuracy of the scanner is determined to be 0.0030 m at 25 m distance.
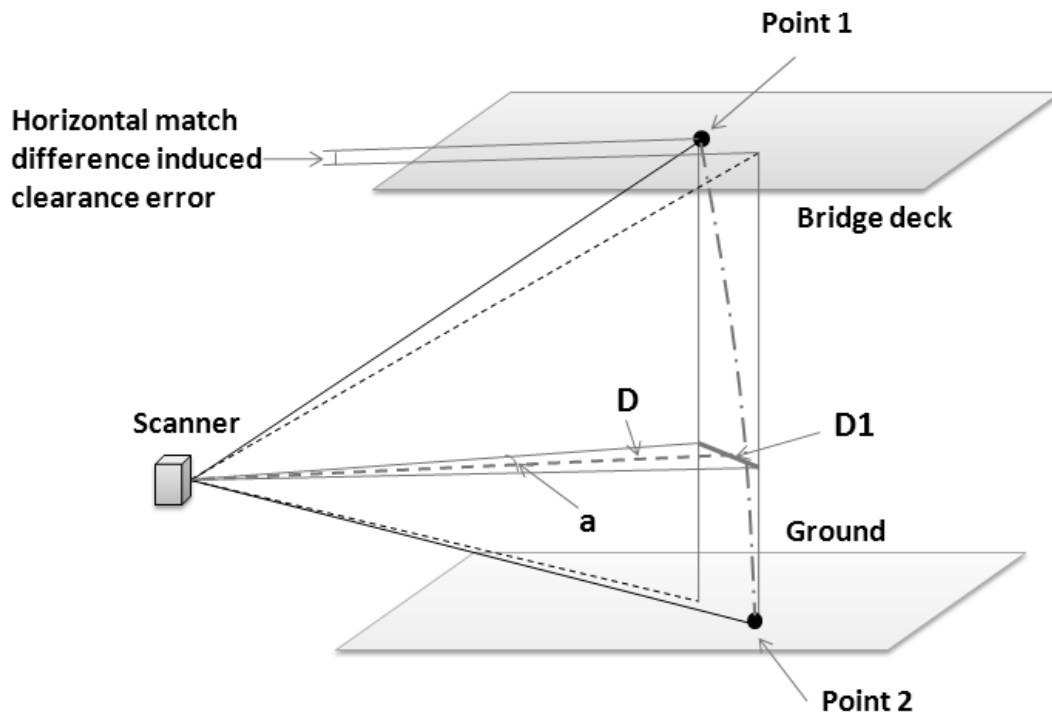
Figure 4-17 Clearance measurement error

Figure 4-18 gives the flow chart of the clearance measurement algorithm. First, the point cloud of bridge deck surface and ground surface are read separately. The ground surface is selected as the basis for the clearance measurement and display. Each point on the ground surface is searched from the deck surface point cloud to find the corresponding point along the same vertical line. In Figure 4-18, StartG_C and StartG_R represent the starting column and row numbers of the point cloud on the ground surface;

EndG_C and EndG_R represent the ending column and row numbers; and StartD_C and EndD_C are the starting and ending column numbers of the point cloud under the deck surface, respectively. The search for the matched pair for each point on the ground started from the end column of the points on the bridge deck, which means that the searching is to find the point with the lowest elevations among the points that share the same X and Y coordinate values. Hence, for the part of a girder surface that is perpendicular to the horizontal plane, only the points on the lowest boundary of the surface are measured. To check whether point (CG, RG) and point (CD, RG) are along the same vertical line, the following criterion is used:

$$h1 \leq 2 * \pi * \frac{Dd}{9000} \qquad (4\text{-}12)$$

where $h1 = \sqrt{(X(CG, RG) - X(CD, RG))^2 + (Y(CG, RG) - Y(CD, RG))^2}$

$$Dd = \sqrt{(X(CD, RG))^2 + (Y(CD, RG))^2 + (Z(CD, RG))^2}$$

and X(CD, RG), Y(CD, RG) and Z(CD, RG) are the coordinate values of point (CD, RG) on the deck surface. $h1$ is the horizontal distance between point (CG, RG) on the ground and point (CD, RG) on the deck surface. Dd is the distance between the scanner and the object point on the deck surface.

Since the scanner has been calibrated before each scan, only the Z coordinate values are needed to measure relative height of the target point to the scanner. Therefore, vertical distance, Cle, between point (CD, RG) and point (CG, RG) can be calculated as

$$Cle = Z(CD, RG) - Z(CG, RG) \qquad (4\text{-}13)$$

After searching all the points on the ground surface, the bridge clearance at each valid ground point can be measured using Eq. (4-13).
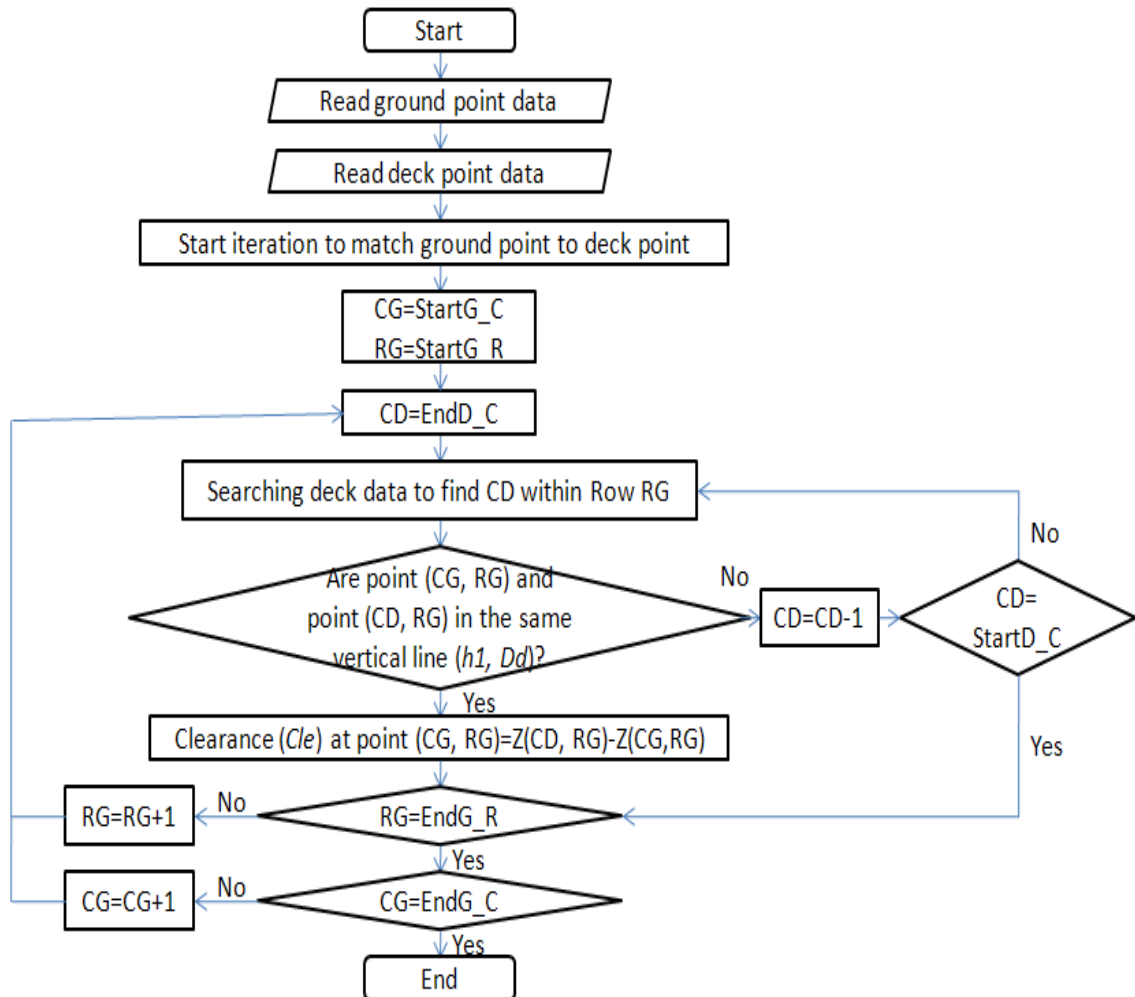
Figure 4-18 Flow chart of clearance measurement program

4.3.3 Bridge Clearance Status in Mecklenburg County, NC

AASHTO (1994) recommended the minimum clearance design requirement for bridges over freeways as 4.88m and recommended an extra 0.15 m of clearance for future resurfacing. Most of the states in the U.S. use a design clearance of 5.03 m for bridges on the national network (Fu 2004; Fuchs et al. 2004). NCDOT sets the design requirement for bridges over interstates and freeways to be 5.03 m, 4.57 m for over local roads bridges and 7.01 m for over rail road bridges, respectively. The clearances also include

0.15 m of clearance of future resurfacing and another 0.15 m for "the flexibility necessary in the coordination of roadway grades with final superstructure depths" (NCDOT 2000). For existing bridges, NCDOT requires a minimum vertical clearance of 4.88 m for over interstate highway bridges and 4.27 m for others.

 States also have their own vehicle height limitations. According to Fu's study (2004), 65% of the states used a limitation of 4.10 m and other states allowed up to 4.40 m for vehicle heights. However, such regulations are often violated. For example, the overheight vehicle detectors that were set up at the West Friendship Weight Station and other stations in Baltimore, MD, have detected vehicle heights reaching 4.50 m between May to July 2001 (Fu et al. 2004).

Public bridges in the Charlotte-Mecklenburg area are maintained both by NCDOT and Charlotte DOT (CDOT). Among the 300 bridges that NCDOT maintained, about 180 bridges are over roadways. Only five (approximately 3%) of the over roadway bridges have minimum vertical clearances under 4.60 m. Two of the five bridges have either collision damage or scrapes under bridge deck. For CDOT maintained eighty bridges, 22 of them are over roadway bridges and thirteen (59%) of them are with the vertical clearance less than 4.60 m, including one closed bridge and one over a parking lot. Ten of the thirteen bridges have either collision damage or scrapes under bridge deck. Although none of the damages have indicated the potential of causing structural failures, they do speed up the deterioration of the structures through concrete spalls, exposure of rebar, deformation of steel bridge component and removal of steel coating. For bridges with minimum vertical clearance higher than 4.60 m, fewer damages are found.

Table 4-5 Selected features of the four studied bridges

Bridge No.		590700	590702	590704	590511
Type		Steel girder concrete deck	Steel girder concrete deck	Concrete girders	Steel
ADT		30600	4800	5100	26000
Percentage of truck		7%	7%	7%	12%
System		Primary	Urban	Urban	Primary
Min clearance	Inventory	4.06m	4.24m	3.76m	4.75m
	LiBE	4.11m	4.25m	3.76m	4.98m*
Damage		Deformation of bracing, scrapes	Concrete spalling, scrapes	Rebar exposing, palling, scrapes	No obvious damage

* For Bridge # 590512, only one span of the bridge has been studied.

4.3.4 Examples

In our study, over 20 bridges in Charlotte-Mecklenburg area have been scanned using a terrestrial LiDAR scanner. In this section, three specific maintained bridges with low clearances studied using LiBE clearance measurement technique, are presented. They are Bridge # 590700, 590702 and 590704. These bridges are all over-roadway railroad bridges built in 1996. They have different structure types, average daily traffics (ADTs), as well as minimum vertical clearances, which are all below the design limits of NCDOT. The photos and clearance plots from LiBE calculations of these bridges are given in Figure 4-19~29. Figure 4-19 and left part of Figure 4-22 are taken from the Lidar Scan images. Figures 4-21, 4-25, 4-26, and 4-29 are the clearance plots generated from LiBE clearance measurement results. Figure 4-20, right part of Figure 4-22, 4-27 and 4-28 are digital photos of corresponding bridges. An overpass Bridge # 590511 without clearance issue is also presented for comparison. Figure 4-32 is the image of the bridge superstructure and Figure 4-33 is its clearance plot. Table 4-5 documents the minimum clearance values from both clearance plots and inventory records for the four bridges.
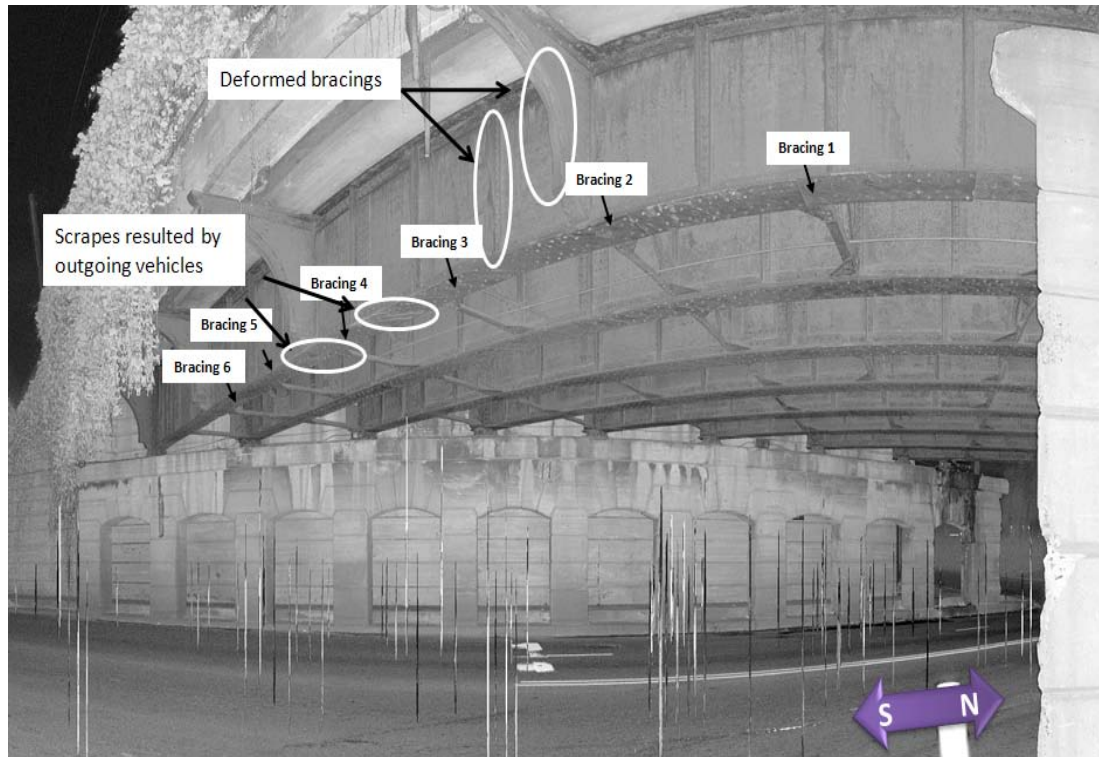
Figure 4-19 Bridge # 590700 (laser scan image, looking north)

Figure 4-20 Bridge # 590700 (digital photo, looking north 07/14/09)

The LiDAR scan data for bridges in service will include noises brought about by moving vehicles. For a typical bridge scan, it may take about 5 to 10 minutes for the scanner head to rotate 360 degree horizontally to finish a full scan. The passing vehicles have much faster speeds than the scanner can scan all the part of their body horizontally, although its vertical point collection speed is fast enough to finish a vertical scan cycle before the vehicle vanished in its field of sight. Therefore in the final scan data, only vertical lines are recorded instead of the whole body of the passing vehicles. These noises will block the scanner's view to certain parts of the structure surface and also induced miscalculations in clearance. As a result, vertical lines above the pavement as shown in Figure 4-19 and Figure 4-22 are the outcomes of passing vehicles during scanning.
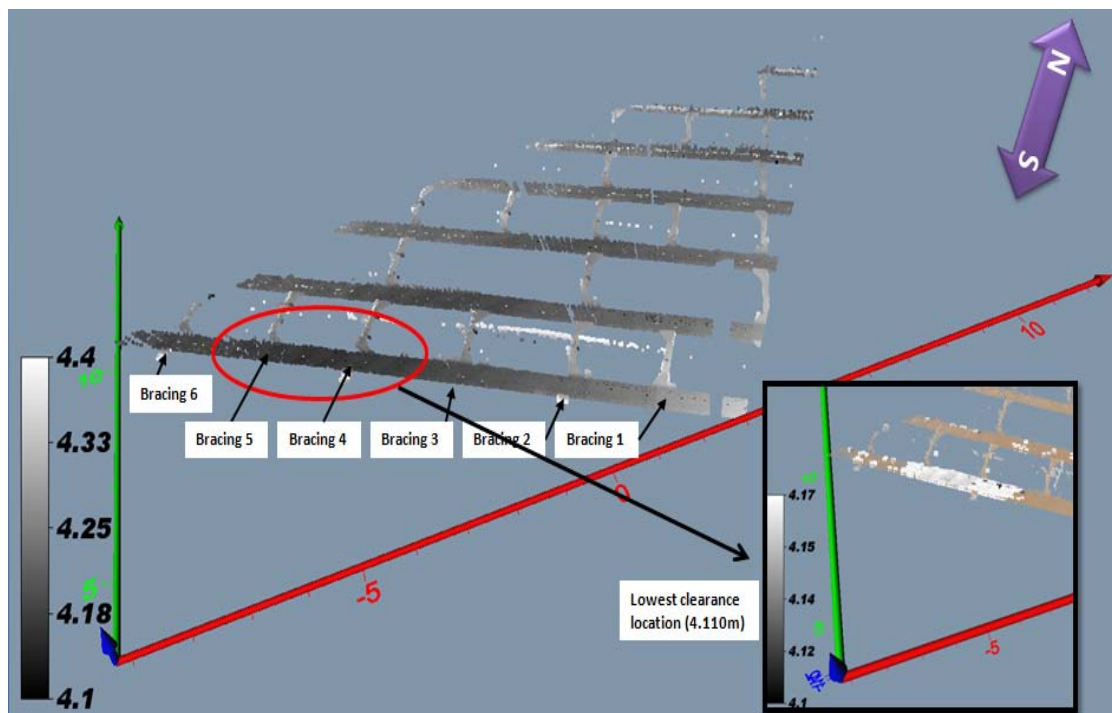
Figure 4-21 Vertical clearance plot of Bridge # 590700

When measuring the minimum vertical clearance of bridges using LiDAR data, the influences of these noises need to be eliminated. First, the data are filtered with reasonable thresholds. The false clearance points may still exits but will be much smaller in size. An array Cl with dimension n ($20 \leq n \leq 100$) is then created to store the smallest clearance values. These clearance data are sorted out with the largest values stored in $Cl(1)$ and the smallest values in $Cl(n)$. Clearance criterion is identified as:

$$Cl(i + 10) - Cl(i) < ac, \ i + 10 \leq n \tag{4-14}$$

where ac is the given accuracy, typically in the range of 0.001~0.05. If the ith clearance data satisfies the criteria in Eq. (4-14), the minimum clearance of a bridge is equal to $Cl(i)$.

Figure 4-22 Laser scan image of Bridge # 590702 (looking west)

Figure 4-23 Digital photo (07/14/09) of Bridge # 590702 (looking west)

Figure 4-21, 4-25, 4-26, and 4-29, are clearance plots of the three low clearance bridges from the scan results. The plots also explicitly display the minimum vertical clearance locations (circled). Figure 4-21 shows the minimum vertical clearance location in an enlarged plot, which is located near the fourth bracing. Figure 4-29 also shows the enlarged minimum clearance location. Instead of showing the location within the scan result for Bridge # 590702, a separate Figure 4-26 is included.

Figure 4-24 Digital photo of Bridge # 590702 (looking east 07/14/09)
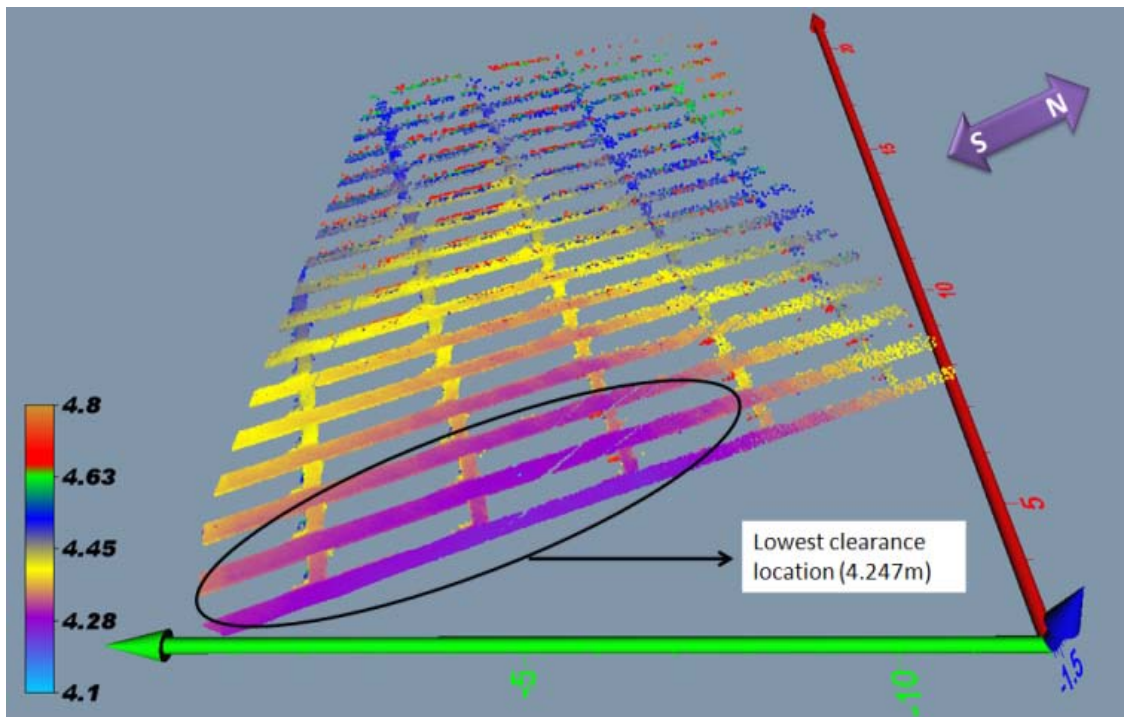
Figure 4-25 Vertical clearance plot of Bridge # 590702
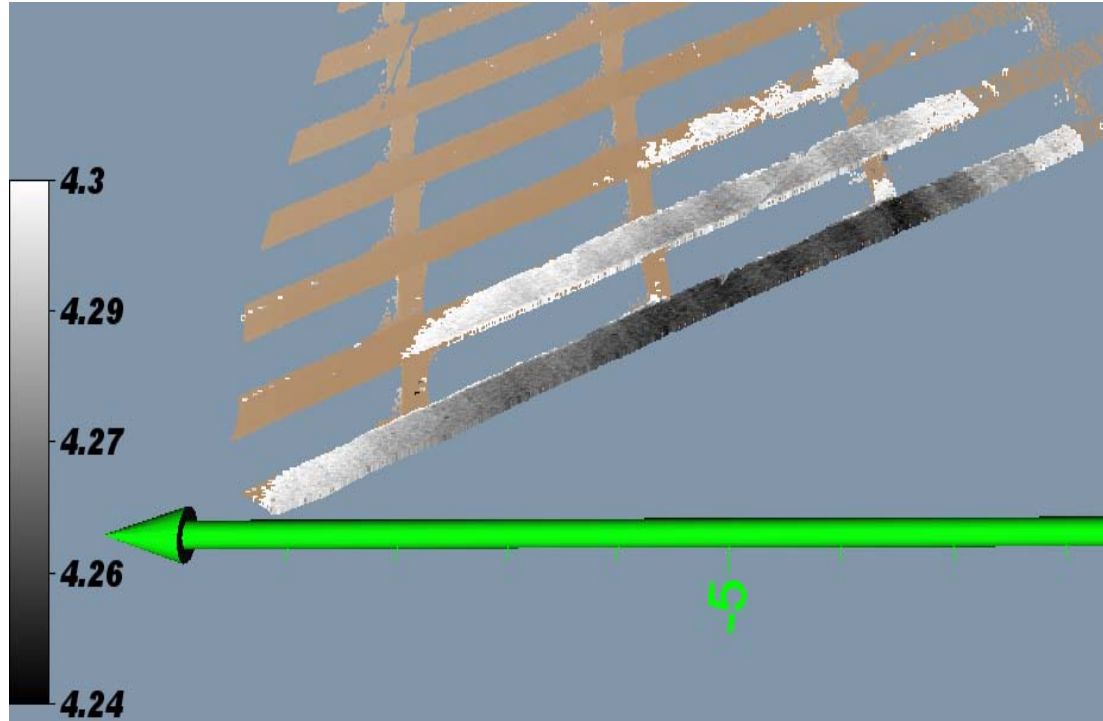
Figure 4-26 Zoom-in view for the lowest clearance locations of Bridge # 590702

Out of the three low clearance bridges, Bridge # 590700 has the highest ADT. Both sides of the bridge have observed steel bracings deformations (circled in Figure 4-19 and Figure 4-31). The clearance plot shown in Figure 4-21 is based on the LiDAR scan at the south side of the bridge. It indicates that the minimum vertical clearance area of this bridge measured is located on the first girder (around bracings 4 and 5). Scrapes on bridge girder can be found at this area. From the locations of these scrapes it can be concluded that they are generated by south travelling vehicles. These scrapes vanished under the second girder, meaning that the clearance increases from the south side to the north side around that location.

With the highest minimum vertical clearance and lowest ADT, Bridge # 590702 has the least damage by vehicle collisions among the three low clearance bridges. Two

concrete loss areas (circled) on the first girder and scrapes under several girders at the east side of the bridge can be seen in the bridge picture (Figure 4-22). From its clearance plot (Figure 4-25), it can also be noticed that the clearance of the bridge increased from the east side to the west side. This explained the vanishing of the nicks on subsequent girders on the east side. The field inspection of the bridge also showed that there was no obvious collision damage on the west side of the bridge (Figure 4-24). The minimum vertical clearance location is between bracing 1 and bracing 4 under the first three girders near the south part of the bridge.

Figure 4-27 Bridge # 590704 (looking south 07/14/09)

Figure 4-28 Bridge # 590704 (looking north 07/14/09)

Bridge # 590704 has the lowest clearance among these three bridges (Table 4-5) and has been damaged mostly by vehicle impacts, even though the ADT of this bridge is almost equal to one sixth of that of Bridge # 590700. The deteriorated state of bridge included exposed steel reinforcement near the center of the deck on the north side of the bridge. The clearance plot in Figure 4-29 shows the highest clearance under the east corner of the bridge and the image in Figure 4-27 also shows less collision damage in that area. At the south side of the bridge, there is also fewer collision induced spallings (Figure 4-28). One possible reason is that this area is near the corner of the roadway; therefore, experienced less traffic. The clearance plot for Bridge # 590704 indicated that the clearance increased from the north side to the south side.
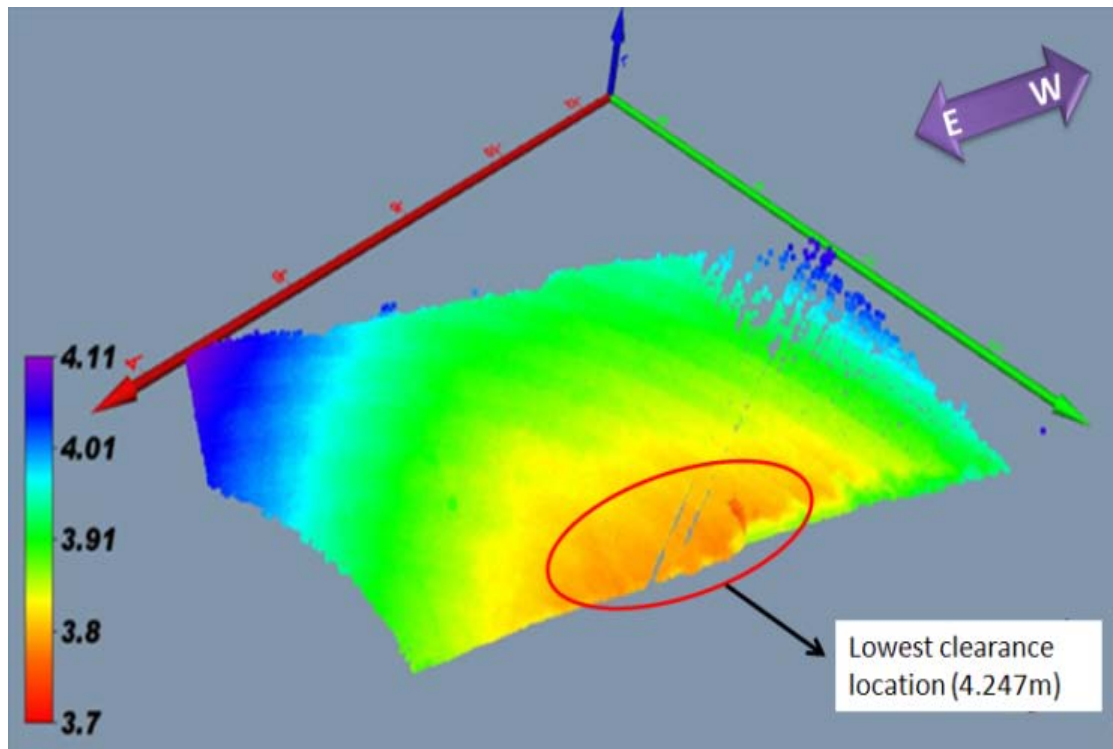
Figure 4-29 Vertical clearance plot of Bridge # 590704 (looking south)
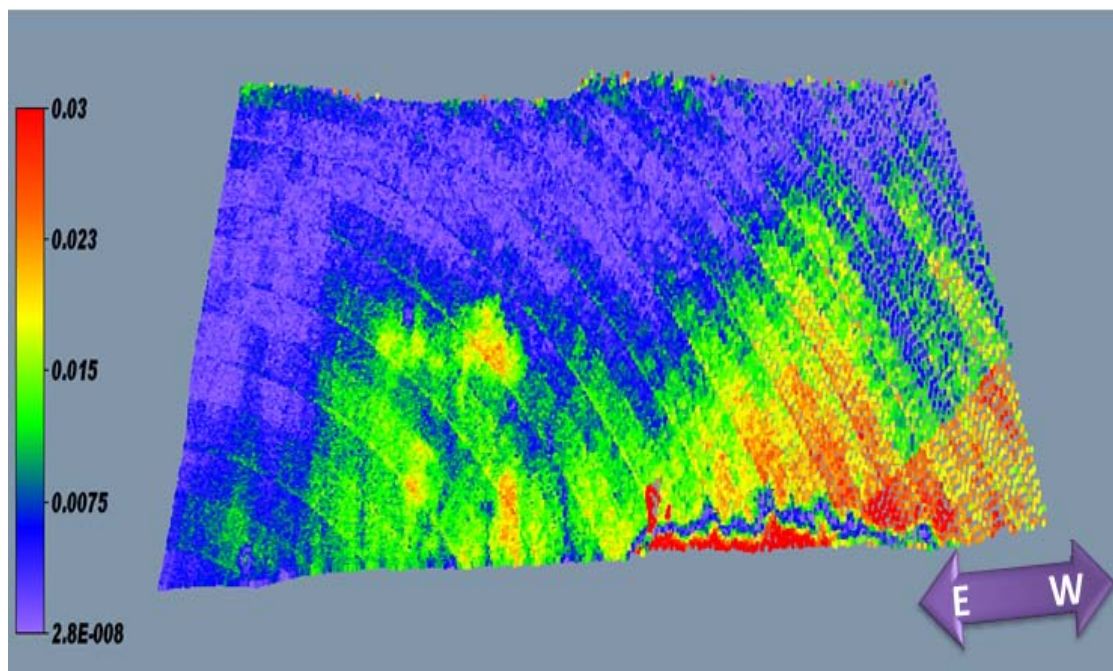
Figure 4-30 Deck surface points rendering (with the distances to the ideal deck plane colored) for Bridge # 590704

Figure 4-30 shows the point cloud rendering of the surface under the 590704 bridge deck. The image shows that the deck surface is smooth except the areas with collision scrapes. The maximum smoothness difference underneath the bridge is about 0.03 m. However, the clearance difference (measured to the pavement surface) of the bridge surface points can reach up to 0.4 m. It is concluded that the pavement height here is the main reason that causes the difference of clearance for this bridge. It is suggested that, flattening the pavement or reducing the pavement height under the bridge as a way to mitigate low clearance induced collision damages.

Figure 4-31 Height of collision damage location for Bridge # 590700

Finally, Figure 4-33 shows the clearance of Bridge # 590511 which increased from the front girder to the inside girders. With the minimum clearance around 4.98 m, which is 0.23 m higher than the design requirement, no obvious collision damage can be found on the girders of this bridge.

Figure 4-32 Superstructure of Bridge # 590511
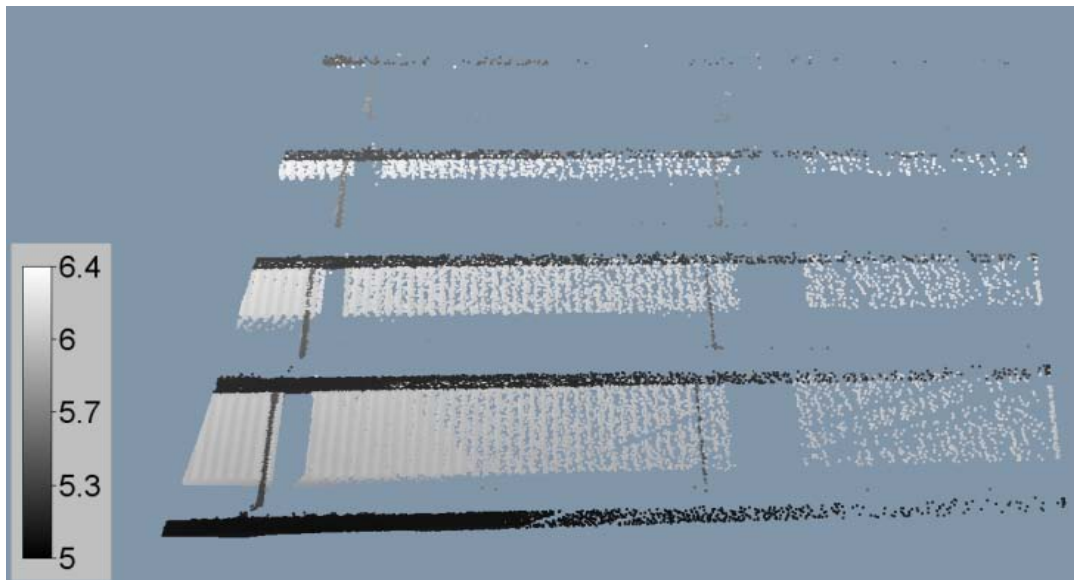
Figure 4-33 Vertical clearance plot of Bridge # 590511

4.3.5 Brief summary

This section discussed the issues that induced by collisions between over height vehicles and low clearance bridges. An automatic bridge clearance measurement tool based on 3D Lidar data is introduced. The collision damage levels of the reported bridges from Mecklenburg, NC, indicate that traffic volume under a bridge is not as significant an issue as allowable bridge clearance. For example, the ADT for Bridge # 590704 is much less than that for Bridge # 590700, yet it has the highest damage scenario for all three low clearance bridges. On the other hand the ADTs under Bridge # 590702 and Bridge # 590704 are almost the same, but Bridge # 590704 obviously has encountered a much larger number of collisions keep than Bridge # 590702.

The case of Bridge # 590704 indicated that the increasing of the bridge clearance to 4.1 m (clearance at the west corner of the bridge in Figure 4-27) can reduce the probability of collisions between the bridge and passing vehicles. The damage traces of Bridge # 590702 show that few vehicle collisions have been taken place for the bridge with minimum clearance higher than 4.5 m (clearance value on the west side of the bridge).

The deformation of steel bracing (circled in Figure 4-19 and Figure 4-31) of Bridge # 590700 shows that the bridge has been hit by vehicles higher than 4.3 m. Since the vehicles cannot pass under the bridge, the bridge through deformation absorbed the energy due to impact. These kind of impacts can threaten the integrity of the bridge and the injure rate of drivers and passengers are high. On the north side of the bridge, a bracing was hit so hard that the rivet heads at that location have been sheared off (Figure 4-31, gray image taken in October 2008). By measuring the heights of the damage

locations from the LiDAR data, the maximum height of the vehicles that caused the damages are estimated to be more than 5.0 m high. Although Bridge # 590700 is over a local road, the clearance of 4.6 m is obviously not enough for it to eliminate collision damage caused by overheight vehicles.

CHAPTER 5: THE APPLICATION OF TERRESTRIAL LIDAR IN BRIDGE STATIC
LOAD TESTING

5.1 Introduction

Bridges are important civil infrastructures that directly relate to the quality of life. Due to the large size of highway bridges, uncertainties exist in the design, material preparation, site condition estimation, and construction control processes. All of these make the prediction of structure performance difficult to achieve. Load testing of bridges has been recognized as a practical method to determine the condition of a bridge (Frýba and Pirner 2001; Orban and Gutermann 2009). Abnormal behaviors of a bridge under load test are a sign for the needs for repair or for more frequent inspections and maintenance works. Swiss code recommended load testing for all bridges over 20 m (Hassan et al. 1995). Czech and Slovak Republics standardized load testing in situ since 1968 (Frýba and Pirner 2001) and requires static load testing for bridges over 18 m. In the U.S., the National Cooperative Highway Research Program (NCHRP) has developed the "*Manual for Bridge Rating through Load Testing*" to evaluate bridge load carrying capacity through load testing (NCHRP 1998).

Load testing results can be used for bridge structure health monitoring, load carrying capacity evaluation (Faber et al. 2000), crack control (Ryu et al. 2007), fatigue failure study (Idriss et al. 1995; Klowak et al. 2006), diagnostics (Nowak et al. 2000), damage detection (Wang et al. 1997), and numerical model creation and updating (Alaylioglu and Alaylioglu 1997; Ataei et al. 2005). Bridges under given static load are often measured for displacement, stress, or strain at selected points using sensors. Strain gauges and displacement transducers are the common tools for strain and displacement measurements (Chan 2001; Klowak and Mufti. 2009). Numerical models may be built and analyzed to compare with test results and to predict the structural condition or performance. Dynamic responses of bridges are often thought to be more realistic in simulating vehicular traffic induced bridge vibration and have been studied extensively for bridge monitoring (Senthilvasan et al. 2002; Gentile and Gallino 2008). Devices such as accelerometer, geophone, cable extension transducer, laser doppler vibrometer, can provide acceleration and velocity information for dynamic analysis (Nassif et al. 2005). However, other than the laser doppler vibrometer, most of the sensors mentioned require direct placement on the bridge, which can be challenging considering the sheer size of the structure.

Terrestrial 3D LiDAR Scanner is a type of remote sensing system that can automatically acquire 3D surface information of the object without physical contact. The relative position of the object surface is achieved by measuring the time the emitted LiDAR light signal travels between the scanner and the object. With a single full scan, all the surrounding surface position information of the scanner can be measured and recorded with accuracy in millimeter range. Fuchs (2004 a&b) first introduced LiDAR

scanner as a method for displacement measurement in bridge static load testing. By comparing the position change of the scan points at each measurement location, deflection of bridge component can be measured. The scanner they used can collect 5×5 grid of points for each scan location. To monitor multiple lines of a bridge during a load test, the scanner needs to be manually placed at multiple locations. The accuracy of this measurement method was about ±0.76mm. Comparing to contact methods for load testing, non-contact methods are more sensitive to noise and they often have lower accuracy. However, non-contact methods are not restricted to the accessibility of the bridge and their measurements eliminate the possible damage to the bridge components through instrument installation. In this dissertation, 3D scanner is used, which can provide the deformation information over a wide area of the bridge surface without changing the scanner position.

In this section, calculations of displacement and strain information are introduced using 3D LiDAR scan results. The developed technique is part of a LiBE system that fully utilized 3D LiDAR scanner for bridge condition monitoring. With the help of 3D data rendering tools, the displacement and strain results of the entire measured surface can be calculated. Therefore, it is easy to identify the deformation pattern and critical positions. A High Performance Steel (HPS) bridge on Langtree Rd. over Interstate I-77 in Iredell County near Charlotte, NC was selected and tested as an example to demonstrate the application of this method. The results prove the potential of using LiDAR scanner in bridge load testing.

5.2 Bridge and load testing description

The bridge studied is a skewed hybrid HPS bridge located on SR1102 over I-77 in Iredell County (TIP I-4411) (Figure 5-1 and Figure 5-2). The bridge consists of two 46 m spans with cast-in-place concrete decking. The welded flanges of the plate girders in high moment areas are made of HPS100W steel (689 N/mm^2) whereas other segments and incidental steel members consist of 345 N/mm^2 and 483 N/mm^2 steel. The length between the two abutments is around 90m and the width of the bridge is around 26 m. The use of hybrid HPS girder systems in bridges is gaining greater popularity and is still a rather new construction as an alternative bridge material in the State of North Carolina. With limited case study experiences, there is a need to evaluate and accurately predict the behavior of such girders under various loading conditions.

High strength, quenched and tempered (Q&T) steels with 689 N/mm^2 yield strength had been available since the 1960s, originally sold under the trademark T-1 Steel, as developed by U.S. Steel (Wasserman and Pate 2000). Historically, research and development efforts were begun in the 1990s as initiated by the FHWA, American iron and Steel Institute (AISI), and the United States Navy to improve the performance of high strength steel (Felkel et al. 2007).

High Performance Steel is comparable to the traditional bridge steels of the American Society for Testing and Materials (ASTM) A709 designation, but with several significant enhancements (ASTM 2000). First, all HPS members are weathering steel grades, but with slightly enhanced weathering characteristics, i.e. a minimum atmospheric corrosion resistance of 6.5 as measured in accordance with ASTM G101 ("Standard Guide for Estimating the Atmospheric Corrosion Resistance of Low-Alloy

Steels" 1997), as opposed to 6.0 for traditional weathering steels. The significance of this

heightened feature of durability cannot be overstated as its implications are toward

reducing life cycle costs. Another benefit of using HPS members is that they exhibit

greater weldability in the higher-strength grades and greater toughness for all potential

grades. These advances were achieved through lower levels of carbon, and certain other

elements, in conjunction with advanced steel-making practices (Mertz 2001).

Figure 5-1 Arial photo of the Hybride HPS Bridge on Langtree Rd (SR1102)

Figure 5-2 Digital photo of the Hybride HPS Bridge on Langtree Rd (SR1102) over I-77

Figure 5-3 Trucks used for bridge load testing

To load test the bridge, two heavy trucks were used and were placed at designed locations on the bridge (Figure 5-3). The weight of Truck A was 25, 237 kg and the weight of Truck B was 24, 865kg. The length of each truck is around 8.0m and the width is around 2.9 m. The distance between the center of the front axle and the center of the

rear axle is 6.2 m and the distance between the outer edges of the each pair of rear axles is 2.5 m. Three loading cases have been carried out as displayed in Figure 5-4. Without changing the position and settings of the scanner, the bridge has been scanned before and after applying the truck loads.

The static load tests of the bridge were performed shortly after bridge construction. Since I-77 is a heavy traffic route, traffic control for strain gage placement is not allowed. The physical constraints inspired the use of 3D LiDAR scanner for static load deflection measurement. The load test was conducted prior to the completion of the second span, hence, only the first span were tested and the results are reported in this section. The FORTRAN source code for displacement measurement is given in APPENDIX G.
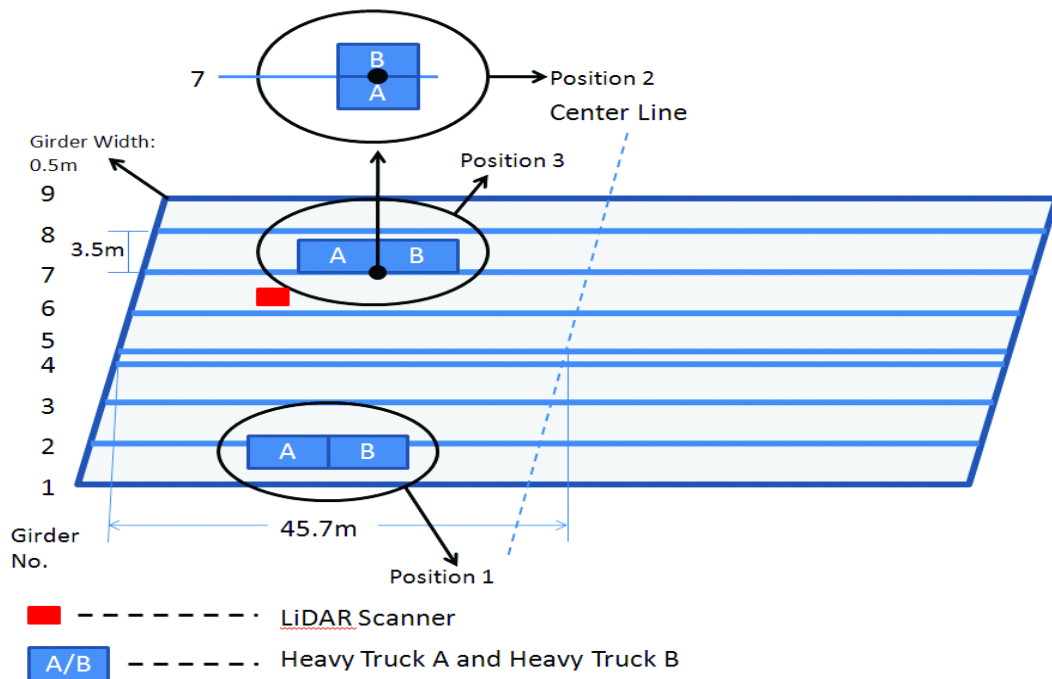
Figure 5-4 Arrangement of girders and the locations of trucks and the scanner

5.3 Automatic displacement measurement using LiDAR data

The LiDAR scanner is placed under a bridge structure, since there was less noise induced by traffic to the underside of a structure. The scanner in this study was placed under one side of the bridge off the road between girder six and girder seven (Figure 5-2). The dimensions of the bridge components can be calculated using the point coordinates. The point coordinates can be obtained easily from the plan view of the scan. Figure 5-3 is the example of the displacement measurements based on point coordinates. In this example, the two trucks were parked on the other side of the bridge other than that shown in Figure 5-3. The geometrical information can help create numerical models for the bridge or can help validate the geometry of the constructed structure.

Typically, one would assure that the deformation at a particular location on the bridge can be determined easily by comparing the coordinate values of the same point on the structure surface before and after loading. Assuming the scanner position has not been moved and that the status of bridge structure remains the same, the scanner can record the information of the same point on the structure in each direction. However, after applying load to a bridge, the superstructure of the bridge will have deformations. Therefore, in the same scan direction, the before and after loading scans will no longer record the same point on the bridge surface. Furthermore, the two scans will also include slight angle difference for each corresponding scan points. Hence, it is not correct to just compare the coordinate values of the scan points from different scan results to get the structural surface deflection.
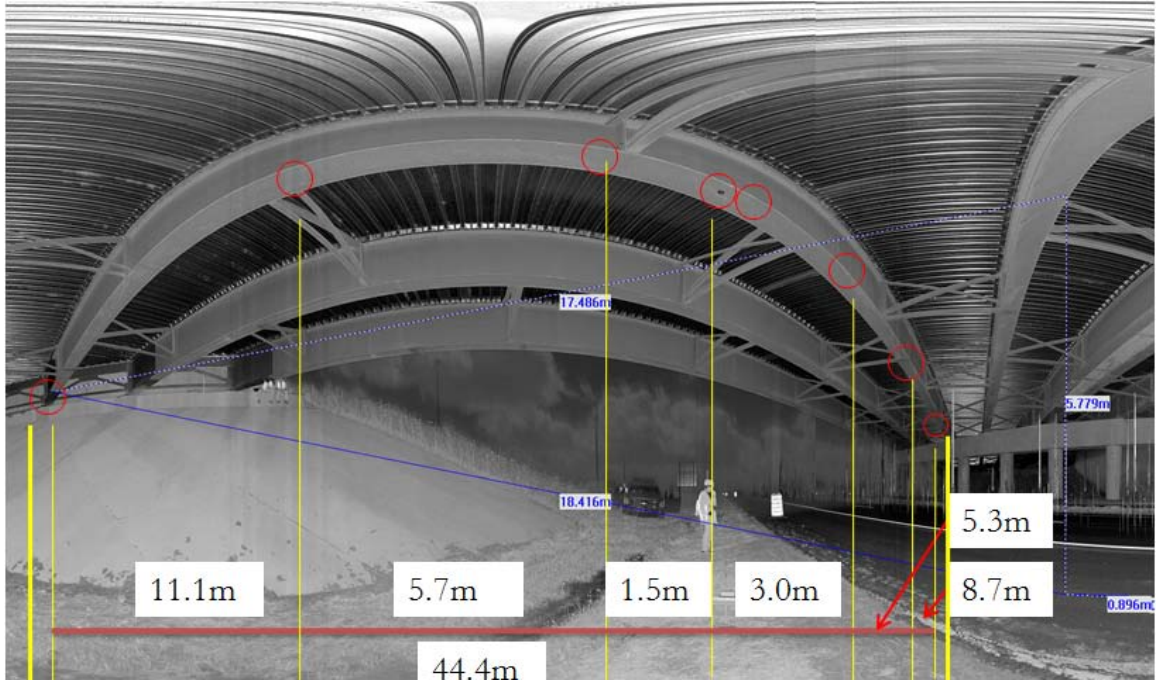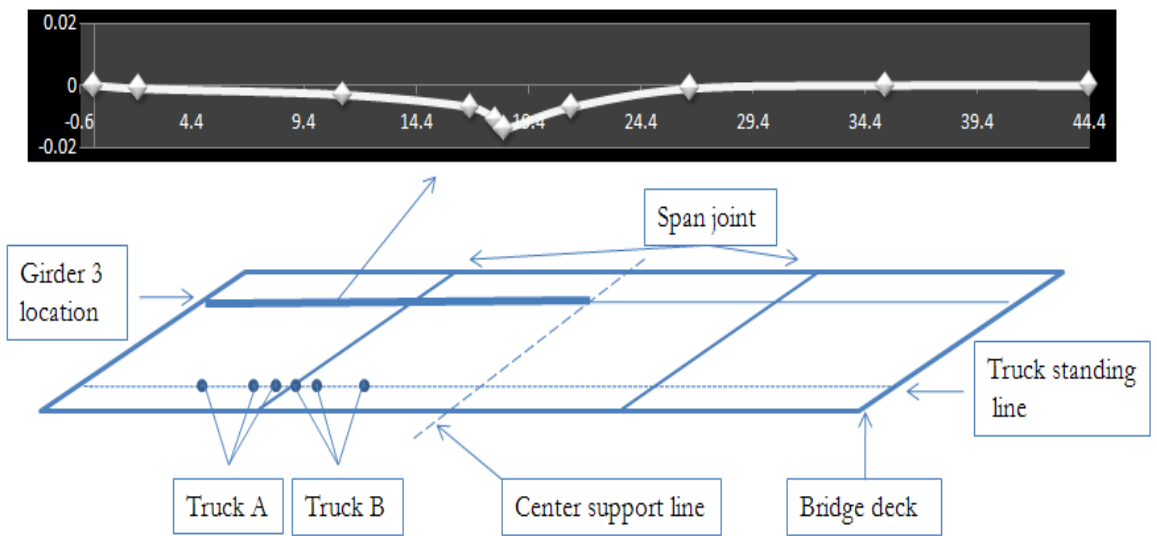
Figure 5-5 Locations of deformation measurement points in the LiDAR scan of the bridge over I-77 and calculated deformation

Without an efficient way to trace every measured point, one way to measure deformation is to match physical points manually. Points with specific features can be selected to compare their coordinate values. For example, the point connects a bracing

and a girder can be easily identified in the scan file. Figure 5-5 shows the deflection curve of the third bridge girder based on comparing the selected point coordinates. Using the manual deformation calculation, it is difficult to find the peak deflection point until the measurements of several locations have been completed. The selection process is time consuming and difficult. Hence an automatic deformation measurement method is developed and introduced below.

Before a bridge scan, the scanner should be calibrated. The elevation of each scan point represents the relative height of the point to the scanner. The coordinate values of each point are then stored along with a column number and a row number assigned representing its horizontal and vertical cycles. Since each vertical scan is completed between a very small horizontal rotation (360˚ /9000 in this dissertation), two points share the same X, Y coordinates are assumed to be in the same vertical scan cycle and therefore share the same vertical cycle number.

In the proposed deformation measurement method of this dissertation, a pseudo reference plane is first created (Figure 5-4). It is a horizontal plane and all the points on the plane share the same Z value. It is assumed that the plane is placed under the bridge superstructure and the points on that plane can be scanned and will not block the scanner's line of sight to the bridge structure. The X and Y coordinates for each scan point on the plane can then be calculated based on the point's scan direction (column and row number) and its Z coordinate. Both the before and after load data for the selected part are searched to find the match points that share the same horizontal position with the points on the pseudo reference plane. Displacement measurement of the bridge surface is achieved by measuring the height difference between the match points.
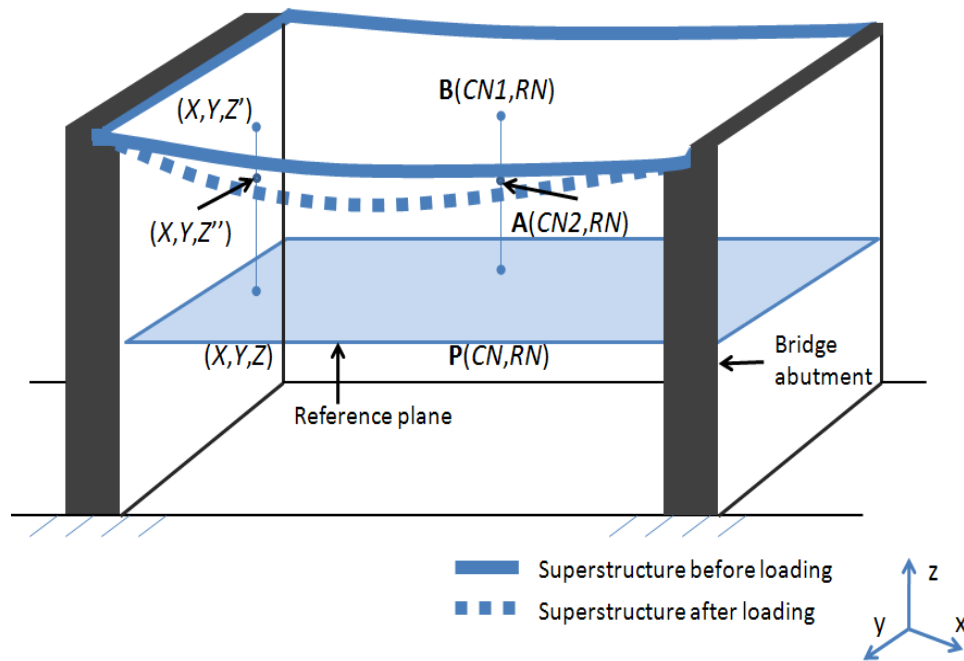
Figure 5-6 The creation of the reference plane

To find the matching for each pseudo point, only points with the same row number to the pseudo point, for both before and after load test datasets, need to be searched. Considering the initial scan angle difference and the errors brought about by noise, the scan points in the row before and after the pseudo points are searched. In Figure 5-6, both $\mathbf{P}(CN, RN)$ and (X, Y, Z) are used to represent points on the reference plane. The former uses column and row numbers and the latter uses the physical coordinates (Figure 5-7). The column number of the scan points in each row is arranged such that the points with the smallest column number have the lowest elevation and the points with the largest column number have the highest elevation. The points in the before and after loading scan datasets are searched starting with the maximum column number in each row. Therefore, in the same vertical line, only the point with the lowest height is selected for deformation measurement.
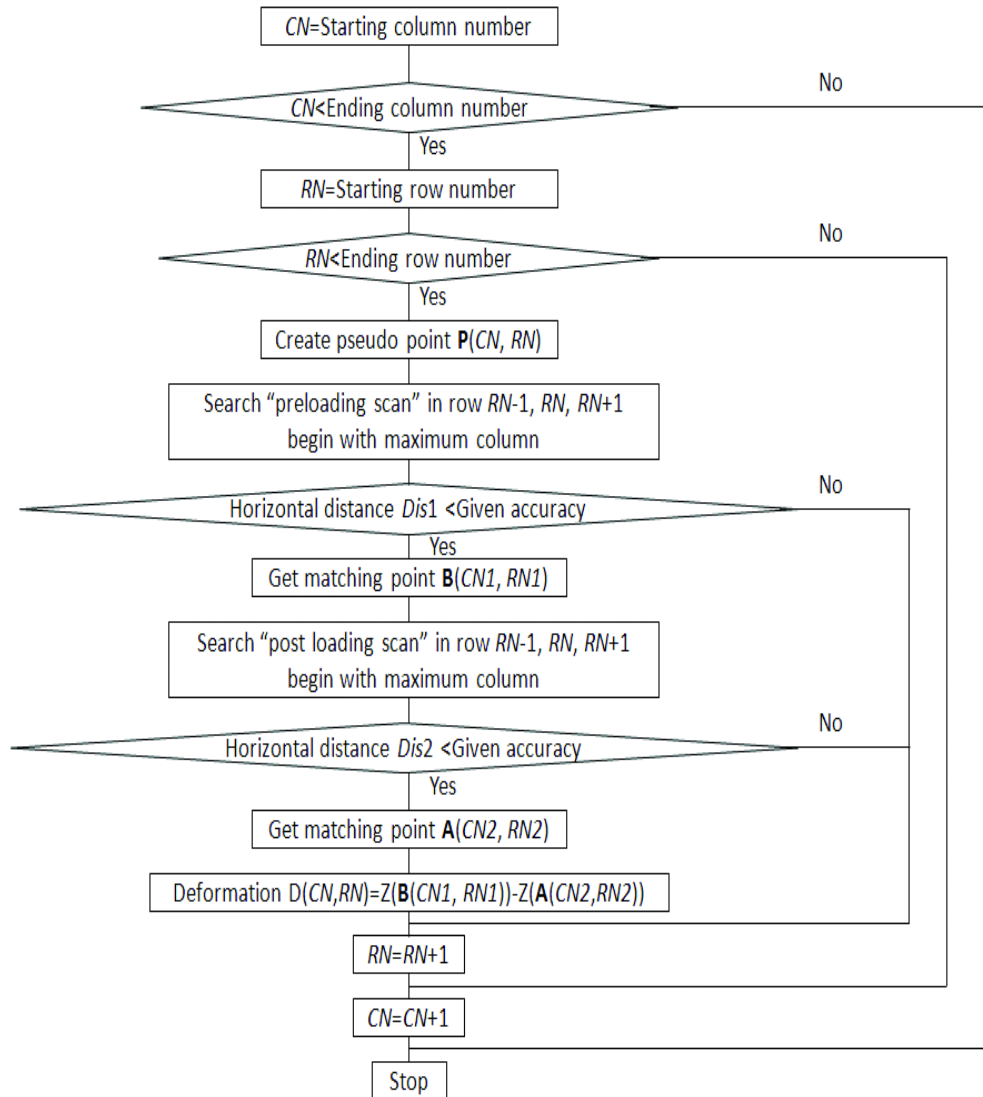
Figure 5-7 Flow chart of finding the match points for the pseudo points on the reference plane

To ensure each reference point has only one match point, the accuracy of the matching process can be chosen as half the distance between any reference point and the incremental point, Δh (Figure 5-8). Therefore, theoretically only one match point is assigned to each point on the reference plane. The match criterion can be expressed as

$$Dis \leq 0.5 \times \Delta h \qquad (5\text{-}1)$$

where

$$Dis = \sqrt{(X(\mathbf{P}(CN,RN)) - X(\mathbf{M}(CNN,RNN)))^2 + (Y(\mathbf{P}(CN,RN)) - Y(\mathbf{M}(CNN,RNN)))^2}$$

$$Dd = \sqrt{X(\mathbf{M}(CNN,RNN))^2 + Y(\mathbf{M}(CNN,RNN))^2 + Z(\mathbf{M}(CNN,RNN))^2}$$

$$r = \sqrt{X(\mathbf{M}(CNN,RNN))^2 + Y(\mathbf{M}(CNN,RNN))^2}$$

$\mathbf{P}(CN,RN)$ is the pseudo point on the reference plane with column number CN and row number RN. $\mathbf{M}(CNN,RNN)$ is the searched point on the bridge surface with column number CNN and row number RNN. RNN is chosen from $RN + 1$, RN, or $RN - 1$. X, Y and Z are the coordinate values for each point. Dis is the horizontal distance between point $\mathbf{P}(CN,RN)$ and point $\mathbf{M}(CNN,RNN)$. Dd is the distance between the scanner and point $\mathbf{M}(CNN,RNN)$, and r is the horizontal distance between them. ac and ar are the average radians between two adjacent points in the same row and in the same column, respectively. ac and ar can be calculated by dividing the average total measured angle by the average total measured points for each vertical or horizontal cycle, respectively.

Table 5-1 Point match accuracy according to distance (all units in meter)

Dd	6	10	15	20	30	40	50	60
ΔR	0.0022	0.0057	0.0092	0.0126	0.0193	0.0259	0.0325	0.0390
ΔC	0.0045	0.0126	0.0283	0.0503	0.1132	0.2012	0.3143	0.4526
Δh	0.0050	0.0138	0.0298	0.0519	0.1149	0.2028	0.3160	0.4543
0.5Δh	0.0025	0.0069	0.0149	0.0259	0.0574	0.1014	0.1580	0.2271
0.2Δh	0.0010	0.0028	0.0060	0.0104	0.0230	0.0406	0.0632	0.0909

Since

$$\Delta C = Z\big(\mathbf{M}(CNN, RNN)\big) \times (\tan(\vartheta + \Delta\vartheta) - \tan(\vartheta))$$
$$= Z\big(\mathbf{M}(CNN, RNN)\big) \times \sin(\Delta\vartheta) / (\cos(\vartheta)\cos(\vartheta + \Delta\vartheta))$$

$$\Delta R \approx \Delta\alpha \times r \qquad\qquad (5\text{-}2)$$

when $\Delta\vartheta \ll \vartheta$, $\sin(\Delta\vartheta) \approx \Delta\vartheta$ and $\cos(\Delta\vartheta + \vartheta) \approx \cos(\vartheta)$. Then

$$\Delta C \approx \Delta\vartheta \times Dd^2 / Z(\mathbf{M}(CNN, RNN))$$

Here $ac = \Delta\vartheta$ and $ar = \Delta\alpha$. Therefore

$$\Delta h \approx \sqrt{(ac \times Dd^2 / Z(\mathbf{M}(CNN, RNN)))^2 + (r \times ar)^2}$$
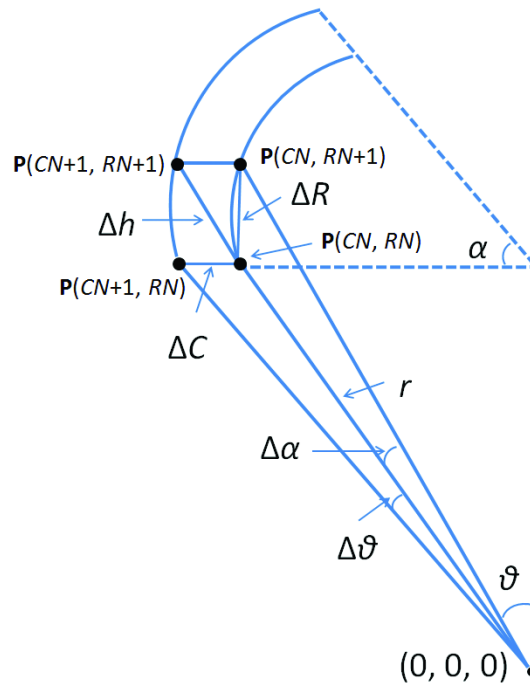
Figure 5-8 Measuring Δh

Based on Eq. (5-1), Table 5-1 gives the matching accuracy for different distance between the point and the scanner. The height of the measured bridge is assumed to be 5.0 m, i.e. $Z\big(\mathbf{M}(CNN, RNN)\big) = 5.0$. $ac = 6.2860e - 4$ and $ar = 6.5270e - 4$ are used in this calculation. From Table 5-1, it can be seen that when the distance is increased to further than 40 m, the match accuracy will be larger than 0.1 m, the LiDAR measured displacement is then considered as reliable. For the sample bridge used in this section, the maximum distance that need to be measured is around 30 m. To obtain more accurate result, the match accuracy has also been increased to $0.2\Delta h$ for comparison. With an accuracy higher than $0.1\Delta h$, only a few match points can be obtained.

5.4 Displacement measurement result

The measured displacements of the seven girders for the three truck locations are given in Figure 5-9-Figure 5-12 for all three load cases, respectively. Most of the results used an accuracy of $0.2\Delta h$, except for Figure 5-10, where accuracy of $0.5\Delta h$ for position 2 is used. The displacement plots are color coded for ease of display. It is shown that near the locations of trucks, bridge girders all have relatively large displacements. Table 5-2 gives the largest displacements that can be measured among the nine girders and their corresponding locations. For load case 3, girder 9 receives the largest displacement value near the location of the trucks. At the edge of the structures, the measured point value often deviates greatly from the mean value of the surrounding area and the point measurement error becomes larger with the increase in distance to the scanner. Therefore, at these locations, the displacement measurements are not accurate.

Table 5-2 Maximum displacement for each loading case and corresponding location

Load Case	1	2	3
Girder No.	1	7	9
Max Displacement (m)	0.017	0.016	0.020
Max Strain (m/m)	5.7e-4 (h=2.226 m)	5.0e-4 (h=3.357 m)	6.2e-4 (h=2.258 m)
Range (m)	25.0-38.6	22.1-27.1	19.8-27.9
Distance range to Scanner (m)	16.7-17.8	8.0-11.8	14.5-20.2

Note: Range is the maximum displacement location along the girder and the zero length is located at the cross section between the corresponding girder and the abutment.

The maximum displacements and distribution factors of each girder for each loading case are given in Table 5-3. To reduce the error brought by the surface roughness and mismatching, girder surface point cloud are divided into many 5×5 point grids and the displacement for each grid is taken as the mean of the center point displacement. The distribution factor for each girder is calculated using the maximum displacement of the girder in each loading case divided by the maximum displacement among all the girders for the three loading cases.

Table 5-3 Maximum displacement (D-in millimeter) and distribution factor (F) of each girder for each loading case

Case No.	1		2		3	
	D	F	D	F	D	F
Girder 1	17	0.85	3	0.15	3	0.15
Girder 2	17	0.85	5	0.25	3	0.15
Girder 3	14	0.70	5	0.25	3	0.15
Girder 4/5	10	0.50	8	0.40	6	0.30
Girder 6	7	0.35	12	0.60	7	0.35
Girder 7	6	0.30	16	0.80	13	0.65
Girder 8	3	0.15	13	0.65	18	0.90
Girder 9	2	0.1	10	0.50	20	1
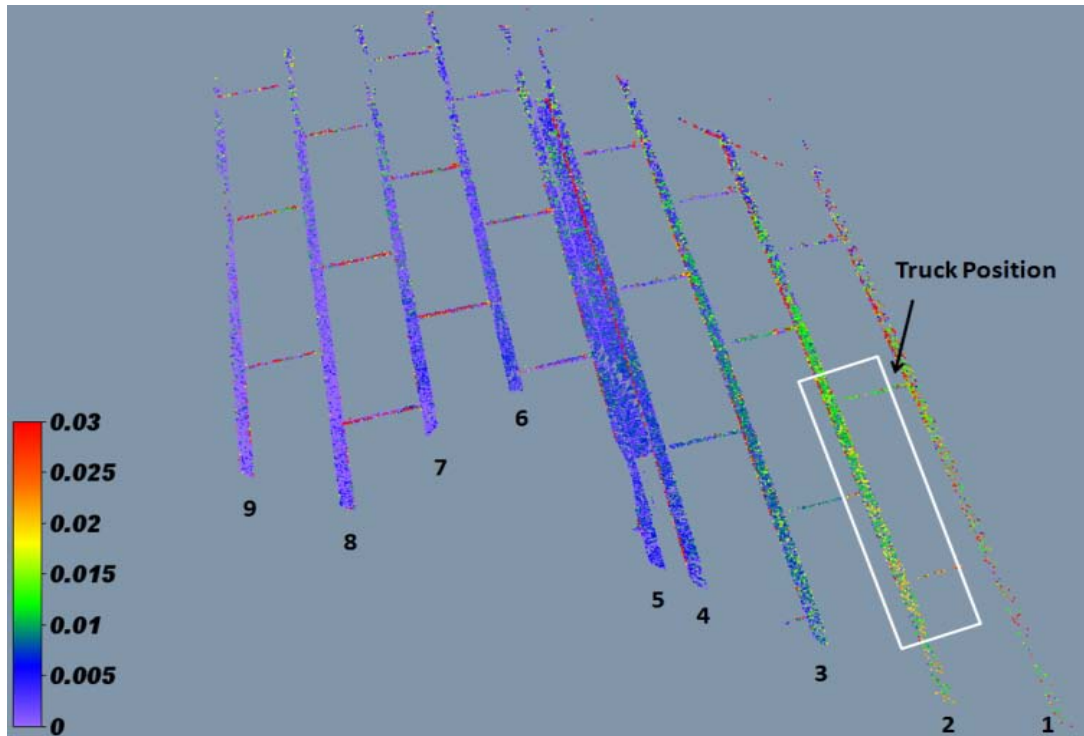
Figure 5-9 Displacement of girders for position 1 (m)
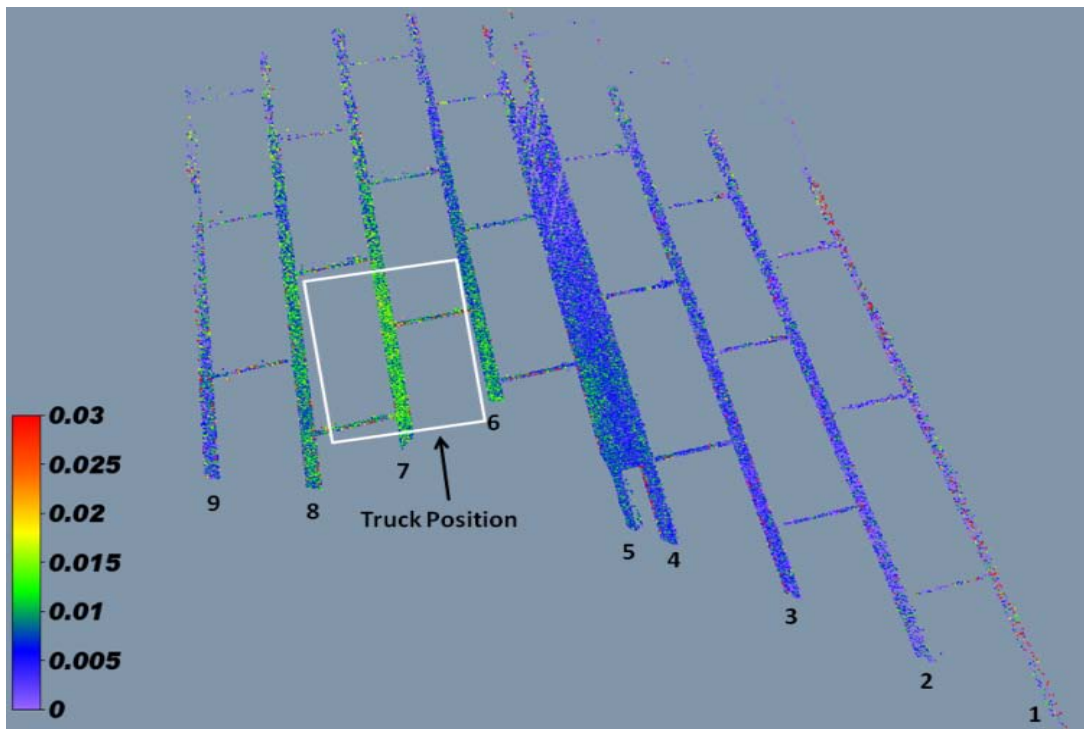
Figure 5-10 Displacement of girders for position 2 $(0.5\Delta h)$ (m)
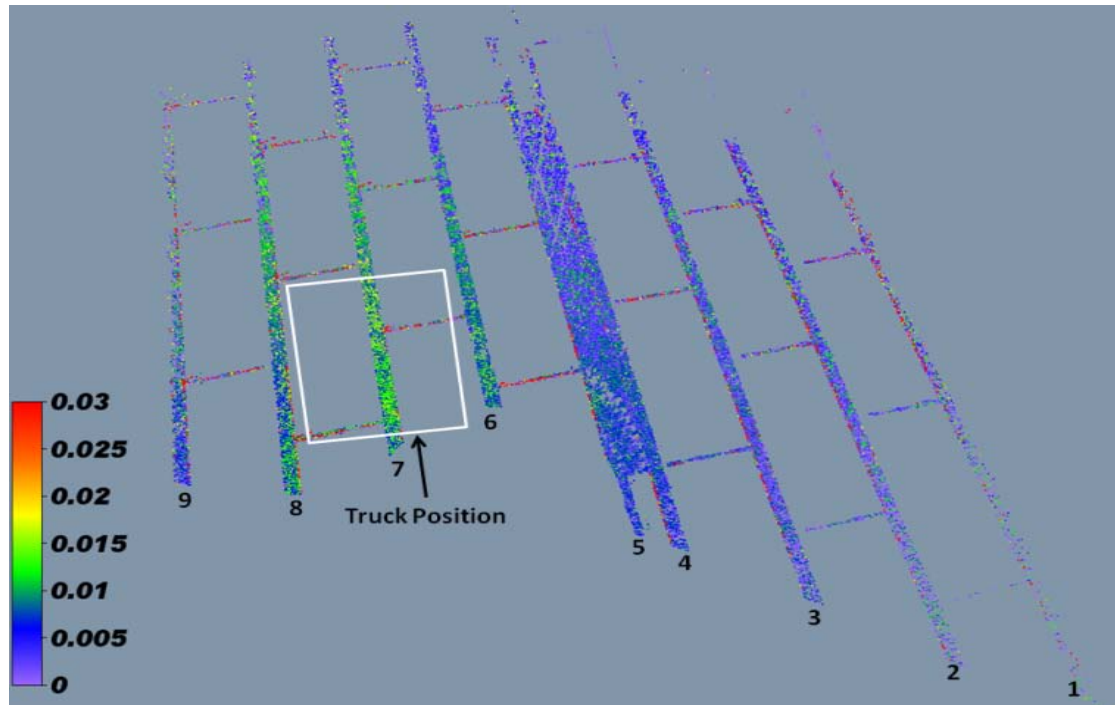
Figure 5-11 Displacement of girders for position 2 (0.2Δh) (m)
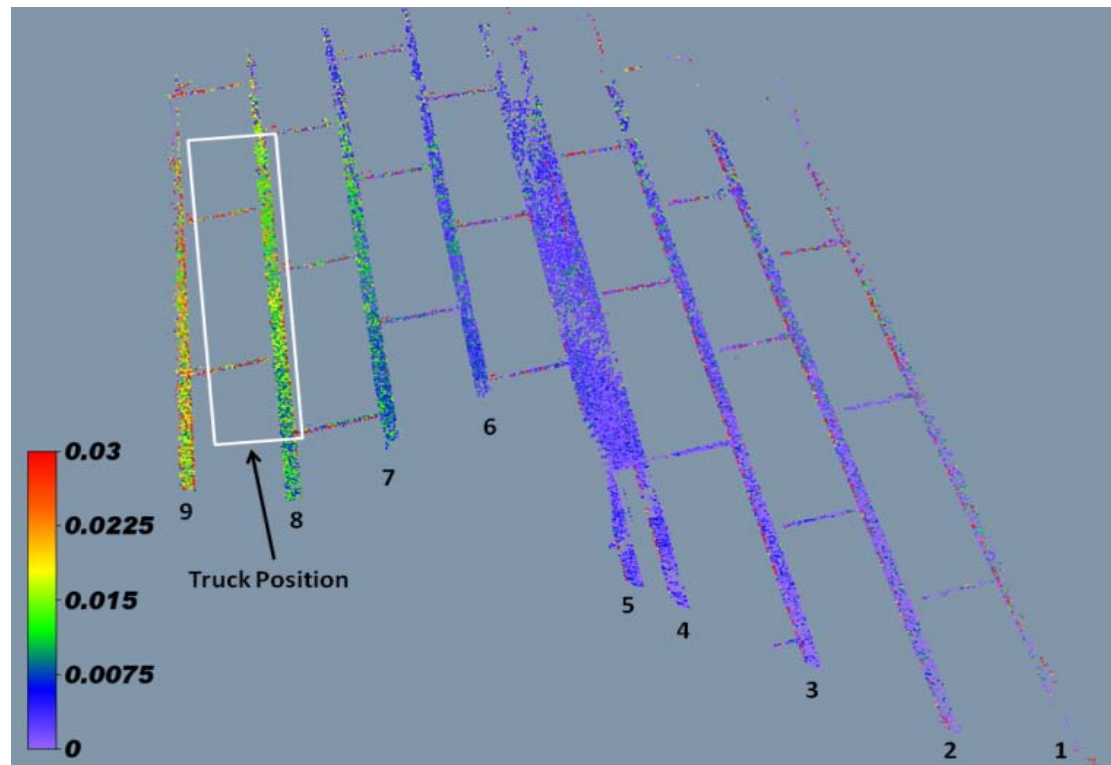
Figure 5-12 Displacement of girders for position 3 (m)

5.5 Strain measurement

According to the moment-curvature relation (Au 1963) for structure elastic deformation, the structural strain can be derived from the deformation curvature of the structure. Based on the derivation,

$$\frac{d^2 v}{d^2 x} = \frac{M}{EI}$$ (5-3)

where v is the vertical displacement of the elastic curve. M is the applied moment. EI represents the bending stiffness of the member. For pure bending, strain is defined as simply

$$\epsilon = -\frac{My}{EI}$$ (5-4)

where y is the distance from the neutral axis of the cross section to the outer edge. Based on finite difference, strain can be calculated as:

$$\epsilon = -\frac{d^2 v}{d^2 x} y \approx \frac{v(x+h) - 2v(x) + v(x-h)}{h^2} y$$ (5-5)

in which h is a small value. Using Eq. (5-5), the strain of the structural component at any location can be calculated from the vertical displacements at that location and nearby locations.

For the loading cases in this section, the maximum strain of the girders is around 0.001 m/m. The distance from the neutral axis of the cross section to the outer edge y is estimated to be 0.8 m. The accuracy for the displacement measurement is 0.001 m. Based on Eq. (5-5), to get reasonable strain value, h should be larger than 1.0 m, which is not correct for local strain measurement. To rectify this problem, higher resolution LiDAR is

needed. The techniques for higher resolution LiDAR range finder are already available. Bosch et al. (2001) proposed a method with the accuracy less than 100 µm and INRS (2009) proposed a low cost instrument with the same accuracy in the range of tens of meters. In this case, the minimum h value will reduce to around 0.3 m. Table 5-2 provides the calculated strain by selecting sample points from the LiDAR data based on Eq. (5-6) with all the h larger than 1.0 m. It is clear that with the increase in the LiDAR range measurement accuracy, the scan data can be used for measuring the strain for the entire recorded surface.

CHAPTER 6: SYSTEM VALIDATION AND LIBE-BASED BRIDGE RATING

6.1 LiDAR scanner range measurement accuracy check

In this dissertation, the basic assumption made is that the LiDAR scanner can provide the resolution for range measurement as it is currently designed. The design distance error of the scanner used in this dissertation is ±3 mm at a distance of 25 m. To validate the range measurement accuracy and repeatability, two tests have been conducted: a 61 cm ruler has been scanned at a distance about 18 m (Figure 6-1) and Bridge # 590084 was scanned from four different locations (Figure 6-2).

Figure 6-1 LiDAR scan for a 61 cm ruler at a distance around 18 m
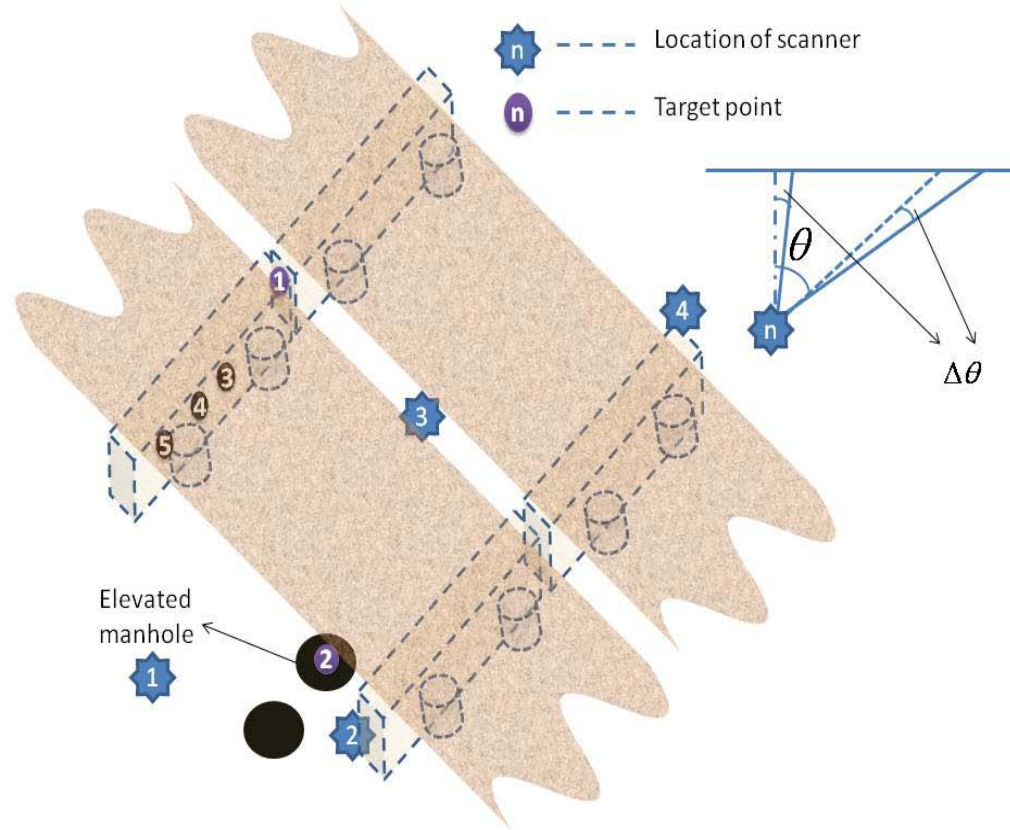
Figure 6-2 Laser position and target points on Bridge # 590084

The maximum scale value of the ruler is 0.610 m. However, the edge-to edge length of the ruler is between 0.610 m and 0.612 m with a +-0.001 m tolerance in measurement deviation. For the LiDAR scan, five sets of points on the two ends of the ruler have been selected from the LiDAR scan of the ruler to measure the length. Each pair of points was selected to have almost the same height (with the same Z value). The X, Y coordinate values of the selected points are given in Table 6-1. All the five length measurement results are between 0.610 m and 0.611 m. The standard deviation is only 1.12E-4 m. This test proves that at the distance around 18 m, the scanner can provide range measurement with the accuracy in millimeters.

Table 6-1 Length measurement for the ruler using the coordinate values of its
boundary points

Pair Number	X (m)	Y (m)	Ruler Length (m)
1	7.304	-16.861	0.611
	6.737	-17.089	
2	7.302	-16.857	0.611
	6.733	-17.080	
3	7.297	-16.845	0.610
	6.726	-17.061	
4	7.297	-16.845	0.611
	6.725	-17.059	
5	7.300	-16.851	0.611
	6.730	-17.071	
Mean			0.611
Standard Deviation			1.12E-4

The purpose for the test on Bridge # 590084 is to demonstrate the effects of

shooting angles and target distances to range measurements. Hence four scans were made

from different physical distances and scan angles to the same scan object. A scan angle

is defined as the angle between the scan direction and the normal of the flat scan object

surface. The range measurement validation is done through comparing the differences of

the measured distance between the five selected reference points and the diameter of a

nearby manhole (Figure 6-3).

The LiDAR measurement resolution is determined by the sensor design, laser

beam width and can be influenced by the distance between the scanner and the object, the

scan angle and the reflectivity of the object surface. The scanner has a scan range

limitation of 76 meters. The further the scan distance, the less reflect energy can be

measured. The distance between two continuous scan points on the bridge surface is also

increased with the increase of scan distance. Therefore the measurement resolution for

particular point is decreased with the increase of scan distance. The scan angle also

influences the distance between two continuous points on the object surface. Object

surface reflectivity is one of the main factors that determine whether the range of the

object can be measured, for example, due to the low reflectivity, water surface can hardly

be measured.

Figure 6-3 Target points and object of Bridge # 590084 (LiDAR image of scan 2)

The validation test details are shown in Table 6-2. As shown, the minimum range

measurement difference between two scans can be less than 2 mm with the scan distance

between 10 m~20 m, for example, the range between point 3 and point 4 in scan 2 and

scan 3, and the distance between point 4 and point 5 in scan 1 and scan 2 (highlighted in

Table 6-2). These points all have the relatively small scan angle. The maximum standard

deviation among the four scans was obtained in measuring the distance between point 1 and point 3. Scan 1 gives the smallest value and differs most from the other three scans. Point 1 and point 3 all have much larger scan angles ($\theta > 45°$) in scan 1 than in other scans. When scanning with a large scan angle, the distance between two continuous scan points is large. This increases the error for selecting the same point on the object surface in a scan image. The same situations are shown in point 4 in scan 1, point 4 and 5 in scan 4. The low deviation values validated the scanner range measurement accuracy and scan repeatability.

Table 6-2 Range measurement comparison of Bridge # 590084 from four different scans

Point No.		Scan 1 (m)	Scan 2 (m)	Scan 3 (m)	Scan 4 (m)	Standard deviation (m)
1-3	Distance between points	6.362	6.427	6.443	6.439	0.0326
	Distance to scanner (1)	21.678	23.389	9.222	26.483	
3-4	Distance between points	1.226	**1.252**	**1.251**	1.235	0.0109
	Distance to scanner (3)	16.010	19.170	11.683	31.663	
4-5	Distance between points	**3.673**	**3.671**	3.686	3.658	0.00993
	Distance to scanner (4)	14.980	18.502	12.487	32.697	
2	Diameter of well	0.681	0.675	0.666		
	Distance to scanner (2)	9.375	5.144	14.599		

6.2 LiBE system accuracy check

In Chapter 5, the point matching accuracy analysis has been performed for bridge displacement measurement. Since clearance measurement also includes a point match process, the conclusions in Chapter 5 can be used for clearance measurement accuracy check. In this section, only the accuracy check for damage detection and quantification in

LiBE are discussed. Section 6.1 has validated the range measurement accuracy of the scanner. Hence, for LiBE system validation, the scan data are used manually to check the accuracy of the LiBE results only.

6.2.1 LiBE system area measurement accuracy check

The pier surface of Bridge # 590255 (Figure 6-4) is selected for LiBE system area measurement accuracy check. The shape of the selected test part in Figure 6-4 is approximately a quadrilateral, therefore, the total area can be measured based on the coordinate values of the four boundary points of that area. The coordinate values of the four boundary points (Table 6-3) of the test part were selected manually from the raw scan data. LiBE measures total test surface area and damage area through adding up the grid areas. The area of each grid is calculated separately based on the coordinate values of the four boundary points of the specified grid. Table 6-4 lists the total surface area measured manually, and that obtained from LiBE system using 98×11 gird and 195×21 grid, respectively. The areas measured by LiBE are close to the rough manual measurement. Although the total grids number increase almost four times from 98×11 gird (10×10 point interval) to 195×21 (5×5 point interval) gird, the area difference is only 0.02%. Comparing to the sheer size bridges, this accuracy should be enough as component size or damage area measurement.

Table 6-3 Test area boundary points information for Bridge # 590255

Boundary Points	1	2	3	4
Scan Column No.	1307	1307	2279	2279
Scan Row no.	4644	4748	4644	4748
X (m)	-9.277	-9.497	-9.230	-9.452
Y (m)	-0.997	-0.373	-1.005	-0.384
Z (m)	8.673	8.839	1.307	1.315

Table 6-4 LiBE surface area measurement check

Test No.	Test Method	Total Area (m^2)
1	Four point area (m2)	4.9188
2	LiBE grids 98×11 (m2)	4.9688
3	LiBE grids 195×21 (m2)	4.9676
Difference between test 1 and 2		1.02%
Difference between test 2 and 3		0.02%
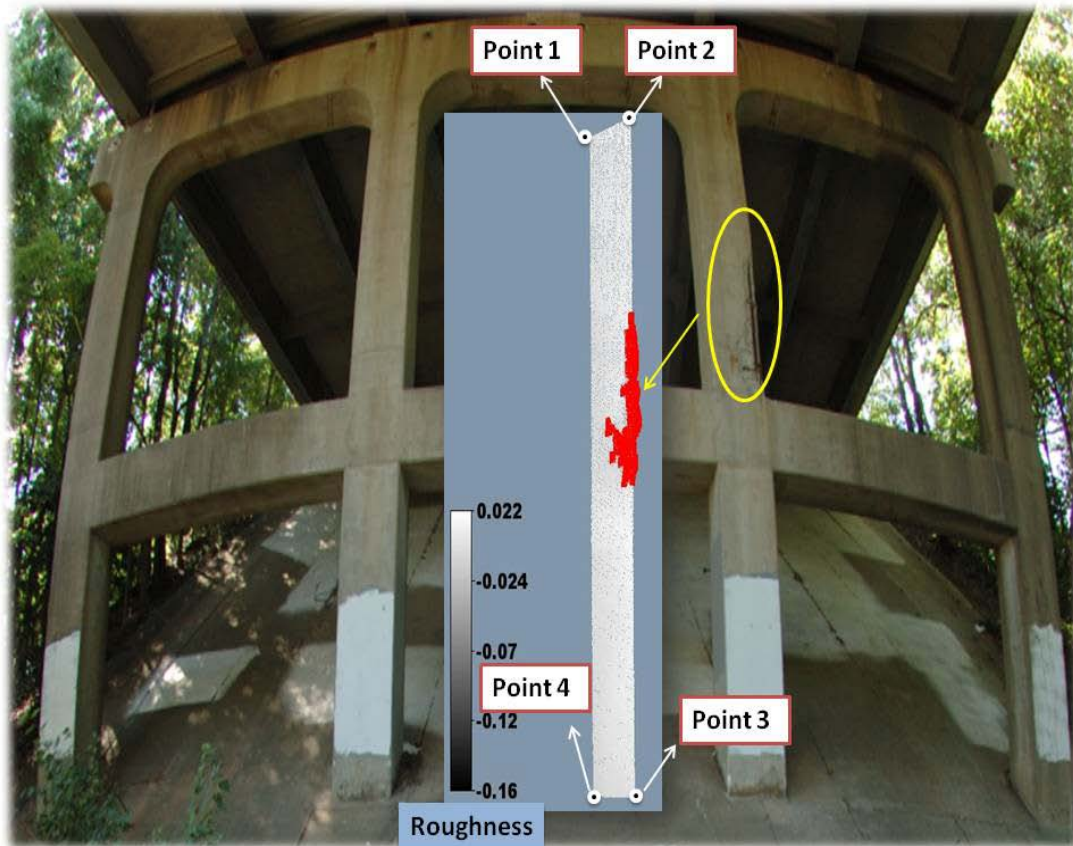
Figure 6-4 Positions of the four boundary points on the selected bridge pier surface

6.2.2 Error analysis and LiBE system improvement for damage detection

The damage detection in LiBE system uses surface roughness and gradient information to select damage points on bridge structure surface. Surface roughness is

measured based on the distance of the points on the surface to a reference plane. Civil

structures often do not have surface smoothness requirement. Even without damage, a flat

bridge surface will have point height difference up to millimeters. Therefore the selected

point interval for measuring surface gradient influences the mean gradients value of the

surface points.

Table 6-5 Surface information of the test bridges

	Distance-Mean (m)	Distance-Deviation (m)	Curvature-Mean (m-1)	Curvature-Deviation (m-1)	Gradient-Mean (m/m)	Gradient-Deviation (m/m)
590147	0.019667	0.022209	9.514335	8.387589	0.426676	11.12911
590255	0.005568	0.008436	11.65266	9.305966	0.308042	11.21692
590179	0.003140	0.002671	11.76624	11.20001	0.221394	11.22567
640024	0.039651	0.035272	159.3901	1444.447	1.235052	10.90800
590702	0.003666	0.002964	15.12206	13.95906	0.206646	11.21868
590704	0.008388	0.006698	34.78929	173.2685	0.404308	11.21902

To standardize the thresholds for damage detection, a new module is added to the

system for calculating the interval of points for gradient calculation to make sure all the

scans use the same point distance for gradient calculations. Table 6-5 compares the mean

value and standard deviation of distance, gradient and curvature of the points on the test

surfaces for different bridges. The bridge surface curvature can be calculated based on

Eq. (6-1)

$$C(\eta, \mathfrak{z}) = \left|\frac{\partial^2 z}{\partial^2 \eta}\right| + \left|\frac{\partial^2 z}{\partial^2 \mathfrak{z}}\right| \tag{6-1}$$

where $C(\eta, \mathfrak{z})$ is the curvature of point $(\eta, \mathfrak{z})$. η and $\mathfrak{z}$ are along the coordinates in the

latitude and longitude directions, respectively.

Surface curvature (second order derivative) is more sensitive to roughness than surface gradient (first order derivative). The mean values of the curvature for bridges in Table 6-5 also coincide with the order of the damage ratio (data for the study bridges are presented in APPEDIX E except for bridge # 590255). Hence the LiBE system is modified to detect damage based on surface roughness and curvature information instead of gradient information. Since the damage ratio is used to determine the thresholds for damage detection, the mean value of the surface curvature can be used to automatically select the thresholds for damage area determination , thus, we moved away from manually setting the adjusting parameters (β_1 and β_2 in Section 4.2). In the ideal case, a flat surface should have the mean values of distance and curvature equal to 0. When a bridge has relatively small mean distance and curvature values, the bridge surface will be recognized as having initial damages. Similarly, when a bridge has a relatively large mean distance value, but has a relatively small mean curvature value, the bridge surface most likely has small, but deep damage areas, such as in the case of Bridge # 590704.

Table 6-6 compares the detected damages for Bridge # 590704 using different threshold values for both distance and curvature. Test No. 1 will be assumed as baseline and uses 0.01 m as the distance threshold, and 15.0 as the curvature threshold to determine whether a point belong to damage or normal construction error. The 15.0 for curvature threshold is calculated from the condition that the vertical distance differential among points for curvature calculations is equal to 0.01 m. It can be seen from the table that the distance threshold has relatively less influence on the damage detection than curvature threshold, and the thresholds influence more on damage area than damage volume. For the changing of distance threshold, the maximum difference of the detected

damage area among all the quantifications is around 10% and the maximum difference of the detected damage volume is around 3%. The change of curvature threshold results in higher damage measurement differences.

Table 6-6 Damage detection and quantification for Bridge # 590147 using different thresholds

Test No.	Distance Threshold (m)	Curvature Threshold (m⁻¹)	Defect No.	Damage Area (m²)	Area Dif (%)	Damage Volume (m³)	Volume Dif (%)
1	0.01	15.0	1	1.6669E-1		1.2580E-2	
			2	1.2959E-1		4.9419E-3	
			3	9.7552E-2		3.8851E-3	
2	0.01	16.5	1	1.5863E-1	-4.83	1.2519E-2	-0.49
			2	1.2959E-1	0.00	4.9419E-3	0.00
			3	8.7692E-2	-10.11	3.6720E-3	-5.49
3	0.01	18.0	1	1.5514E-1	-6.93	1.2488E-2	-0.73
			2	1.2492E-1	-3.61	4.8881E-3	-1.09
			3	8.2190E-2	-15.75	3.6256E-3	-6.68
4	0.01	13.5	1	1.7585E-1	5.49	1.2618E-2	0.30
			2	1.4500E-1	11.88	5.1065E-3	3.33
			3	1.0553E-1	8.18	3.9407E-3	1.43
5	0.01	12.0	1	1.9786E-1	18.70	1.2770E-2	1.51
			2	1.7064E-1	31.68	5.3707E-3	8.68
			3	1.4144E-1	44.99	4.6944E-3	20.83
Deviation		Curvature-2.42 m⁻¹		0.0214 m²		0.000294 m³	
6	0.011	15.0	1	1.6669E-1	0.00	1.2580E-2	0.00
			2	1.1670E-1	-9.95	4.8227E-3	-2.41
			3	9.4773E-2	-2.85	3.8556E-3	-0.76
7	0.012	15.0	1	1.5993E-1	-4.06	1.2496E-2	-0.67
			2	1.1670E-1	-9.95	4.8227E-3	-2.41
			3	9.4773E-2	-2.85	3.8556E-3	-0.76
8	0.009	15.0	1	1.7147E-1	2.87	1.2625E-2	0.36
			2	1.2959E-1	0.00	4.9419E-3	0.00
			3	9.7552E-2	0.00	3.8851E-3	0.00
9	0.008	15.0	1	1.7515E-1	5.08	1.2660E-2	0.64
			2	1.3111E-1	1.17	4.9553E-3	0.27
			3	9.7552E-2	0.00	3.8851E-3	0.00
Deviation		Distance-0.00158 m		0.00639 m²		6.180E-5 m³	

By comparing with actual bridge image, the detection result from test No. 5 is most close to the actual condition. Comparing to other detection results, test No. 5 contains more damage areas on the boundary of the damages with low depth. These low depth damage areas have little influence to the bridge condition, but will account for more total damaged area. The thresholds can be set higher to exclude the boundary area and result in more reasonable results.

6.2.3 Influence of scan angle for damage detection and quantification

To study the influence of the scan angle for damage detection and quantification, and further validate the damage quantification function of LiBE, an experiment has been carried out. A shipping box with a 0.076 m × 0.089 m rectangular hole is used to simulate a flat surface that has damage (Figure 6-5). A small paper box with the dimension of 0.076 m × 0.089 m × 0.057 m has been attached to the hole inside the shipping box to control the depth of the damage.
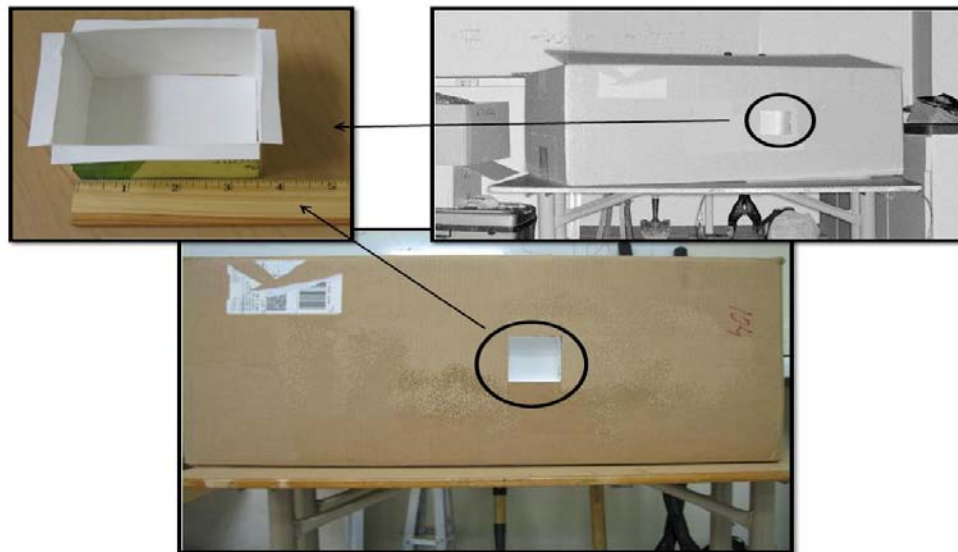
Figure 6-5 Experiment design

The surface of the shipping box has been scanned twice with the hole opposite to the scanner at the distance around 4 m and 2.5 m respectively. Two additional scans have also been recorded with the damage surface placed oblique to the scan direction (Figure 6-6). The box surface data has been analyzed by LiBE and the quantification results are given in Table 6-7. Different grid sizes have been used to detect the simulated damage.
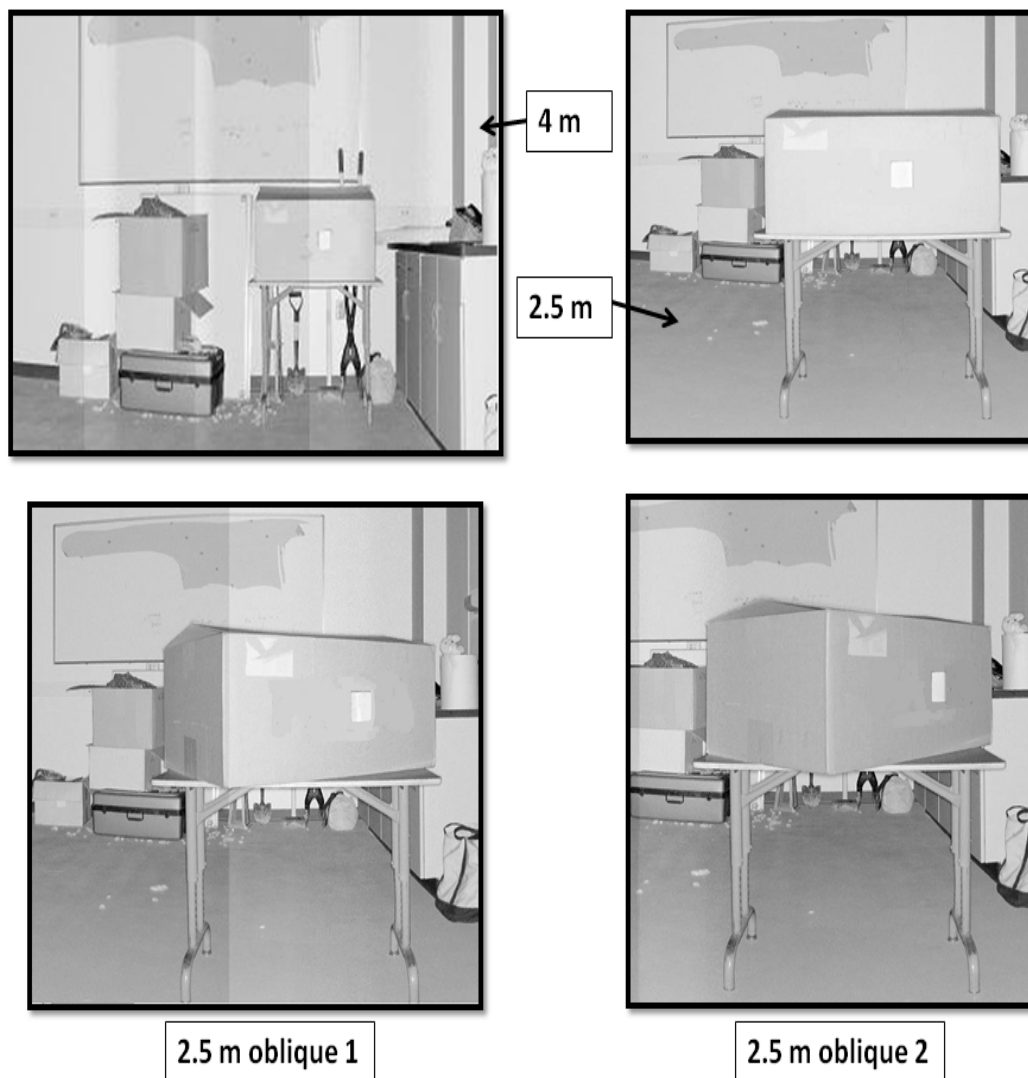
Figure 6-6 Four LiDAR scans for the shipping box

Due to the corrugated design of the shipping box, instead of being ideally flat, the box surface has fluctuation up to several millimeters. Since bridge component surface is not ideally flat, these test results are still validated. In the case of 0.003 m surface flatness deviation, the damage volume on the shipping box could change around 2.03E-5 m^3, which results in 5.2% volume quantification deviation. Most quantification results in Table 6-7 are smaller than this deviation except oblique 1. This proves the efficiency of the damage detection function of LiBE. Table 6-7 also indicates that the change of gird size and scan distance did influence the quantification result of the damage, but still in the allowable range.

Table 6-7 Quantification of the damage based on different scans

Test	Grid Size	Damage Area (m^2)	Area Deviation	Damage Volume (m^3)	Volume Deviation
Design Value		6.77E-3		3.87E-4	
2.5 m – oblique 1	3	6.60E-3	-2.5%	2.80E-4	-27.6%
2.5 m – oblique 2	3	6.97E-3	3.0%	3.92E-4	1.3%
2.5 m	3	7.01E-3	3.5%	4.07E-4	5.2%
2.5 m	5	7.14E-3	5.5%	4.12E-4	6.5%
4 m	3	7.02E-3	3.7%	3.73E-4	-3.6%
4 m	5	6.91E-3	2.1%	3.57E-4	-7.8%

Since the scanner can only get the information of the object in its line of sight. Accurate quantification of a damage in LiBE should be based on the overall measurement of the damage surface points. If the damage surface points and the scanner form a convexity set in Euclidean space, all the damage surface range information can be recorded with certain resolution. For a convex set, each point on a straight line that connects any pair of points within the set should belong to the set. Therefore, if the

scanner and the damage surface form a convexity space, no point will block the view of the scanner to any point on the damage surface. Ignoring the shape of the damage surface, to obtain as much information about the damage as possible, the scanner should be placed right opposite to the damage.

The high deviation of volume quantification from test oblique 1 in Table 6-7 shows the influence of partial scan of the damage. However, small deviation can be found for damage area quantification. This can be explained through Figure 6-7. The oblique scan of the damage makes only part of the damage surface be measured. Therefore the volume quantification just counts volume of the red part of the damage in test oblique 1. Since the scanner averages the ranges measured by the laser pulses within the beam width at each scan point, at the edge of an object, if the range of points on the two sides of the edge differs a lot, the range of the edge will be recorded in between the ranges of the points on the two sides. Due to the influence of the scan angle, the points at right side of front left edge in the scanner's view are on the back surface of the damage. The front left edge of the damage is virtually measured as shown Figure 6-7. Although the left surface of the damage cannot be scanned, the scan points on the front left edge of damage can still be classified as damaged points by the program. Therefore, the scan angle will not influence the quantification of the damage area, which can be seen from the results of test oblique 1 in Table 6-7.
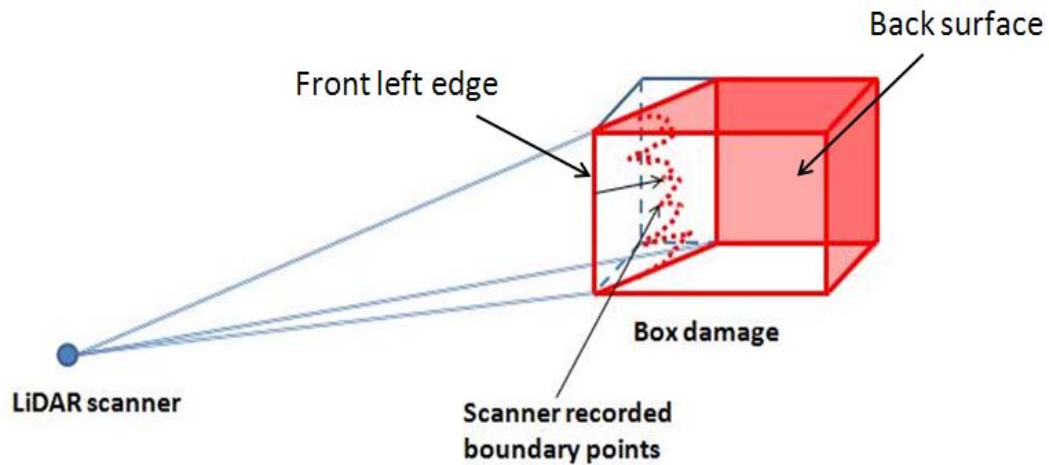
Figure 6-7 Influence of scan angle

6.3 Bridge clearance rating in LiBE

Bridge inspection record defines the bridge component rating as: 0-2 to be critical, 3-4 to be poor, 5-6 to be fair and 7-9 to be good. Hence, for bridge clearance evaluation using LiBE, a 0-9 scale rating is also adopted. Specifically, rating 8-9 represent effective bridge system with nearly new condition; 6-7 represent no structure service required; 4-5 are for questionable structures; 2-3 represent potential structural problem and immediate services are required, and 0-1 indicate no traffic allowed. Most of the clearance issues will not cause the failure of the entire bridge structure, and the clearance measurement itself cannot provide in-depth damage evaluation for determining maintenance requirements for the bridge structure. Therefore the minimum rating based on clearance condition is set to 4.

Based on NCDOT bridge policy (NCDOT 2000), the design limits of bridge vertical clearance and minimum requirements for a bridge to remain in service are summarized in Table 6-8. The clearances should also include 0.15 m of clearance for

future resurfacing and another 0.15 m for "the flexibility necessary in the coordination of roadway grades with final superstructure depths" (NCDOT 2000). The clearance evaluation using LiBE will only consider safety and not economy, which means the higher the clearance, the higher the bridge rating.

Table 6-8 Bridge vertical clearance requirements for North Carolina

	Over local/collector roads/streets	Over interstates/ freeways /arterials	Over railroad
Design limit	4.57 m~4.72 m	5.03 m~5.18 m	7.01 m~7.16 m
Extra-consideration	4.87 m~5.02 m	5.33 m~5.48 m	7.31 m~7.46 m
Minimum clearance to remain in service	4.27 m	4.88 m	6.70 m*

In LiBE system, if a bridge has a minimum vertical clearance larger than the design limit plus the extra consideration for resurfacing and construction difference, the bridge is thought to be in good clearance condition and can get a rating of 9. If the clearance is in the range of the design limit plus the extra considerations, the bridge can get a rating of 8. If the clearance value drops into the range of design limit, it still can get a rating of 7. A rating 6 is given to the bridge that have a minimum clearance value larger than the minimum requirement to be in service and lower than the requirements for rating 7. Based on the study of bridge vertical clearance in section 4.2, it can be seen that a local bridge with clearance lower than 4.10 m or an interstate (freeways /arterials) bridge with a clearance lower than 4.50 m will encounter much more collision damages than a bridge

with higher clearance. Hence, the thresholds of 4.10 mm for local bridges and 4.50 m for interstate bridges are selected to determine if a bridge should be rated 4 or 5, and the structure is thought to be questionable in these cases. Table 6-9 provides the detailed rating criteria. The selected for scan bridges (around 20) have been evaluated based on these criteria. Final ratings for the applicable bridges are given in Appendix C.

Table 6-9 Bridge minimum vertical clearance rating criteria

Rating	Local Road	Interstate/Freeway	Railroad
9	>5.02 m	>5.48 m	>7.46 m
8	4.87 m~5.02 m	5.33 m~5.48 m	7.31 m~7.46 m
7	4.57 m~4.87 m	5.03 m~5.33 m	7.01 m~7.32 m
6	4.27 m~4.57 m	4.88 m~5.03 m	6.70 m~7.01 m
5	4.10 m~4.27 m	4.50 m~4.88 m	<6.70 m
4	<4.10 m	<4.50 m	--

6.4 Bridge damage rating based on LiBE Damage Detection

Reinforced concrete bridge components are vulnerable to water and chloride attacks. These attacks will result in the corrosion of the inner reinforcements. The corrosion, if not detected, can gradually reduce the strength of the girder, and the reinforcement volumetric expansions due to oxide formation will result in concrete delamination (Liu and Frangopol 2004). The depth of the reinforcements to the concrete surface is called "concrete cover". The concrete cover is one of the main factors that determine the corrosion potential of the reinforcements under the same environmental condition (Roberts 2004).

Bridge component ratings based on damage level, which is assessed by LiBE, adopts a 0-100 scale. The size of the damage on a concrete, reinforced concrete or pre-stressed concrete bridge components can reflect the corrosion situation, the intensity of impact load, or the overload level at particular location. The variables LiBE selected to evaluate damage include the total area the damage covers, the total mass loss, the maximum depth within the damage, and the average depth within the damage. These information can be obtained automatically from LiBE system.

For bridge rating based on damage quantification, the bridge member with the worst condition is selected for primary evaluation, and the rating of that member is used as the rating of the whole bridge for simplification. Pillai and Menon (2003) provided the recommended concrete cover based on the "severity of environmental exposure conditions" (as shown in Table 6-10). For bridge rating based on surface damage, both the damage ratio, γ, and average depth, AD, are considered as the main parameters. The damage ratio is equal to the total area of damages divided by the total area of the measured bridge surface. Assume the worst condition, when the bridge receives a rating of 0, the damage ratio should be equal to 1.0 and the average damage depth exceeds the maximum concrete cover requirement ($AD \geq 0.075\,m$) at extreme environment condition. The damage ratio should count more than the average depth of the damage in the final rating of a bridge. The mass loss on the bottom surface of a bridge member increases the risk of the corrosion of the rebars that carry the largest tension stress, which may result in member failure. Therefore, in the bridge rating equations (Eq. (6-2) and Eq. (6-3)), the damage ratio receives a weight of 0.7 and average depth receives a weight of 0.3. The maximum depth of the damage is also considered in the bridge final rating.

$$R = 100 \times [1.0 - 0.7 \times \sqrt{\gamma} - 0.3 \times \left(\frac{AD}{0.075}\right)^{\frac{AD}{M}}] \tag{6-2}$$

$$R = 100 \times [1.0 - 0.7 \times \sqrt{\gamma} - 0.3 \times \left(\frac{AD}{0.075}\right)^{\sqrt{\frac{M}{AD}}}] \qquad \text{IF} \quad A > 0.075 \tag{6-3}$$

where R is the final rating. γ represents the damage ratio. AD is the average depth of the

damages on the test bridge member and M is the maximum depth of the damage. All the

selected 21 bridges in Charlotte-Mecklenburg area and the Bridge # 640024 in

Wilmington NC has been evaluated based on the detectable damage by the LiBE system.

The final ratings of the test bridges are given in APPENDIX D.

Table 6-10 Nominal cover requirement based on exposure condition (Pillai and Menon 2003)

Exposure condition	Nominal cover (mm)	Remarks
Mild	20	Can be reduced by 5mm for main rebars less than 12mm dia
Moderate	30	
Severe	45	Can be reduced by 5mm if concrete grade is M35 or higher
Very Severe	50	
Extreme	75	

CHAPTER 7: CONCLUSIONS

The research conducted in this dissertation verified that remote sensing imageries, especially the LiDAR scanning technique, can provide useful bridge health related information that can be used for transportation infrastructure management. The 3-D LiDAR scanner collects surface topology data along its line-of-sight with high accuracy. Due to the ease of operation and large amount of spatial information produced, the 3-D LiDAR scanner has many potential applications in SHM. This dissertation introduced three such applications, which have been developed and integrated into the LiBE automated evaluation software system: 1) automatic bridge defect detection and quantification, 2) clearance measurement, and 3) load testing. Results from a small sample of bridges tested to date in North Carolina and California demonstrate the efficiency of LiDAR application for bridge health monitoring.

The following summarized the conclusions of this study:

- The 3D surface data cloud generated from LiDAR scan can be used to quantify visible damage volumes. Proper defect detection and quantification of bridge structure surface defects can help identify potential stability problems. The proposed damage detection approach, LiBE, can detect relatively large defect on flat surfaces.

- Distance-, gradient- and curvature-based damage quantification methods have been adopted for defective area detection. The gradient-based and curvature-based methods are good at identifying the edge of a defect, but they are weak in keeping the integrity of the defect; the distance-based method in contract is good at keeping the integrity of the defect, but weak in identifying the edge of a defect. The test result also indicated that surface curvature is more sensitive to damage.

- Using detailed remote sensing data, specific bridge damage mechanisms can be isolated allowing forensic investigation to be performed. Example using bridge # 590147 indicated that even subtle sitting (height) differentials can result in high stress concentration and induce early distress in the pile caps of a bridge substructure. LiDAR can provide realistic quantification of mass loss in case of concrete members. This information will help bridge inspector to better quantify bridge damages.

- The proposed methodologies and examples demonstrate that 3D laser scanner can be useful tools for determining bridge clearances and LiBE can be an effective technique to quantify bridge damages (Section 4.3).

- A method for bridge displacement measurement during load testing based on LiDAR scan data has been introduced. A high performance high strength steel bridge near Charlotte, NC has been studied using this method. The scan data have been used to measure the displacement of the entire bridge surface during three load scenario. The measured displacements are used to validate the construction of the highway bridge, which shows that the bridge experienced tolerable displacements under the specified loads.

- By combining the bridge component dimension measurement function, the LiDAR scan data and LiBE analysis result can be used for FE model creation and updating. A strain measurement method using the scan data is proposed at the end of this section, which shows the potential of using LiDAR techniques for structural surface strain measurement over large area. However, the strain measurement should require higher resolution LiDAR systems.

- The LiDAR scan records of bridges can provide bridge managers direct information on current conditions of the bridge. The LiDAR-based bridge measurements and evaluations are repeatable. With the utilization of LiDAR technology and an automated data processing system, bridge inspection accuracies can be improved significantly. More accurate bridge inspections and damage evaluations can lead to better maintenance decisions.

- The accuracy of the LiDAR scanner used in this dissertation has been validated and it proves that the scanner can provide bridge surface data with the accuracy as it is designed. The accuracy of the damage detection and quantification from LiBE system has also been validated. The analysis demonstrated the validity of the proposed methods.

- Gird size and scan distance did influence the quantification result of damage, but still in the allowable range.

- To get accurate measurement of the damage volume, the scanner should be placed opposite to the damage and the scan angle won't influence the quantification of damage area.

- Compared to onsite visual bridge inspection and close range photographing, remote sensing-based bridge inspection is more sensitive to noise brought by traffic, shadows, moisture, and lighting conditions. Bridge monitoring also requires that remote sensing imagery reach a certain degree of resolution in order to detect possible problems. Since different bridges have different properties, not all of the problems associate with a bridge can be identified from the top view. However, with visual access of a bridge superstructure within the range of 70 meters, the LiDAR tested and included in this project to date has demonstrated the ability of data collection and damage analysis for bridges. In summary, as an emerging inspection assistant tool, remote sensing data should be further explored with a collaborative effort by RITA, FHWA and AASHTO in order to consider standards that may promulgated for general bridge monitoring related application.

Based on the study of this dissertation, the benefits of using terrestrial LiDAR for bridge monitoring include the following points:

- LiDAR data can be used for 3D quantification for the damage on bridge surface, which is hard to be accomplished based on traditional 2D digital images.

- LiDAR data can provide the clearance value of the entire bridge surface and the minimum vertical clearance location can be easily identified using the developed LiBE system.

- LiBE can calculate the displacement of the entire bridge surface based on LiDAR data and strain can also be calculated.

- LiDAR data can be used in forensic engineering for damage reasoning.

CHAPTER 8: RECOMMENDATIONS FOR FUTURE STUDIES

Terrestrial 3D LiDAR technology provides surface 3D information with high speed and high accuracy, while most of the current sensors perform measurements only in 2D. Therefore it can be used for structural dimension measurement as well as feature quantification. The past works using 2D imageries can all be extended to 3D through LiDAR technology, which will result in more accurate assessment of structures.

The derived methodologies in this dissertation for the application of LiDAR data can also be used in satellite or airborne LiDAR-based infrastructure surface defect detection. Finding the links between surface damage and internal structure problems and implementing the results to the automatic damage detection program are the works need to be improved. With proper LiDAR-based software development, bridge inspectors could obtain the bridge structural problems just with a single scan. This will become a valuable contribution for bridge inspection, since it will be a fast, simple and accurate inspection tool. Other types of infrastructure like buildings and highways can also use laser scanner for health monitoring. The surface damages of buildings and highway pavements could be quantified. The structure displacement of buildings can also be measured.

REFERENCES

AASHTO. 1980. Guide for bridge maintenance management. American Association of State Highway and Transportation Officials, Washington, D.C.

AASHTO. 1987. AASHTO manual for bridge maintenance. American Association of State Highway and Transportation Officials, Washington, D.C.

AASHTO. 1994. A policy on geometric design of highways and streets. American Association of State Highway and Transportation Officials, Washington, D.C., 559.

Abdalla M. 2004. 3GR for Road Safety Integration of GIS, GPS, GSM and Remote Sensing, for Road Safety. Proceedings of the Eighth International Conference, Beijing, China.

Abdel-Qader I, O Abudayyeh, M ASCE, ME Kelly. 2003. Analysis of edge-detection techniques for crack identification in bridges. Journal of Computing in Civil Engineering 17(4): 255-263.

Abdel-Qader I, S Pashaie-Rad, O Abudayyeh, S Yehia. 2006. PCA-Based algorithm for unsupervised bridge crack detection. Advances in Engineering Software 37: 771-778.

Abudayyeh O, MA Bataineh, I Abdel-Qader. 2004. An imaging data model for concrete bridge inspection. Advances in Engineering Software 35(8-9): 473-480.

ACE. 2003. Engineering and design remote sensing. Department of the Army, U.S. Army Corps of Engineers, Washington, DC.

Achenbach JD. 2009. Structural health monitoring-what is the prescription. Mechanics Research Communications 36(12): 137-142.

AGA. 2007. Costs Less, Lasts Longer. American Galvanizers Association. <http://www.galvanizeit.org/images/uploads/publicationPDFs/CLLL.pdf>. (Accessed Nov.6 2009).

Ahn Y, P Shanmugam, JH Ryu, JC Jeong. 2006. Satellite detection of harmful algal bloom occurrences in Korean waters. Harmful Algae 5(2): 213-231.

Alaylioglu H and A Alaylioglu. 1997. Dynamic structural assessment of a highway bridge via hybrid FE model and in situ testing. Computers & Structures 63(3): 439-453.

Al-Qadi IL and S Lahouar. 2004. Ground penetrating radar: State of the practice for pavement assessment. Materials Evaluation 62(7): 759-763.

Al-Qadi IL and S Lahouar. 2005. Measuring rebar cover depth in rigid pavements with ground-penetrating radar. Transportation Research Record 1907: 81-85.

Amekudzi AA and R Baffour. 2002. Using Remote Sensing, Image Processing and GIS Techniques for Transportation Infrastructure and Environmental Capital Asset Management.

ASCE. 2002. Proceedings of the Seventh International Conference on Applications of Advanced Technology in Transportation, Boston Marriot, Cambridge, MA.

Anon. 1989. How to maintain local bridges at the least cost. Better Roads 59(5): 29-30.

ASCE. 2005. Report Card for America's Infrastructure-Bridges [C]. America Society of Civil Engineering.

ASCE. 2009. Infrastructure report card 2009. American Society of Civil Engineering.

ASCE/SEI-AASHTO. 2009. White Paper on Bridge Inspection and Rating. Journal of Bridge Engineering 14(1): 1-5.

ASTM. 1997. Standard test methods for measuring and compensating for emissivity using infrared imaging radiometers. American Society for Testing and Materials, E1862-97R02E01, Pennsylvania, USA.

ASTM. 2000. Standard specification for carbon and high-strength low-alloy structural steel shapes, plates, and bars and quenched-and-tempered alloy structural steel plates for bridges. American Society for Testing and Materials.

Ataei S, AA Aghakouchak, MS Marefat, S Mohammadzadeh. 2005. Sensor fusion of a railway bridge load test using neural network. Expert Systems with Applications 29: 678-683.

Au T. 1963. Elementary structural mechanics, Prentice Hall, Englewood Cliffs, New Jersey: 368-377.

Avdelidis NP, A Moropoulou, DP Almond. 2004. Passive and active thermal nondestructive imaging of materials. Electro-Optical and Infrared Systems: Technology and Applications, London, United Kingdom: 126-140.

Baba N and K Ono. 1987. Design and construction of a long span, wide trussed langer girder bridge. Annual Report of Roads: 29-42.

Benson RC. 2000. Overview of geophysical and non-destructive methods for characterization of roads and bridges. GeoDenver 2000: Use of Geophysical Methods in Construction, Denver, CO, USA.

Better Road. 2009. <http://obr.gcnpublishing.com/articles/may03c.htm>. (Accessed April 12, 2009).

Birge SL. 1985. Highway dimensions from photolog. Technical Papers, 51st Annual Meeting, ASP-ACSM Convention: Theodolite to Satellite: 29-38.

Birk RJ, T Stanley, GI Snyder, TA Hennig, MM Fladeland, F Policelli. 2003. Government programs for research and operational uses of commercial remote sensing data. Remote Sensing of Environment 88: 3-16.

Biswas P. 2004. Implement ability of the WDBN remote system for bridge integrity monitoring at the county level. Master Thesis, The University of Alabama at Birmingham, Birmingham, Alabama.

Bosch T, S Pavageau, D D'Alessandro, N Servagent, V Annovazzi-Lodi, S Donati. 2001. A low-cost, optical feedback LiDAR range-finder with chirp-control. Instrumentation and Measurement Technology Conference. Proceedings of the 18th IEEE 2: 1070-1074.

Brent RJ. 1996. Applied Cost-Benefit Analysis. Edward Elgar, Cheltenham and Lyme: 3-6.

Brinckerhoff P. 1993. Bridge Inspection and Rehabilitation: A Practical Guide. Wiley-IEEE, New York, Chapter 1: 1-11.

Brown CJ and GW Roberts. 2008. Monitoring infrastructure using global navigation satellite systems. Insight: Non-Destructive Testing and Condition Monitoring 50(10): 570-571.

Burleigh D and R Bohner. 1999. Thermal nondestructive testing (TNDT) of adhesively bonded composite reinforcements applied to concrete civil structures. Part of SPIE Conference on Nondestructive Evaluation of Bridges and Highways III, SPIE, 3587, Newport Beach, California.

Butenuth M, BM Straub, C Heipke, F Willrich. 2003. Tree supported road extraction from arial images using global and local context knowledge. Computer Vision System - Lecture Notes in Computer Science 2626/2003: 162-171.

Caceres JJ and KC Slatton. 2007. Improved classification of building infrastructure from airborne Lidar data using spin images and fusion with ground-based Lidar. Urban Remote Sensing Joint Event, Paris, France.

Cai H and W Rasdorf. 2008. Modeling road centerlines and predicting lengths in 3-D using LIDAR point cloud and planimetric road centerline data. Computer-Aided Civil and Infrastructure Engineering 23(3): 157-173.

Carrara WG, RS Goodman, RM Majewski. 1995. Spotlight synthetic aperture radar. Artech House, Boston, London.

CCRS. 2009. Fundamentals of remote sensing. Canada Centre for Remote Sensing. <http://www.ccrs.nrcan.gc.ca/resource/tutor/fundam/pdf/fundamentals_e.pdf>. (Accessed Nov. 6, 2009).

Chan THT, ZX Li, JM Ko. 2001. Fatigue analysis and life prediction of bridges with structural health monitoring data — Part II: application. International Journal of Fatigue 23(1): 55-64.

Chase SB. 2005. The role of sensing and measurement in achieving FHWA's strategic vision. Sensing Issues in Civil Structure Health Monitoring: 23-32.

Chase SB and G Washer. 1997. Non-Destructive evaluation for bridge management in the next century. Public Roads 61(1).

Chaudhuri D and A Samal. 2008. An automatic bridge detection technique for multispectral images. IEEE Transactions on Geoscience and Remote Sensing 46(9): 2720-2727.

Chen S, et al. 2007. IRSV System for Transportation Infrastructure Operations and Management. Quarterly Report. USDOT-RITA.

Chen S, E Hauser, R Eguchi, W Liu, C Rice, Z Hu, C Boyle, H Chung. 2009. Bridge Health Monitoring Using Commercial Remote Sensing. Proceeding of the 7th International Workshop on Structural Health Monitoring, Stanford, CA.

Chona R, SK Khanna, KJ Kmiec. 1995. Application of high resolution geometric Moire method to fracture problems. Experimental Techniques 19(6): 10-13.

Chung HC and M Shinozuka. 2004. Highway surface distress inspection using remote sensing. Engineering, Construction, and Operations in Challenging Environments: Earth & Space 2004, ASCE: 231-238.

Clark MR, DM McCann, MC Forde. 2003. Application of infrared thermography to the non-destructive testing of concrete and masonry bridges. NDT & E International 36: 265-275.

Consolazio GR and DR Cowan. 2003. Nonlinear analysis of barge crush behavior and its relationship to impact resistant bridge design. Computers & Structures 81(8-11): 547-557.

Corrosion Doctors. Silver Bridge Collapse. <http://www.corrosion-doctors.org/Bridges/Silver-Bridge.htm>. (Accessed Nov.6, 2009).

Czepiel E. 1995. Bridge Management Systems Literature Review and Search. ITI Technical Report, No.11, Northwestern University BIRL Industrial Research Laboratory.

Dawson M and H Shenton. 2005. Evaluation of Steel Bridge Girders Damaged by over-height Vehicle Collision. A worksheet submitted to NSF-REU, <http://www.gogetpapers.com/Essays/AASHTO_design_standards/5>. (Accessed Nov.6, 2009).

DigitalGlobe. 2009. <http://www.digitalglobe.com/index.php/82/Content+Collection+Systems>. (Accessed Nov.6, 2009).

Dunker KF and BG Rabbat. 1990. Performance of highway bridges. Concrete International 12(8): 40-42.

Dutta A and S Talukdar. 2004. Damage detection in bridges using accurate modal parameters. Finite Elements in Analysis and Design 40: 287-304.

Eguchi RT, M Eeri, B Mansouri. 2005. Use of Remote Sensing Technologies for Building Damage Assessment after the 2003 Bam, Iran, Earthquake—Preface to Remote Sensing Papers. Earthquake Spectra 21(S1): S207-S212.

Eihoz M. 2006. Use of GIS technique as decision support tool for sanitary landfill sitting. Solid Waste Technology and Management: 521-530.

Faber MH, DV Val, MG Stewart. 2000. Proof load testing for bridge assessment and upgrading. Engineer Structures 22(12): 1677-1689.

Faro Technology. 2007. FARO Laser Scanner LS 840/880.

FHWA. 2002. Bridge Inspector's Reference Manual. Federal Highway Administration, U.S. Department of Transportation, No. FHWA NHI 03-002.

FHWA. 2005. National Bridge Inspection Standard. Federal Highway Administration. U.S. Department of Transportation, No. FHWA-2001-8954.

Felkel JP, DC Rizos, PH Ziehl. 2007. Structural performance and design evaluation of HPS 70W bridge girders. J. Constructional Steel Res. v63: 909-921.

Filho JNO, YY Su, H Song, LY Liu, YMA Hashash. 2005. Field tests of 3D laser scanning in urban excavation. International Conference on Computing in Civil Engineering, ASCE, Cancun, Mexico.

Frýba L and M Pirner. 2001. Load tests and modal analysis of bridges. Engineering Structures 23(1): 102-109.

Forzieri G, M Gardenti, F Caparrini, F Castelli. 2008. A methodology for the pre-selection of suitable sites for surface and underground small dams in arid areas: A case study in the region of Kidal, Mali. Physics and Chemistry of the Earth, Parts A/B/C 33(1-2): 74-85.

Fratini M, M Pieraccini, D Dei, F Parrini, G Bartoli, C Atzeni. 2007. An experimental comparison of Interferometric radar vs. accelerometers for monitoring of large structures. 4th European Radar Conference, EURAD, Munich, Germany: 99-102.

Fuchs PA, GA Washer, SB Chase, M Moore. 2004a. Application of Laser-Based Instrumentation for Highway Bridges. Journal of Bridge Engineering 9(6): 541-549.

Fuchs PA, GA Washer, SB Chase, M Moore. 2004b. Laser-based Instrumentation for Bridge Load testing. Journal of Performance of constructed facilities 18(4): 213-219.

Fu CC, JR Burhouse, GL Chang. 2004. Overheight vehicle collisions with highway bridges. Transportation Research Record (TRB) No. 1865: 80-88.

Gafy ME and Y Abdelrazig. 2004. Remote Sensing Framework for Transportation Infrastructure Environment Assessment. Proceedings of the Ninth Biennial ASCE Aerospace Division International Conference on Engineering, Construction, and Operations in Challenging Environments. League City/Houston, TX.

Gentile C and N Gallino. 2008. Ambient vibration testing and structural evaluation of an historic suspension footbridge. Advances in Engineering Software 39(4): 356-366.

GeoEye. 2009. <http://www.geoeye.com/CorpSite/corporate/>. (Accessed Nov.6, 2009).

Ghose MK, AK Dikshit, SK Sharma. 2006. A GIS-based transportation model for solid waste disposal - a case study on Asansol municipality. Waste Management 26: 1287-1293.

Girardeau-Montaut D, M Roux, R Marc, G Thibault. 2005. Change detection on points cloud data acquired with a ground laser scanner. Workshop "Laser scanning 2005", Enschede, the Netherlands.

Glantz P, ED Nilsson, W Hoyningen-Huene. 2009 Estimating a relationship between aerosol optical thickness and surface wind speed over the ocean. Atmospheric Research 92(1): 58-68.

Glennie C. 2007. A kinematic terrestrial LIDAR scanning system. 20th International Technical Meeting of the Satellite Division of The Institute of Navigation 2007, ION GNSS 2007, Fort Worth, TX, United states.

Google Earth. <http://earth.google.com/>. (Accessed Nov.6, 2009).

Grivas DA, BC Schultz, G Mason. 1997. A framework for using satellite and airborne remote sensing technology in infrastructure performance assessment. Proceedings of the 1997 Speciality Conference on Infrastructure Condition Assessment: Art, Science, Practice, ASCE, Boston, MA, USA.

Guralnick SA and ES Suen. 1991. Real-time inspection of pavement by Moire patterns. Applications of Optical Engineering: Proceedings of OE/Midwest '90, Rosemont, IL, USA: 664-677.

Han Y, H Zheng, Q Cao, Y Wang. 2007. An effective method for bridge detection from satellite imagery. 2nd IEEE Conference on Industrial Electronics and Applications, Harbin, China: 2753-2757.

Harik IE, AM Shaaban, H Gesund, GYS Valli and ST Wang. 1990. United States bridge failures 1951-1988. Journal of performance of constructed facilities 4(4): 272-77.

Hassan M, O Burdet, R Favre. 1995. Ultrasonic measurements and static load tests in bridge evaluation. NDT & E International 28(6): 331-337.

Herold M, DA Roberts, ME Gardner, PE Dennison. 2004. Spectrometry for urban area remote sensing—Development and analysis of a spectral library from 350 to 2400 nm. Remote Sensing of Environment 91(3-4): 304-319.

Herold M and D Roberts. 2005. Spectral characteristics of asphalt road aging and deterioration: Implications for remote-sensing applications. Applied Optics 44(20): 4327-4334.

Herold M, ME Gardner, V Noronha, A Dar, DA Roberts. 2006. Pectrometry and hyperspectral remote sensing of urban road infrastructure. Online journal of space communication. <http://satjournal.tcom.ohiou.edu/Issue03/abst_herold.html>. (Accessed May 6, 2009).

Hinz S and A Baumgartner. 2000. Road extraction in urban areas supported by context objects. International Archives of Photogrammetry and Remote Sensing 33(B3/1): 405-412.

Hinz S and A Baumgartner. 2003. Automatic Extraction of Urban Road Networks from Multi-View Aerial Imagery. ISPRS Journal of Photogrammetry and Remote Sensing 58(1-2): 83-98.

Horberry T, M Halliday, AG Gale. 2002. Bridge strike reduction: optimizing the design of markings. Accident Analysis & Prevention 34: 581-588.

Hite MC, R Desroches, RT Leon. 2006. Evaluation of the performance of bridge steel pedestals under seismic loads. Structures Congress 2006, St. Louis, MO, United States: 171.

Huertas A and R Nevatia. 2000. Detecting changes in aerial views of manmade structures. Image Vis. Comput. 18(8): 583-596.

Huston DR. 1999. Ground penetrating radar for concrete bridge health monitoring applications. Proceedings of 1999 Nondestructive Evaluation of Bridges and Highways III 3587: 170-179.

Idriss RL, KR White, SP Chang. 1995. Evaluation and testing of a fracture critical bridge. NDT & E International 28(6): 339-347.

INRS. 2009. Low cost high-precision LiDAR range finder (LRF). Institut national de la recherché scientifique.

InSiteful Imagery. 2007. <http://www.insitefulimagery.com/about.htm>. (Accessed May 6, 2009).

Jandu AS. Inspection and Maintenance of Highway Structures in England. Bridge Engineering 161 (BE3): 111-114.

Jelalian AV. 1992. Laser radar systems. Artech House, Boston, London.

Jensen J and D Cowen. 1999. Remote sensing of Urban/Suburban infrastructure and socio-economic attributes. Photogrammetric Engineering & Remote Sensing 65(5): 611-622.

Jiang JJ, XZ Lu, JQ Guo. 2002. Study for real-time monitoring of large-span bridge using GPS. Progress in Safety Science and Technology, Taian, China: 308-312.

Jiang R, DV Jáuregui, and K White. 2008. Close-range photogrammetry applications in bridge measurements: literature review. Measurement 41: 823-834.

Jivacate I and FT Najafi. 2003. The Current Status of Bridge Management Systems. Proceedings of Canadian Society for Civil Engineering Annual Conference, Moncton, NB, Canada: 1622-1631.

Kayen R, RT Pack, J Bay, S Sugimoto, H Tanaka. 2006. Terrestrial-LIDAR visualization of surface and structural deformations of the 2004 Niigata Ken Chuetsu, Japan, earthquake. Earthquake Spectra 22(S1): S147-S162.

Keskinen A. 2007. Mapping road infrastructure in developing countries applying remote sensing and GIS-The case of the Taita Hills, Kenya. Master Dissertation, Deparment of Geography. Helsinki, University of Helsinki.

Kim KH, JH Lee, BG Lee. 1997. Congestion data acquisition using high resolution satellite imagery and frequency analysis techniques. International Geoscience and Remote Sensing Symposium (IGARSS), Singapore: 331-334.

Klowak C, A Memon, A Mufti. 2006. Static and fatigue investigation of second generation steel-free bridge decks. Cement and Concrete Composites 28(10): 890-897.

Klowak CS and AA Mufti. 2009. Behaviour of bridge deck cantilever overhangs subjected to a static and fatigue concentrated load. Construction and Building Materials 23(4): 1653-1664.

Ko JM and YQ Ni. 2005. Technology developments in structural health monitoring of large-scale bridges. Engineering Structures 27: 1715–1725.

Lee JJ and M Shinozuka. 2006. A vision-based system for remote sensing of bridge displacement. NDT & E International 39(5): 425-431.

Lefevre RJ. 2000. Radar bridge clearance sensor. IEEE 2000 International Radar Conference, Alexandria, VA, USA, 660-665.

Lichti DD and SJ Gordon. 2004. Error propagation in directly georeferenced terrestrial laser scanner point clouds for cultural heritage recording. WSA2 Modeling and Visualization, Athens, Greece.

Liu M and DM Frangopol. 2004. Optimal bridge maintenance planning based on probabilistic performance prediction. Engineering Structures 26(7): 991-1002.

Liu W. 2008. Logistic Study for the Application of Remote Sensing in Bridge Management. EMGT 6920 & INES 8090 Logistics Engineering and Management Class Term Project Report, UNC Charlotte.

Liu W, S Chen, E Hauser. 2009. Remote sensing for bridge health monitoring. SPIE Optics + Photonics, San Diego, California, No.7456-13.

Lomenie N, J Barbeau, R Trias-Sanz. 2003. Integrating textural and geometric information for an automatic bridge detection system. 2003 IGARSS: Learning From Earth's Shapes and Colours, Toulouse, France: 3952-3954.

Luo Y, Y Xue, SB Zhong. 2005. Road extraction from IKONOS image using Grid computing platform. International Geoscience and Remote Sensing Symposium (IGARSS), Seoul, South Korea IEEE.

Lwin MM. 2006. The important roles of bridge maintenance and management on transportation safety and efficiency. Proceedings of the 3rd International Conference on Bridge Maintenance, Safety and Management - Bridge Maintenance, Safety, Management, Life-Cycle Performance and Cost. Washington, DC: 47-51.

Maser KR. 1995. Evaluation of bridge decks and pavements at highway speed using ground-penetrating radar. Nondestructive Evaluation of Aging Bridges and Highways, SPIE, Oakland, CA, USA.

Merkle WJ and JJ Myers. 2006. Load testing and load distribution response of Missouri bridges retrofitted with various FRP systems using a non-contact optical measurement system. Transportation Research Board 85th Annual meeting, Washington, D.C.

Mertz DR. 2001. Trends in design and construction of steel highway bridges in the United States. Prog. Struct. Engrg, Mater v3: 5-12.

Miceli M, J Duke, M Horne. 2003. Thermal infrared inspection of FRP bridge decks for health monitoring. Thermosense XXV 5073: 328-338.

Morain SA. 2002. Critical Infrastructure Protection Using Image Intelligence from Space-based and Aerial Sensors. ASME International Mechanical Engineering Congress and Exposition, New Orleans, LA: 159-168.

Moropoulou A. 2002. Infrared thermography and ground penetrating radar for airport pavements assessment. Nondestructive Testing and Evaluation 18(1): 37-42.

Moulton LK, H GangaRao, GT Halvorsen. 1985. Tolerable movement criteria for highway bridges. U.S. Department of Transportation, Federal Highway Administration, No. FHWA-RD-85-107, McLean, Virginia.

Nassif HH, M Gindy, J Davis. 2005. Comparison of LiDAR Doppler vibrometer with contact sensors for monitoring bridge deflection and vibration. NDT & E International 38(3): 213-218.

NCDOT. 2000. Bridge policy. North Carolina Department of Transportation: Highway Design Branch / Design Services Unit. <http://www.ncdot.org/doh/preconstruct/altern/value/manuals/>. (Accessed Nov. 6, 2009).

NCDOT. 2007. NC Bridge Information. North Carolina Department of Transportation. <http://www.ncdot.org/doh/operations/dp_chief_eng/maintenance/bridge/>. (Accessed April 12, 2009).

NCHRP (National Cooperative Highway Research Program). 1998. Manual for Bridge Rating Through Load Testing. Research Result Digest 234, Transportation Research Board, Washington, D.C.

NCDOT TSG. 2007. Annual Average Daily Traffic Volume-2007 spreadsheet. Traffic Survey Group. <http://www.ncdot.org/doh/preconstruct/tpb/traffic_survey/>. (Accessed Nov. 6, 2009).

NCRST. 2000. National Consortia on Remote Sensing in Transportation. <http://www.ncgia.ucsb.edu/ncrst/research/ncgia.html>. (Accessed Nov. 6, 2009).

Neves LC, DM Frangopol, PJS Cruz. 2006. Multi-Objective Probabilistic Optimization of Bridge Lifetime Maintenance: Novel Approach. Proceedings of the 3rd International Conference on Bridge Maintenance, Safety and Management - Bridge Maintenance, Safety, Management, Life-Cycle Performance and Cost, Washington, DC: 539-541.

Nowak AS, S Kim, PR Stankiewicz. 2000. Analysis and diagnostic testing of a bridge. Computers & Structures 77(1): 91-100.

NSTPRSC. 2007. Transportation for Tomorrow: Report of the National Surface Transportation Policy and Revenue Study Commission. National Surface Transportation Policy and Revenue Study Commission.

NSTIFC. 2009. Paying Our Way. Report of the National Surface Transportation Infrastructure Financing Commission, National Surface Transportation Infrastructure Financing Commission.

Orban Z and M Gutermann. 2009. Assessment of masonry arch railway bridges using non-destructive in-situ testing methods. Engineering Structures 31(10): 2287-2298.

OMB. 2009. Budget assumptions, OMB Circular No. A-94. Office of Management and Budget. <http://www.whitehouse.gov/omb/circulars/a094/a94_appx-c.html>. (Accessed Nov. 6, 2009).

Owen E. Montreal bridge collapse: design and inspection criticized. <www.nce.co.uk/.../196733.article>. (Accessed Apr. 12, 2009).

Papaelias MP, C Roberts, CL Davis. 2008. A review on non-destructive evaluation of rails: state-of-the-art and future development. Proceedings of the Institution of Mechanical Engineers, Part F: Journal of Rail and Rapid Transit 222: 367-384.

Parcharidis I, M Foumelis, P Kourkouli, U Wegmuller, E Lagios, V Sakkas. 2008. Continuous risk assessment of structures in areas of ground deformation susceptibility by persistent scatterers InSAR: Preliminary result of the Rio-Antirio bridge (Greece). Fringe 2007 Workshop "Advances in SAR Interferometry from Envisat and ERS Missions", Frascati, Italy.

Parekh IR. 1986. Comprehensive Bridge Posting Policy. Transportation Research Record 1083: 35-45.

Park JH, JT Kim, R Yeon-Sun, JM Lee. 2007. Monitoring Cracks and Prestress-Loss in PSC Girder Bridges Using Vibration-based Damage Detection Techniques. Proc. of SPIE 6532: 65321V.

Park JH, R Tateishi, K Wikantika, JG Park. 1999. Potential of high resolution remotely sensed data for urban infrastructure monitoring. Proceedings of the 1999 IEEE International Geoscience and Remote Sensing Symposium, Hamburg, Ger. 2(1999): 1137-1139.

Patricio MA and D Maravall. 2007. A novel generalization of the gray-scale histogram and its application to the automated visual measurement and inspection of wooden pallets. Image and Vision Computing 25: 805-816.

Pedersen PT, S Valsgård, D Olsen, S Spangenberg. 1993. Ship impacts: Bow collisions. International Journal of Impact Engineering 13(2): 163-187.

Perera SC. 1995. Integration of Remote Sensing Data with GIS Technology for the Acceleration of the Activities in National Mapping Agencies. Asian Conference on Remote Sensing.

Pieraccini M, G Luzi, D Mecatti, M Fratini, L Noferini, L Carissimi, G Franchioni, C Atzeni. 2004. Remote sensing of building structural displacements using a microwave interferometer with imaging capability. NDT & E International 37(7): 545-550.

Pieraccini M, L Noferini, D Mecatti, C Atzeni, G Teza, A Galgaro, N Zaltron. 2006. Integration of radar interferometry and laser scanning for remote monitoring of an urban site built on a sliding slope. IEEE Transactions on Geoscience and Remote Sensing 44(9): 2335-2342.

Pieraccini M, F Parrini, M Fratini, C Atzeni, P Spinelli, M Micheloni. 2007. Static and dynamic testing of bridges through microwave interferometry. NDT&E International 40: 208-214.

Pieraccini M, M Fratini, F Parrini, C Atzeni, G Bartoli. 2008. Interferometric radar vs. accelerometer for dynamic monitoring of large structures: An experimental comparison. NDT & E International 41(4): 258-264.

Pillai SU, D Menon. 2003. Reinforced concrete design. Tata McGraw-Hill. Delhi. 169-179.

Qiao P, M Yang, MS Ayman. 2004. Impact analysis of I-Lam sandwich system for over-height collision protection of highway bridges. Engineering Structures 26(7): 1003-1012.

Quiñones-Rozo CA, YMA Hashash, LY Liu. 2008. Digital image reasoning for tracking excavation activities. Automation in Construction 17(5): 608-622.

Ramey GE, AR Wolff, RL Wright. 1997. DOT management actions to enhance bridge durability/longevity. Practice Periodical on Structural Design and Construction 2(3): 125-130.

Ribarsky W, E Hauser, SE Chen, W Tolone, SW Lee, R Chang, W Liu, R Vatcha, X Wang. 2009. Integrated Remote Sensing and Visualization (IRSV) System for Transportation Infrastructure Operations and Management. Poster Presentation, Transportation Research Board Annual Meeting, Washington D.C.

Righiniotis TD. 2004. Simplified calculations involving the maximum load on bridge fatigue details under inspection. Part I: Fracture. Journal of Constructional Steel Research 60: 809-824.

Rizzo P, I Bartoli, FL Scalea, S Coccia, M Fateh. 2005. High-speed defect detection in rails by non-contact guided ultrasonic testing. Health Monitoring and Smart Nondestructive Evaluation of Structural and Biological Systems IV San Diego, CA, USA: 274-284.

Roberts GW, CJ Brown, X Meng, PRB Dallard. 2007. Using GPS to measure the deflections and frequency responses of the London Millennium bridge. Bridge Design, Construction and Maintenance - Proceedings of the two-day International Conference organized by the Institution of Civil Engineers, ICE, Beijing, China: 487-496.

Roberts GW, XL Meng, M Meo, A Dodson, E Cosser, E Iuliano, A Morris. 2003. A remote bridge health monitoring system using computational simulation and GPS sensor data. Proceedings of the 11th FIG Symposium on Deformation Measurements, Santorini, Greece.

Roberts RL. 2004. Determining the depth of reinforcing bars in a concrete structure using electromagnetic signals. U.S. Patent 6772091.

Rodriguez-Valverde MA, P Ramon-Torregrosa, A Paez-Duenas, MA Cabrerizo-Vilchez, R Hidalgo-Alvarez. 2008. Imaging Techniques Applied to Characterize Bitumen and Bituminous Emulsions. Advances in Colloid and Interface Science 136: 93-108.

Rolander DD, BM Phares, BA Graybeal, ME Moore, GA Washer. 2001. Highway Bridge Inspection: State-of-the-Practice Survey. Transportation Research Record N1794: 73-81.

Roper WE and S Dutta. 2006. Oil Spill and Pipeline Condition Assessment Using Remote Sensing and Data Visualization. Sixth Biennial Fresh Water Spill Symposium, Portland, OR.

Rosati G, G Boschetti, A Biondi, A Rossi. 2009. Real-time defect detection on highly reflective curved surfaces. Optics and Lasers in Engineering 47(3-4): 379-384.

Ryu HK, YJ Kim, SP Chang. 2007. Crack control of a continuous composite two-girder bridge with prefabricated slabs under static and fatigue loads. Engineer Structures 29(6): 851-864.

Sabins FF. 1997. Remote Sensing: Principles and Interpretation. New York: W. H. Freeman & Co. Price: xiii + 494.

Sakagami T, S Kubo, S Nakamura, Y Kawashima, T Komiyama. 2002. Application of lock-in data processing for thermographic NDT of concrete structures. Proceedings of SPIE 4710: 552-7.

Sasmal S and K Ramanjaneyulu. 2008. Condition evaluation of existing reinforced concrete bridges using fuzzy based analytic hierarchy approach. Expert Systems with Applications 35(3): 1430-1443.

Saxena A. 2001. Monitoring of urban infrastructure in cities and its fringe areas through remote sensing. Proceeding of the 22nd Asian Conference on Remote Sensing, Singapore.

Scheer J. 2000. Versagen von Bauwerken, Band 1: Brücken, Ernst & Sohn, Berlin.

Schulz K, E Cadario, H Gross, H Hammer, A Thiele, U Thoennessen, U Soergel, D Weydahl. 2007. Detection and feature extraction of bridges in airborne and spaceborne SAR image data. Proceedings of SPIE 6749: 67490U.

Senthilvasan J, DP Thambiratnam, GH Brameld. 2002. Dynamic response of a curved bridge under moving truck load. Engineer Structures 24(10): 1283-1293.

Sgrenzaroli M. 2005. Cultural heritage 3D reconstruction using high resolution laser scanner: new frontiers data processing. CIPA 2005 XX International Symposium, Torino, Italy.

Sharma H, S Hurlebaus, P Gardoni. 2008. Development of a bridge bumper to protect bridge girders from overheight vehicle impacts. Computer-Aided Civil and Infrastructure Engineering 23: 415-426.

Shin H and DA Grivas. 2003. How Accurate Is Ground-Penetrating Radar for Bridge Deck Condition Assessment? Transportation Research Record 1845: 139-147.

Shinozuka M and K Loh. 2004. Remote Sensing with the Synthetic Aperture Radar (SAR) for Urban Damage Detection. Proceedings of the Ninth Biennial ASCE Aerospace Division International Conference on Engineering, Construction, and Operations in Challenging Environments, League City/Houston, TX.

Shrive NG. 2005. Intelligent Structural Health Monitoring: A civil engineering perspective. IEEE International Conference on Systems, Man and Cybernetics, Waikoloa, HI, United States IEEE.

Simonetto E and H Oriot. 1999. 3D extraction from airborne SAR imagery. Proceedings of the 1999 Remote Sensing for Earth Science, Ocean, and Sea Ice Applications, Florence, Italy SPIE.

Sivakumar B, F Moses, G Fu, M Ghosn. 2007. Legal truck loads and AASHTO legal loads for posting. Transportation Research Board 575: 82.

Soergel U, A Thiele, H Gross, U Thoennessen. 2007. Extraction of bridge features from high-resolution InSAR data and optical images. Urban Remote Sensing Joint Event, Paris, France.

Stewart MG. 2001. Reliability-based assessment of ageing bridges using risk ranking and life cycle cost decision analyses. Reliability Engineering & System Safety 74(3): 263-273.

Stoeckeler EG. 1970. Use of aerial color photography for pavement evaluation studies. Highway Res. Record 319: 40-57.

Stramondo S, C Bignami, M Chini, N Pierdicca, A Tertulliani. 2006. Satellite radar and optical remote sensing for earthquake damage detection: results from different case studies. International Journal of Remote Sensing 27: 4433-4447.

Tarchi D, H Rudolf, M Pieraccini, C Atzeni. 2000. Remote monitoring of buildings using a ground-based SAR: Application to cultural heritage survey. International Journal of Remote Sensing 21(18): 3545-3551.

Teza G, A Galgaro, F Moro. 2009. Contactless recognition of concrete surface damage from laser scanning and curvature computation. NDT&E International 42: 240-249.

Thompson PD and JO Sobanjo. 2003. Florida DOT project-level bridge management models. Journal of Bridge Engineering 8(6): 345-352.

TRB. 2000. Conference: Remote Sensing for Transportation. Transportation Research Board, Washington, D.C. <http://onlinepubs.trb.org/Onlinepubs/conf/reports/remote_sensing_1.pdf>. (Accessed Nov.6, 2009).

Tralli DM, RG Blom, V Zlotnicki, A Donnellan, DL Evans. 2005. Satellite remote sensing of earthquake, volcano, flood, landslide and coastal inundation hazards. ISPRS Journal of Photogrammetry and Remote Sensing 59(4): 185-198.

Tsai MY, YC Chen, SWR Lee. 2008. Correlation between Measurement and Simulation of Thermal Warpage in PBGA With Consideration of Molding Compound Residual Strain. Components and Packaging Technologies, IEEE Transactions on 31(3): 683-690.

Uddin W. 2002. Evaluation of airborne LiDAR digital terrain mapping for highway corridor planning and design. Pecora 15/ Land Satellite information IV/ ISPRS Commission I/FIEOS, American Society for Photogrammetry & Remote Sensing, Denver.

University of Cambridge. Bridge failure database. <http://www.bridgeforum.com/dir/collapse/type/unknown.html>. (Accessed Nov.6, 2009).

U.S. Census Bureau. 2000. North Carolina County- Population, Housing Units, Area, and Density. <http://factfinder.census.gov/servlet/GCTTable?ds_name=DEC_2000_SF1_U&geo_id=04000US37&_box_head_nbr=GCT-PH1&format=ST-2>. (Accessed Nov.6, 2009).

UTC. 2001. 4th National Transportation Asset Management Workshop. Midwest Regional University Transportation Center, Madison, WI. <http://www.mrutc.org/outreach/workshop/program/>. (Accessed Nov.6, 2009).

Wang L, L Yang, D Huang, Z Zhang, G Chen. 2008. An impact dynamics analysis on a new crashworthy device against ship–bridge collision. International Journal of Impact Engineering 35(8): 895-904.

Wang ML, G Heo, D Satpathi. 1997. Dynamic characterization of a long span bridge: A finite element based approach. Soil Dynamics and Earthquake Engineering 16(7-8): 503-512.

Washer GA. 1998. Developments for the non-destructive evaluation of highway bridges in the USA. NDT & E International 31(4): 245-9.

Washer GA, R Fenwick, N Bolleni, J Harper, S Alampalli. 2008. Thermal Imaging for Bridge Inspection and Maintenance. Tenth International Conference on Bridge and Structure Management, Transportation Research Board.

Wasserman E and H Pate. 2000. Tennessee's experience with high performance steel: an owner's prospective. Steel Bridge Design and Construction for the new Millennium with Wmphasis on High Performance Steel: Conference Proceedings, Lincoln, NE, National Bridge Research Organization: 138-145.

Weil GJ. 1998. Remote sensing of voids in large concrete structures: Runways, taxiways, roads, bridges, & building walls & roofs. Proceedings of SPIE - The International Society for Optical Engineering 3436(n1): 305-316.

Welch R. 1974. Skylab-2 Photo Evaluation. Photogrammetric Engineering and Remote Sensing 40: 1221-1224.

Welch R. 1976. Skylab S-190B ETC Photo Quality. Photogrammetric Engineering and Remote Sensing 42: 1057-1060.

Welch R. 1982. Spatial resolution requirements for urban studies. International Journal of Remote Sensing 3(2): 139-146.

Wong KY, KL Man, WY Chan. 2001. Application of global position system to structural health monitoring of cable-supported bridges. Proc. SPIE 4337: 390.

Wu F. 2005. Recognition of bridges by integrating satellite SAR and optical imagery. 2005 IEEE International Geoscience and Remote Sensing Symposium, Seoul, Korea, Republic of: 3939-3941.

Yang Y, H Ma, V Song. 2006. Automated targets detection based on level set evolution using radar and optical imagery. Geoinformatics 2006: Remotely Sensed Data and Information, Wuhan, China.

Yao L, P Yao, R Wang, X Meng. 2008. GPS-based dynamic monitoring and analysis of Nanpu bridge deformation. Journal of Tongji University 36(12): 1633-1636+1664.

Yehia S, O Abudayyeh, I Abdel-Qader, A Zalt. 2008. Ground-penetrating radar, chain drag, and ground truth: Correlation of bridge deck assessment data. Transportation Research Record 2044: 39-50.

Yelf R and A Carse. 2000. Audit of a road bridge superstructure using ground penetrating radar. The 8th International Conf. on Ground Penetrating Radar, Goldcoast: 249-254.

Zhang R and E Aktan. 2005. Design considerations for sensing system to ensure data quality. Sensing Issues in Civil Structure Health Monitoring: 281-290.

Zhao Z and C Chen. 2001. Concrete bridge deterioration diagnosis using fuzzy inference system. Advances in Engineering Software 32(4).

APPENDIX A: BRIDGE REPAIR PLAN OF MECKLENBURG COUNTY IN NCDOT
2007-2013 STIP (NCDOT 2007)

Location	Year Built	Right of way	Construction	Total	
Mallard Creek No.147	1938	$300	$3,400	$3,700	Mecklenburg: Average cost per bridge-$1,173.5 (Thousand Dollar)
Mcintyre creek No.134	1958	$5	$330	$336	
Gar Creek No. 100	1960	$40	$500	$540	
Reedy Creek No. 177	1970	$100	$750	$850	
Irvins Creek No. 36	1953	$230	$1,010	$1,240	
Creasy creek No. 38	1945	$25	$350	$375	
Broad Creek No.51	1925	$210	$600	$810	Beaufort: Average cost per bridge-$1,299.7 (Thousand Dollar)
Pungo Creek No. 43	1925	$90	$900	$990	
Broad Creek No. 104	1953	$31	$1,600	$1,631	
Runyon Creek No. 103	1947	$225	$4,900	$5,175	
Pungo Creek No. 21	1939	$80	$1,000	$1,080	
Jack Creek No.59	1949	$50	$560	$613	
Aggie Run No.5	1974	$150	$1,650	$1,801	
Durham Creek No.42	1966	$50	$526	$593	
Blounts Creek No.81	1972	$50	$526	$593	
Horse Branch Creek No. 67	1965	$225	$900	$1,133	
Chocowinity Creek No. 68	1966	$272	$950	$1,230	
Chocowinity Creek No. 69	1964	$50	$985	$1,040	
Tranters Creek No.8	1935	$180	$3,150	$3,337	
Latham Creek No.84	1962		$1,100	$1,100	
Tranters Creek No. 90	1970		$1,640	$1,640	
Big Swamp No.6	1971	$70	$1,185	$1,360	
Big Swamp No.272	1959		$600	$600	
Canal No.140	1962	$90	$1,150	$1,240	
Bath Creek No.135	1967	$50	$650	$711	
Creek No. 39	1969	$25	$825	$850	
Horsepen Swamp No. 40	1966	$35	$410	$450	
Durham Creek No.14	1966	$50	$560	$618	
US 64-221 No.117	1956	$2,200	$4,400	$6,600	Rutherford County: Average cost per bridge - $1,828.5 (Thousand Dollar)
Broad River No.7	1925	$1,000	$2,000	$3,000	
Broad River No.87	1926	$300	$3,400	$3,700	
Broad River No.270	1917	$35	$2,139	$2,174	
Creek No.526	1970	$50	$1,050	$1,100	
Fork of Cathy's Creek No. 37	1952	$150	$2,100	$2,252	
Creek No.217	1952	$90	$750	$840	
Holland's Creek No.35	1952	$50	$560	$610	
Cathey's Creek No.41	1963	$60	$850	$911	
Clinchfield Railroad	1950	$50	$650	$700	

No. 69				
Puzzle Creek No.76	1967	$180	$1,800	$1,981
Webb Creek No. 351	1950	$5	$525	530
First Broad River No.202	1952	$30	$1,150	$1,180
Creek No.32	1952	$90	$1,150	$1,240
Floyds Creek No. 144	1950	$50	$560	$610

APPENDIX B: STATISTIC OF BRIDGE FAILURE IN THE U.S. AFTER 1967
(CORROSION DOCTORS; UNIVERSITY OF CAMBRIDGE; FHWA 2002; SCHEER
2000)

Bridge Name	Location	Built Year	Collapse year	Reason	Type
U.S. Highway 35 Silver Bridge	West Virginia and Kanauga, Ohio. Across Ohio river.	1928	1967	Fatigue cracking (FCM)	Steel
Chesapeake Bay Bridge	Annapolis		1970	Ship Impact	
Kaslaski River Bridge	Illinois		1970	Design error	
Motorway bridge	Junction Antelope Valley		1971	Earthquake	
Sidney-Lanier Bridge	Brunswick, Georgia		1972	Ship Impact	
Chesapeake Bay Bridge	Annapolis		1972	Ship Impact	
Motorway bridge	near Pasadena, California	1972	1972	Design error	
Lake Pontchartrain bridge	Lake Pont		1974	Ship Impact	
Lafayette Street bridge	St-Paul, Minnesota	1905	1975	Brittle failure of new steel	
Fulton Yates Bridge	Henderson, Kentucky		1976	Overloading during refurbishment	
Pass Manchac Bridge	Louisiana		1976	Ship Impact	
Bridge over Passiac River	Union Avenue		1977	Ship Impact	
Benjamin Harrison Memorial Bridge	Hopewell, Virginia		1977	Ship Impact	
Southern Pacific Railroad Bridge	Louisiana		1978	Ship Impact	
Interstate 17 Bridge	Black Canyon, Arizona		1978	Flood	
Southern Rail Bridge	Indiana	1910	1979	Overload	
Interstate 10 Bridge	Phoenix, Arizona		1979	Flood	
bridge near Rockford	Rockford		1979	Design error	Concrete
Bridge over the	Washington		1979	Wind and

Hood canal				storm	
Alabama Rail Bridge	Alabama		1979	Train Impact	
Truss bridge in Trenton	Wisconsin (Milwaukee River)		1980	Truck Impact	
Sunshine Skyway Bridge	St.Petersburg, Florida		1980	Ship Impact	
Syracuse bridge	New York		1982	Design Error	
Saginaw bridge	Saginaw		1982	Design Error	
bridge in East Chicago	Indianapolis		1982	Design Error	
Connecticut Turnpike Bridge	Greenwich (Mianus River)	1958	1983	Fatigue cracking (FCM)	Steel
Walnut street viaduct over Interstate 20	Denver, Colorado		1985	Design Error	
Schoharie Bridge	New York		1987	Flood and Storm	
Bridge in El Paso	Texas		1987	Design Error	
Motorway bridge near Seattle			1988	Design Error	
Truss bridge in Shepherdsville	Kentucky		1989	Truck Impact	
San Francisco Oakland Bay Bridge	California		1989	Earthquake	
Cypress Freeway	Oakland, California		1989	Earthquake	
Bridge in Baltimore			1989	Design Error	
bridge in Los Angeles	Los Angeles		1989	Design Error	Box girder
Herbert C. Bonner Bridge	North Carolina		1990	Ship Impact	
Motorway bridge	junction Antelope Valley		1992	Earthquake	
Truss bridge near Mobile	Alabama		1993	Ship Impact	
Truss bridge in Concord	New Hampshire		1993	Construction Error	
Interstate 5 Bridge	Los Angeles, California		1994	Earthquake	
Twin bridges, Interstate 5	(Arroyo Pasajero River), Coalinga, California		1995	Scour of Foundation	
composite bridge	Clifton		1995	Construction	

	(Tennessee River)			Error	
Walnut Street Bridge	Harrisburg, Pennsylvania (Susquehanna River)		1996	Scour and Ice damage	
Bridge over Hatchie River	Covington, Tennessee		1999	Scouring and undermining of the foundations	
Concord pedestrian bridge	Concord, NC	1995	2000	Deterioration	Concrete
Queen Isabella Causeway	Texas		2001	Ship Impact	
Tewksbury Township pony truss bridge	Hunterdon County, New Jersey		2001	Truck Impact	
Turkey Creek Bridge	Sharon Springs, Kansas		2002	Fire	
Marcy bridge			2002	Design Error	
Interstate 40 Bridge	Oklahoma (Webber Falls)		2002	Ship Impact	
Highway 14 overpass, 60 miles south of Dallas	Texas (over Interstate 45)		2002	Truck Impact	
Imola Avenue Bridge	Napa, California		2003	Construction Error	
Kinzua Viaduct	North-central Pennsylvania	1900	2003	Tornado	steel bridge
West Grove Bridge	Silver Lake, Kansas		2004	Train Impact	
Shannon Hills Drive Bridge	Arkansas		2004	Overload	
Rural bridge near Shelby	North Carolina (Beaver Dam creek)		2004	Washed out	
McCormick County bridge	east of Mount Carmel (Little river), South Carolina		2004	Debris	
Lee Roy Selmon Expressway	Tampa Bay, Florida		2004	Flood	
Interstate 95 Bridge	Bridgeport, Connecticut		2004	Impact	
Interstate 70 Bridge	Denver, Colorado		2004	Design Error	
Interstate 20	Pecos, Texas (Salt		2004	Flood	

Bridge	Draw River)				
Interstate 10 Bridge	Escambia Bay, Florida		2004	Hurricane	
Bridge northwest of Norcatur	(Sappa Creek), Kansas		2004	Overload	
Bridge near Pawnee City	Nebraska		2004	Design Error	
Wooden bridge in Pico Rivera	California		2005	Fire	
Laurel Mall Pedestrian Bridge	between the parking and shopping areas		2005	Deterioration	
Interstate 70 Lake View Drive Bridge	Washington County (Pennsylvania)		2005	Deterioration	
I35-W bridge	Minneapolis		2007	Deterioration	
K&I bridge	Indiana		2008	Aged and debris	

APPENDIX C: LiBE CLEARANCE MEASUREMENTS FOR THE 20 SELECTED
BRIDGES AND CORRESPONDING RATINGS

Bridge Number	Sufficiency Rating	Type	Bridge over	Clearance Inventory (m)	LiBE Measured (m)	Clearance Rating
590084	82.1	PPC Cored Slab	Green way & Water	---	---	---
590140	77.5	RC Girder	Green way & Water	---	---	---
590147	47.5	RC Girder	Green way & Water	---	---	---
590179	72.3	Concrete	Railroad	6.325	6.333	5
590239	78.2	Steel	Railroad	6.782	6.993	6
590296	94.7	Prestressed Concrete	Railroad			
590511	80.4	RC Deck	Highway	4.750	4.980*	6
590512	80.4	RC Deck	Highway	5.588	4.980*	6
590038	30.4	RC Deck	Water	---	---	---
590049	48.4	RC Deck	Water	---	---	---
590059	11.8	Steel Plank	Water	---	---	---
590108	100	RC Deck	Railroad	7.010	7.090	7
590161	63.7	Steel	Water	---	---	---
590165	48.2	Steel	Water	---	---	---
590355	70.3	RC Deck	Highway	5.004	4.870	5
590177	29.1	Steel	Water	---	---	---
590255	77.7	Steel	Railroad	7.290	10.993*	10
590376	84.83	Steel	Water	---	---	---
590379	29.3	Prestressed Concrete	Water	---	---	---
590700		Steel	Highway	4.064	4.110	4
590702		Steel	Local Road	4.242	4.250	5
590704		Concrete	Local Road	3.759	3.760	4

* Only part of these bridges have been scanned for evaluation

APPENDIX D: LiBE DEFECT DETECTION AND QUANTIFICATION FOR THE SELECTED BRIDGES AND CORRESPONDING RATINGS

Bridge Number	Sufficiency Rating	Defect No.	Area (m2)	Volume (m3)	Damage Ratio (γ)	Maximum Depth (M) (m)	Average Depth (A) (m)	LiDAR Defect Rating (R)
590179	72.3	1	8.53E-2	5.37E-4	0.0792	0.031	1.01E-02	62.2
590255	77.7	1	2.87E-1	7.09E-3	0.0578	0.162	2.98E-02	57.8
590140	77.5					N/A		
590147	47.5	1	1.76E-1	1.26E-2	0.0727	0.259	9.00E-02	55.9
		2	1.45E-1	5.11E-3				
		3	1.06E-1	3.94E-3				
590084	82.1					N/A		
590239	78.2					N/A		
590059	11.8					N/A		
590161	63.7					N/A		
590165	48.2					N/A		
590177	29.1					N/A		
590296	94.7					N/A		
590376	84.83					N/A		
590379	29.3					N/A		
590511	80.4					N/A		
590512	80.4					N/A		
590038	30.4					N/A		
590049	48.4					N/A		
590108	100					N/A		
590355	70.3					N/A		
590700						N/A		
590702		1	2.06E-2	3.39E-4	0.0056	0.042	1.64E-02	78.2
590704		1	4.42E-1	1.40E-2	0.0799	0.080	3.54E-02	56.1
640024	30.1	1	5.07E-1	2.85E-2	0.2169	0.332	5.61E-02	38.8

APPENDIX E: DEFECT DETECTION AND QUANTIFICATION PROGRAM

```
Program main

Write (*,*) 'Please enter the bridge number'
read (*,*) Bridgenumber
write (*,*) 'Please enter the section name you create of the
analysis part'
Read (*,*) Sectionname
write(9,*) 'Bridge number=', Bridgenumber
write(9,*) 'Section name=', Sectionname
read (1,*) Start_C, Start_R

N_interC=1
NR_grid=1
Accuracy=0.005
bet1=1.0
bet2=1.0
maxid=0.0
I=1
K=1
NR=0
read(1,*)Column, Row, X(i,1),Y(i,1),Z(i,1)
End_R=Start_R
if(Row.ne.Start_R)then
   k=k+1
endif
do
  j=2
  StartR(i)=Row
  if(Start_R.gt.StartR(i))Start_R=StartR(i)
  do
    read(1,*)Column, Row, X(i,j),Y(i,j),Z(i,j)
            if(Column.gt.(i+Start_C-1))then
              X(i+1,1)=X(i,j)
              Y(i+1,1)=Y(i,j)
              Z(i+1,1)=Z(i,j)
              X(i,j)=0.0
              Y(i,j)=0.0
              Z(i,j)=0.0
              EndR(i)=j-1
              if(j.Gt.NR)NR=j
                    k=k+1
                    exit
            else
            endif
            do
              if(Row.gt.(StartR(i)+j-1))then
                            write(*,*)Column, Row,
StartR(i)+j-1,j,k
                    k=k+1
                        j=j+1
                        X(i,j)=X(i,j-1)
                        Y(i,j)=Y(i,j-1)
                        Z(i,j)=Z(i,j-1)
                            X(i,j-1)=0.0
                        Y(i,j-1)=0.0
                        Z(i,j-1)=0.0
                        else
                            exit
            endif
        enddo
            j=j+1
    end do
    if(Column.gt.10000)then
      X(i+1,1)=0.0
                Y(i+1,1)=0.0

                Z(i+1,1)=0.0
      If(StartR(i)+j-2.gt.End_R)End_R=StartR(i)+j-2
                EndR(i)=j-1
                exit
    else
      i=i+1
                End_C=Column
    If(StartR(i-1)+j-2.gt.End_R)End_R=StartR(i-1)+j-2
    endif
end do
N_Grid=End_C/N_interC+1
NC=i
write(*,*)'auto plane creation: y or n'
read(*,*)autoplane
if(autoplane.eq.'y')then
  call
Initialplane(Start_C,End_C,EndR,End_R,X,Y,Z,a,b,c,T,Accu
racy)
else
  call Initialplane1(a,b,c,T)
endif
write(6,*)'plane',a,b,c
M=0
Do i=1, End_C-Start_C+1
  Do j=1, Endr(i)
                If(X(i,j).lt.900)then
If((abs(X(i,j))+abs(Y(i,j))+abs(Z(i,j))).gt.0.0001)then
  call Distance(a,b,c,x(i,j),y(i,j),z(i,j),D(i,j))

ran(i,j)=sqrt(X(i,j)**2+Y(i,j)**2+Z(i,j)**2)


evend=evend+abs(D(i,j))
                                        M=M+1
                            endif
                    endif
          end do
end do
evend=evend/M
write(9,*)'evend',evend
scandis=1.0/sqrt(a**2+b**2+c**2)
Do i=1, End_C-Start_C+1
  Do j=1, EndR(i)
          If(X(i,j).lt.900)then
                    call Pointrotate(X(i,j),Y(i,j),Z(i,j),T)
                else
                endif
          end do
end do
write(6,*)T
ZC=0.0
ZR=0.0
write(*,*)'please enter the interval for calculating the
gredient'
read(*,*)int1
write(6,*)'interval=',int1
M=0
Even=0.0
D_max=0.0
vard=0.0
Do ii=1, floor((End_C-Start_C+1)/3.0)
        i=ii*3
  Do jj=1, floor(Endr(i)/3.0)
```

```
                j=Jj*3
if(ran(i,j).gt.0.0001.and.(abs(X(i,j))+abs(Y(i,j))+abs(Z(i,j))).lt
.900)then
int=IDNINT(int1*10.0*scandis/(ran(i,j)**2))
                        if(int.lt.1)int=1
                If(i.gt.int.and.i.lt.End_C-Start_C-
int+2.and.(j+StartR(i)-StartR(i+int)).gt.0.and.(j+StartR(i)-
StartR(i-int)).gt.0)then
                        If((abs(X(i-int,j+StartR(i)-StartR(i-
int)))+abs(Y(i-int,j+StartR(i)-StartR(i-int)))+abs(Z(i-
int,j+StartR(i)-StartR(i-
int)))).lt.200.and.(abs(X(i+int,j+StartR(i)-
StartR(i+int)))+abs(Y(i+int,j+StartR(i)-
StartR(i+int)))+abs(Z(i+int,j+StartR(i)-
StartR(i+int)))).lt.200)then
If((abs(X(i+int,j+StartR(i)-
StartR(i+int)))+abs(Y(i+int,j+StartR(i)-
StartR(i+int)))).gt.0.0001.and.(abs(X(i-int,j+StartR(i)-
StartR(i-int)))+abs(Y(i-int,j+StartR(i)-StartR(i-
int)))).gt.0.0001)then
                if(sqrt((X(i+int,j+StartR(i)-StartR(i+int))-X(i-
int,j+StartR(i)-StartR(i-int)))**2+(Y(i+int,j+StartR(i)-
StartR(i+int))-Y(i-int,j+StartR(i)-StartR(i-
int)))**2).lt.0.001)then

ZC=4.0*(Z(i+int,j+StartR(i)-StartR(i+int))-2.0*Z(i,j)+Z(i-
int,j+StartR(i)-StartR(i-int)))/(0.001**2)
                elseif((abs(X(i,j))+abs(Y(i,j))).gt.0.001)then

ZC=4.0*(Z(i+int,j+StartR(i)-StartR(i+int))-2.0*Z(i,j)+Z(i-
int,j+StartR(i)-StartR(i-int)))/((X(i+int,j+StartR(i)-
StartR(i+int))-X(i-int,j+StartR(i)-StartR(i-
int)))**2+(Y(i+int,j+StartR(i)-StartR(i+int))-Y(i-
int,j+StartR(i)-StartR(i-int)))**2)
                        endif
                    endif
                endif
                endif
                If(j.gt.int.and.j.lt.endr(i)-int+1)then
                        If((abs(X(i,j-int))+abs(Y(i,j-
int))+abs(Z(i,j-
int))).lt.200.and.(abs(X(i,j+int))+abs(Y(i,j+int))+abs(Z(i,j+int
))).lt.200)then
IF((abs(X(i,j+int))+abs(Y(i,j+int))+abs(Z(i,j+int))).gt.0.0001.
and.(abs(X(i,j-int))+abs(Y(i,j-int))+abs(Z(i,j-
int))).gt.0.0001)then
                if(sqrt((X(i,j+int)-X(i,j-int))**2+(Y(i,j+int)-
Y(i,j-int))**2).lt.0.001)then
                        ZR=4.0*(Z(i,j+int)-2.0*Z(i,j)+Z(i,j-
int))/(0.001**2)
                        elseif((abs(X(i,j))+abs(Y(i,j))).gt.0.001)then

                                ZR=4.0*(Z(i,j+int)-
2.0*Z(i,j)+Z(i,j-int))/((X(i,j+int)-X(i,j-int))**2+(Y(i,j+int)-
Y(i,j-int))**2)
                        endif
                                        endif
                                endif
                        endif
If((abs(X(i,j))+abs(Y(i,j))+abs(Z(i,j))).gt.0.0001)then
                        Dis=abs(ZC)+abs(ZR)
                                Even=Even+(Dis)

if((Dis).gt.D_max)D_max=(Dis)
                vard=vard+(abs(D(i,j))-evend)**2
                                        M=M+1
                        endif
                    endif
                end do
end do
```

```
even=even/M
vard=sqrt(vard/M)
 write(9,*)'vardis=',vard
 write(9,*)'evengrad=',even
if(evend.lt.0.01.and.even.lt.15.0)then
  evend=evend+vard
  even=15.0-0.25*(15.0-even)
elseif(evend.gt.0.01.and.even.lt.15.0)then
  evend=0.01
  even=15.0-0.25*(15.0-even)
elseif(evend.lt.0.01.and.even.gt.15.0.and.even.lt.30.0)then
  evend=evend+vard/2.0
  even=1.75*even
elseif(evend.gt.0.01.and.even.gt.15.0.and.even.lt.30.0)then
  evend=0.01
  even=1.75*even
elseif(evend.gt.0.01.and.even.gt.30.0)then
  evend=evend-vard/2.0
  even=even*(1.0+even/30.0)
elseif(evend.lt.0.01.and.even.gt.30.0)then
  evend=evend+vard/2.0
  even=even*(1.0+even/30.0)
endif
NGeven=0.0
Geven=0.0
pGeven=0.0
p=0.0
var=0.0
M=0.0
Do i=1, End_C-Start_C+1
   Do j=1, Endr(i)
if(ran(i,j).gt.0.0001.and.(abs(X(i,j))+abs(Y(i,j))+abs(Z(i,j))).lt
.900)then
            int=IDNINT(int1*10.0*scandis/(ran(i,j)**2))
                    if(int.lt.1)int=1
   If(i.gt.int.and.i.lt.End_C-Start_C-int+2.and.(j+StartR(i)-
StartR(i+int)).gt.0.and.(j+StartR(i)-StartR(i-int)).gt.0)then
   If((abs(X(i-int,j+StartR(i)-StartR(i-int)))+abs(Y(i-
int,j+StartR(i)-StartR(i-int)))+abs(Z(i-int,j+StartR(i)-
StartR(i-int)))).lt.200.and.(abs(X(i+int,j+StartR(i)-
StartR(i+int)))+abs(Y(i+int,j+StartR(i)-
StartR(i+int)))+abs(Z(i+int,j+StartR(i)-
StartR(i+int)))).lt.200)then
IF((abs(X(i+int,j+StartR(i)-
StartR(i+int)))+abs(Y(i+int,j+StartR(i)-
StartR(i+int)))).gt.0.0001.and.(abs(X(i-int,j+StartR(i)-
StartR(i-int)))+abs(Y(i-int,j+StartR(i)-StartR(i-
int)))).gt.0.0001)then
        if(sqrt((X(i+int,j+StartR(i)-StartR(i+int))-X(i-
int,j+StartR(i)-StartR(i-int)))**2+(Y(i+int,j+StartR(i)-
StartR(i+int))-Y(i-int,j+StartR(i)-StartR(i-
int)))**2).lt.0.001)then
ZC=4.0*(Z(i+int,j+StartR(i)-StartR(i+int))-2.0*Z(i,j)+Z(i-
int,j+StartR(i)-StartR(i-int)))/(0.001**2)
            elseif((abs(X(i,j))+abs(Y(i,j))).gt.0.001)then
 ZC=4.0*(Z(i+int,j+StartR(i)-StartR(i+int))-2.0*Z(i,j)+Z(i-
int,j+StartR(i)-StartR(i-int)))/((X(i+int,j+StartR(i)-
StartR(i+int))-X(i-int,j+StartR(i)-StartR(i-
int)))**2+(Y(i+int,j+StartR(i)-StartR(i+int))-Y(i-
int,j+StartR(i)-StartR(i-int)))**2)
                endif
                    endif
                endif
                        endif
If(j.gt.int.and.j.lt.endr(i)-int+1)then
 If((abs(X(i,j-int))+abs(Y(i,j-int))+abs(Z(i,j-
int))).lt.200.and.(abs(X(i,j+int))+abs(Y(i,j+int))+abs(Z(i,j+int
))).lt.200)then
IF((abs(X(i,j+int))+abs(Y(i,j+int))+abs(Z(i,j+int))).gt.0.0001.
```

```fortran
and.(abs(X(i,j-int))+abs(Y(i,j-int))+abs(Z(i,j-int))).gt.0.0001)then
              if(sqrt((X(i,j+int)-X(i,j-int))**2+(Y(i,j-int)-Y(i,j-int))**2).lt.0.001)then
ZR=4.0*(Z(i,j+int)-2.0*Z(i,j)+Z(i,j-int))/(0.001**2)
              elseif((abs(X(i,j))+abs(Y(i,j))).gt.0.001)then
ZR=4.0*(Z(i,j+int)-2.0*Z(i,j)+Z(i,j-int))/((X(i,j+int)-X(i,j-int))**2+(Y(i,j+int)-Y(i,j-int))**2)
              endif
              endif
                              endif
              endif
              If((abs(X(i,j))+abs(Y(i,j))+abs(Z(i,j))).lt.900)thenIf((abs(X(i,j))+abs(Y(i,j))+abs(Z(i,j))).gt.0.0001)then
                              Dis=abs(ZC)+abs(ZR)
              if(maxid.lt.abs(D(i,j)))then
                      maxid=abs(D(i,j))
                                      endif
if(-D(i,j).gt.evend*bet2)NGeven((i/N_interC+1),((j+StartR(i)-Start_R)/(N_interC)+1))=NGeven((i/N_interC+1),((j+StartR(i)-Start_R)/(N_interC)+1))+1
              Geven((i/N_interC+1),((j+StartR(i)-Start_R)/(N_interC)+1))=Geven((i/N_interC+1),((j+StartR(i)-Start_R)/(N_interC)+1))+abs(D(i,j))
              pGeven((i/N_interC+1),((j+StartR(i)-Start_R)/(N_interC)+1))=pGeven((i/N_interC+1),((j+StartR(i)-Start_R)/(N_interC)+1))+1
if(((j+StartR(i)-Start_R)/(N_interC)+1).gt.NR_grid)NR_grid=((j+StartR(i)-Start_R)/(N_interC)+1)
              if(Dis.gt.even*bet1)then
Neven((i/N_interC+1),((j+StartR(i)-Start_R)/(N_interC)+1))=Neven((i/N_interC+1),((j+StartR(i)-Start_R)/(N_interC)+1))+1
                              endif
                              if(((j+StartR(i)-Start_R)/(N_interC)+1).gt.NR_grid)NR_grid=((j+StartR(i)-Start_R)/(N_interC)+1)

              write(2,82)Start_C+i-1,StartR(i)+j-1,X(i,j),Y(i,j),Z(i,j),(Dis),D(i,j) !
                                      var=var+((Dis)-even)**2
                                      M=M+1
                              endif
                      endif
                  endif
                  end do
end do
var=sqrt(var/M)
write(9,*)'vargrad=',var
M=1
defectv=0.0
tarea=0.0
tdarea=0.0
do i=1,N_grid
  do j=1,NR_grid
          if(pGeven(i,j).gt.(N_interC**2/8))then
                  p(i,j)=Neven(i,j)/pGeven(i,j)
                  Geven(i,j)=Geven(i,j)/pGeven(i,j)
                  pGeven(i,j)=NGeven(i,j)/pGeven(i,j)
                  else
                    pGeven(i,j)=0.0
                          p(i,j)=0.0
                          pGeven(i,j)=0.0
                  endif
          end do
end do
  do i=1,N_grid
          do j=1,NR_grid
if(pGeven(i,j).gt.0.5.and.p(i,j).gt.0.5)then
          if(C_Grid(i,j).lt.1)then
                        C_Grid(i,j)=M
                                      call
omnidirection(i,j,M,C_Grid,pGeven,p)
                      M=M+1
                          endif
              endif
          end do
  end do
        do i=1,N_grid
          do j=1,NR_grid
                          do
              Empty_check=0
              if(C_Grid(i,j).gt.0)then
                  N1=(i-1)*N_interC+1
                  N2=i*N_interC+1
                          do
          M1=(j-1)*N_interC+Start_R-StartR(N1)+1
M4=(j-1)*N_interC+Start_R-StartR(N1)+N_interC+1
              if(M4.le.1)then
                  N1=N1+1
              if(N1.gt.N2)then
              Empty_check=1
              exit
              endif
              else
              if(M1.le.0)M1=1
                  exit
              endif
              end do
              if(Empty_check.eq.1)exit
                          do
          M2=(j-1)*N_interC+Start_R-StartR(N2)+1
M3=(j-1)*N_interC+Start_R-StartR(N2)+N_interC+1
              if(M3.le.1)then
              N2=N2-1
              if(N1.gt.N2)then
              Empty_check=1
                  exit
              endif
              else
              if(M2.le.0)M2=1
                  exit
              endif
              end do
              if(Empty_check.eq.1)exit
                          do
If((abs(X(N1,M1))+abs(Y(N1,M1))+abs(Z(N1,M1))).gt.0.0001.and.X(N1,M1).lt.900)then
                      exit
                      else
              if(M1+StartR(N1).lt.M4+StartR(N1))then
                          M1=M1+1
                      else
write(*,*)'row of 1st point greater than 4th point'
              if(N1.lt.N2)then
                  N1=N1+1
                      else
              Empty_check=1
                  exit
              endif
              do  !
M1=(j-1)*N_interC+Start_R-StartR(N1)+1
M4=(j-1)*N_interC+Start_R-StartR(N1)+N_interC+1
              if(M4.le.1)then
              N1=N1+1
              if(N1.gt.N2)then
```

```
                              Empty_check=1
                                    exit
                                  endif
                                   else
                            if(M1.le.0)M1=1
                                    exit
                                  endif
                                end do !
                            if(N1.gt.N2)then
                                Empty_check=1
                                      exit
                                    endif
                                    endif
                                    endif
        end do
              if(Empty_check.eq.1)exit
                        do
If((abs(X(N2,M2))+abs(Y(N2,M2))+abs(Z(N2,M2))).gt.0.00
01.and.X(N2,M2).lt.900)then
                              exit
                               else
if(M2+StartR(N2).lt.M3+StartR(N2))then
                                            M2=M2+1
                                             else
write(*,*)'row of 2nd point greater than 3rd point'
                            if(N2.gt.N1)then
                                    N2=N2-1
                                          else
                           Empty_check=1
                                        exit
                                    endif
                            do  !
M2=(j-1)*N_interC+Start_R-StartR(N2)+1
M3=(j-1)*N_interC+Start_R-StartR(N2)+N_interC+1
                                if(M3.le.1)then
                                    N2=N2-1
                                if(N1.gt.N2)then
                            Empty_check=1
                                            exit
                                    endif
                                    else
                            if(M2.le.0)M2=1
                                exit
                             endif
                                end do !
                          if(N1.gt.N2)then
                                  Empty_check=1
                                        exit
                                    endif
                                    endif
                                    endif

          end do
              if(Empty_check.eq.1)exit
                        do
If((abs(X(N2,M3))+abs(Y(N2,M3))+abs(Z(N2,M3))).gt.0.00
01.and.X(N2,M3).lt.900)then
                              exit
                               else
if(M3+StartR(N2).gt.M2+StartR(N2))then
                                      M3=M3-1
                                          else
                          Empty_check=1
                                        exit
                                    endif
                                  endif
                                end do
                  if(Empty_check.eq.1)exit
                                do
If((abs(X(N1,M4))+abs(Y(N1,M4))+abs(Z(N1,M4))).gt.0.00
```

```
01.and.X(N1,M4).lt.900)then
                                exit
                                 else
          if(M4+StartR(N1).gt.M1+StartR(N1))then
                                          M4=M4-1
                                            else
                          Empty_check=1
                                                exit
                                  endif
                                 endif
                               end do
                 if(Empty_check.eq.1)exit
Area=abs(X(N1,M1)*Y(N2,M2)-
X(N2,M2)*Y(N1,M1)+X(N2,M2)*Y(N2,M3)-
X(N2,M3)*Y(N2,M2)+X(N2,M3)*Y(N1,M4)-
X(N1,M4)*Y(N2,M3)+X(N1,M4)*Y(N1,M1)-
X(N1,M1)*Y(N1,M4))/2.0
defectv(C_Grid(i,j))=defectv(C_Grid(i,j))+(Area*Geven(i,j))
defecta(C_Grid(i,j))=defecta(C_Grid(i,j))+(Area)
                    tarea=tarea+Area
                           tdarea=tdarea+(Area)
                                           else
          N1=(i-1)*N_interC+1

N2=i*N_interC+1
                    N11=N1
                        N22=N2
                            do
          M1=(j-1)*N_interC+Start_R-StartR(N1)+1
M4=(j-1)*N_interC+Start_R-StartR(N1)+N_interC+1
                          if(M4.le.1)then
                                N1=N1+1
if(N1.gt.N2)then
          Empty_check=1
              exit
            endif
             else
          if(M1.le.0)M1=1
                  exit
                endif
                end do
              if(Empty_check.eq.1)exit
                        do
          M2=(j-1)*N_interC+Start_R-StartR(N2)+1
M3=(j-1)*N_interC+Start_R-StartR(N2)+N_interC+1
                          if(M3.le.1)then
                                N2=N2-1
                          if(N1.gt.N2)then
                            Empty_check=1
                                exit
                                endif
                   else
          if(M2.le.0)M2=1
                exit
              endif
            end do
          if(Empty_check.eq.1)exit
 do
If((abs(X(N1,M1))+abs(Y(N1,M1))+abs(Z(N1,M1))).gt.0.00
01.and.X(N1,M1).lt.900)then
                  exit
                   else
if(M1+StartR(N1).lt.M4+StartR(N1))then
            M1=M1+1
             else
if(N1.lt.N2)then
N1=N1+1
             else
Empty_check=1
```

```
                exit
            endif
             do !
M1=(j-1)*N_interC+Start_R-StartR(N1)+1
M4=(j-1)*N_interC+Start_R-StartR(N1)+N_interC+1
                                    if(M4.le.1)then
                                    N1=N1+1
                                    if(N1.gt.N2)then
                    Empty_check=1
                                        exit
                                    endif
                                    else
                    if(M1.le.0)M1=1
                        exit
                        endif
                            end do
                    if(N1.gt.N2)then
                    Empty_check=1
                                    exit
                                endif
                    endif
                    endif
                    end do
                if(Empty_check.eq.1)exit
        do
If((abs(X(N2,M2))+abs(Y(N2,M2))+abs(Z(N2,M2))).gt.0.00
01.and.X(N2,M2).lt.900)then
                    exit
                    else
if(M2+StartR(N2).lt.M3+StartR(N2))then
                        M2=M2+1
                            else
                    if(N2.gt.N1)then
                                N2=N2-1
                                    else
                        Empty_check=1
                                    exit
                                endif
                                do !
M2=(j-1)*N_interC+Start_R-StartR(N2)+1
M3=(j-1)*N_interC+Start_R-StartR(N2)+N_interC+1
                                    if(M3.le.1)then
                                    N2=N2-1
                                    if(N1.gt.N2)then
                    Empty_check=1
                                    exit
                                    endif
                                    else
                        if(M2.le.0)M2=1
                            exit
                        endif
                        end do !
            if(N1.gt.N2)then
            Empty_check=1
                                exit
                        endif
                    endif
                    endif
                    end do
                    if(Empty_check.eq.1)exit
do
If((abs(X(N2,M3))+abs(Y(N2,M3))+abs(Z(N2,M3))).gt.0.00
01.and.X(N2,M3).lt.900)then
                    exit
                    else
        if(M3+StartR(N2).gt.M2+StartR(N2))then
                                M3=M3-1
                                    else
                        Empty_check=1
                                    exit
```

```
                        endif
                    endif
                    end do
                    if(Empty_check.eq.1)exit
do
If((abs(X(N1,M4))+abs(Y(N1,M4))+abs(Z(N1,M4))).gt.0.00
01.and.X(N1,M4).lt.900)then
                        exit
                        else
            if(M4+StartR(N1).gt.M1+StartR(N1))then
                                M4=M4-1
                                else
            write(*,*)'row of 4th point less than 1st point'
                            Empty_check=1
                                        exit
                            endif
                            endif
                        end do
                if(Empty_check.eq.1)exit
Area=abs(X(N1,M1)*Y(N2,M2)-
X(N2,M2)*Y(N1,M1)+X(N2,M2)*Y(N2,M3)-
X(N2,M3)*Y(N2,M2)+X(N2,M3)*Y(N1,M4)-
X(N1,M4)*Y(N2,M3)+X(N1,M4)*Y(N1,M1)-
X(N1,M1)*Y(N1,M4))/2.0
                tarea=tarea+Area
endif                                       exit
                            end do
    end do
    end do
If(M.eq.1)then
    write(*,*)'no defect detected'
    write(9,*)'no defect detected'
else
write(9,*)'Total Detected Defect Number:', M-1
write(9,*)'-----Defect Number-----Volume of the defect------
Area of the defect------'
Do K=1,M-1
    write(*,*)K,defectv(K),defecta(K)
    write(9,*)K,defectv(K),defecta(K)
    do i=1,N_grid
        do j=1,NR_grid
            If(C_Grid(i,j).eq.K)then
                                do ii=(i-
1)*N_interC+1,i*N_interC
    if((j)*N_interC+Start_R-StartR(ii).gt.0)then
    MM=(j-1)*N_interC+Start_R-StartR(ii)+1
    if((j-1)*N_interC+Start_R-StartR(ii)+1.le.0)MM=1
            do jj=MM,(j)*N_interC+Start_R-StartR(ii)
If(X(ii,jj).lt.900)then
            If((abs(X(ii,jj))+abs(Y(ii,jj))+abs(Z(ii,jj))).gt.0.00
01)then

write(8,81)k,i,j,X(ii,jj),Y(ii,jj),Z(ii,jj),D(ii,jj)!k,Start_C+ii-
1,StartR(ii)+jj-1,X(ii,jj),Y(ii,jj),Z(ii,jj)
                                        endif
                            endif
                                end do
                            endif
                        enddo
                    endif
            end do
end do
end do
endif

write(9,*) 'Maxidepth=', Maxid
write(9,*) 'Rating=', tdarea/tarea
write(9,*) 'total area=', tarea
write(*,*)tarea
80      format(i6,i6,D19.6,D19.6,D19.6)
```

```
81    format(i6,i6,i6,D19.6,D19.6,D19.6,D19.6)
82    format(i6,i6,D19.6,D19.6,D19.6,D19.6,D19.6)
end

Subroutine
Initialplane(Start_C,End_C,EndR,End_R,X,Y,Z,a,b,c,T,Accu
racy)
Implicit none
Integer :: NC,NR,MC1,MC2,MR1,MR2
Integer :: Start_C, End_C,End_R,MC,EndR(2000)
Real*8 :: X(2000,3000),Y(2000,3000),Z(2000,3000)
Real*8 :: Err,Ave1(3),Ave2(3),Ave3(3),D,Accuracy
real*8 :: CL, CX, CY, CZ, DL, DM, DN, EL, EM, EN
Real*8 :: a,b,c
Real*8, dimension(3,3) :: T


MC1=2
MR1=2
MC2=End_C-Start_C
MC=(Start_C+End_C)/2-Start_C+1
Do
  MR2=EndR(MC2)-1
    do
                call
Localpointcheck(MC1+1,MR1+1,X,Y,Z,Err,Ave1)

      if(X(MC1,MR1).lt.100)then
                exit
      else
                MR1=MR1+3
      endif
    enddo
  do
    call Localpointcheck(MC2-1,MR2-1,X,Y,Z,Err,Ave2)

    if(Ave2(1).lt.100)then
                exit
        else
                MR2=MR2-3
        endif
  enddo
        NC=MC
  do
    NR=4
        do

If((abs(X(NC,NR))+abs(Y(NC,NR))+abs(Z(NC,NR))).lt.0.00
01)then
                NC=NC+1
                else
                  exit
                endif
        end do

        call
Localpointcheck(NC+1,NR,X,Y,Z,Err,Ave3)
        if(Ave3(1).lt.100)then
                exit
        else
                NR=NR+3
        endif
  enddo
    call
Threepointplane(Ave1(1),Ave1(2),Ave1(3),Ave2(1),Ave2(2)
,Ave2(3),Ave3(1),Ave3(2),Ave3(3),a,b,c)
        NC=MC
        do
          NR=EndR(NC)/2
```

```
If(X(NC,NR).eq.0.0.and.Y(NC,NR).eq.0.0.and.Z(NC,NR).eq
.0.0)then
                NC=NC-1

        else
          exit
        endif
    end do
    call
Distance(a,b,c,x(NC,NR),y(NC,NR),z(NC,NR),D)

    If(D.gt.Accuracy*10)then
      MR1=MR1+1
                MC1=MC1+1
                MC2=MC2-1
                MC=MC+1
                write(*,*)D
                pause
    else
      exit
    endif
end do
call ch(a,b,c,CL,CX,CY,CZ,DL,DM,DN,EL,EM,EN)
call
Coordinatematrix(CX,CY,CZ,DL,DM,DN,EL,EM,EN,T)

End Subroutine

Subroutine Initialplane1(a,b,c,T)
Implicit none
Real*8 :: Ave1(3),Ave2(3),Ave3(3)
real*8 :: CL, CX, CY, CZ, DL, DM, DN, EL, EM, EN
Real*8 :: a,b,c
Real*8, dimension(3,3) :: T
                write(*,*)"Begin reading 3 reference points"
                write(*,*)'first point x value'
                read(*,*)AVe1(1)
                write(*,*)'first point y value'
                read(*,*)AVe1(2)
                write(*,*)'first point z value'
                read(*,*)AVe1(3)
                write(*,*)'second point x value'
                read(*,*)AVe2(1)
                write(*,*)'second point y value'
                read(*,*)AVe2(2)
                write(*,*)'second point z value'
                read(*,*)AVe2(3)
                write(*,*)'third point x value'
                read(*,*)AVe3(1)
                write(*,*)'third point y value'
                read(*,*)AVe3(2)
                write(*,*)'third point z value'
                read(*,*)AVe3(3)
                write(6,*)'reference points'

write(6,*)Ave1(1),Ave1(2),Ave1(3),Ave2(1),Ave2(2),Ave2(
3),Ave3(1),Ave3(2),Ave3(3)
        call
Threepointplane(Ave1(1),Ave1(2),Ave1(3),Ave2(1),Ave2(2)
,Ave2(3),Ave3(1),Ave3(2),Ave3(3),a,b,c)
call ch(a,b,c,CL,CX,CY,CZ,DL,DM,DN,EL,EM,EN)
call
Coordinatematrix(CX,CY,CZ,DL,DM,DN,EL,EM,EN,T)

End Subroutine

Subroutine tangent(C1,X,Y,Z,X1,Y1,Z1)
implicit none
  Real*8, intent(in) :: X,Y,Z,X1,Y1,Z1
```

```
   Real*8 :: C1(3), NL
                    NL=Sqrt((X1-X)**2+(Y1-Y)**2+(Z1-
Z)**2)

                    C1(1)=(X1-X)/NL
                    C1(2)=(Y1-Y)/NL
                    C1(3)=(Z1-Z)/NL
End subroutine

Subroutine Localpointcheck(M,N,X,Y,Z,Err,Ave)
Integer :: M,N,I
Real*8 :: X(2000,3000),Y(2000,3000),Z(2000,3000),Err,
Ave(3),A(8)
A(1)=sqrt((X(M,N+1)-X(M,N))**2+(Y(M,N+1)-
Y(M,N))**2+(Z(M,N+1)-Z(M,N))**2)
A(2)=sqrt((X(M,N-1)-X(M,N))**2+(Y(M,N-1)-
Y(M,N))**2+(Z(M,N-1)-Z(M,N))**2)
A(3)=sqrt((X(M+1,N+1)-X(M,N))**2+(Y(M+1,N+1)-
Y(M,N))**2+(Z(M+1,N+1)-Z(M,N))**2)
A(4)=sqrt((X(M-1,N+1)-X(M,N))**2+(Y(M-1,N+1)-
Y(M,N))**2+(Z(M-1,N+1)-Z(M,N))**2)
A(5)=sqrt((X(M+1,N)-X(M,N))**2+(Y(M+1,N)-
Y(M,N))**2+(Z(M+1,N)-Z(M,N))**2)
A(6)=sqrt((X(M-1,N)-X(M,N))**2+(Y(M-1,N)-
Y(M,N))**2+(Z(M-1,N)-Z(M,N))**2)
A(7)=sqrt((X(M+1,N-1)-X(M,N))**2+(Y(M+1,N-1)-
Y(M,N))**2+(Z(M+1,N-1)-Z(M,N))**2)
A(8)=sqrt((X(M-1,N-1)-X(M,N))**2+(Y(M-1,N-1)-
Y(M,N))**2+(Z(M-1,N-1)-Z(M,N))**2)
Err=0.0
Do I=1,8
           Err=Err+A(I)
End do
Err=Err/8.0
Ave(1)=(X(M+1,N+1)+X(M+1,N)+X(M+1,N-
1)+X(M,N+1)+X(M,N)+X(M,N-1)+X(M-1,N+1)+X(M-
1,N)+X(M-1,N-1))/9.0
Ave(2)=(Y(M+1,N+1)+Y(M+1,N)+Y(M+1,N-
1)+Y(M,N+1)+Y(M,N)+Y(M,N-1)+Y(M-1,N+1)+Y(M-
1,N)+Y(M-1,N-1))/9.0
Ave(3)=(Z(M+1,N+1)+Z(M+1,N)+Z(M+1,N-
1)+Z(M,N+1)+Z(M,N)+Z(M,N-1)+Z(M-1,N+1)+Z(M-
1,N)+Z(M-1,N-1))/9.0
End Subroutine

Subroutine
Threepointplane(X1,Y1,Z1,X2,Y2,Z2,X3,Y3,Z3,a,b,c)
Real*8 :: X1,Y1,Z1,X2,Y2,Z2,X3,Y3,Z3,a,b,c,D
D=X1*Y2*Z3+X3*Y1*Z2+X2*Y3*Z1-X3*Y2*Z1-
X1*Y3*Z2-X2*Y1*Z3
a=(-1.0)/D*(Y2*Z3+Y1*Z2+Y3*Z1-Y2*Z1-Y1*Z3-Y3*Z2)
b=(-1.0)/D*(X1*Z3+X3*Z2+X2*Z1-X3*Z1-X1*Z2-X2*Z3)
c=(-1.0)/D*(X1*Y2+X3*Y1+X2*Y3-X3*Y2-X2*Y1-
X1*Y3)
End Subroutine

Subroutine Distance(a,b,c,x,y,z,D)
Real*8 :: a,b,c,x,y,z,D
D=(a*x+b*y+c*z+1)/sqrt(a**2+b**2+c**2)
End Subroutine

subroutine ch(a,b,c,CL,CX,CY,CZ,DL,DM,DN,EL,EM,EN)
implicit none
         real*8, intent(in) :: a,b,c
         real*8, intent(out) :: CL, CX, CY, CZ, DL, DM,
DN, EL, EM, EN
         real*8 :: H,H1
         CX=a
         CY=b
         CZ=c
         CL=sqrt(CX**2+CY**2+CZ**2)
```

```
         CX=CX/CL
         CY=CY/CL
         CZ=CZ/CL
         DL=-a/(a**2+b**2)
         DM=-b/(a**2+b**2)
         DN=1/c
         H=sqrt(DL**2+DM**2+DN**2)
         DL=DL/H
         DM=DM/H
         DN=DN/H
         EL=1/a
         EM=-1/b
         EN=0.0
         H1=sqrt(EL**2+EM**2+EN**2)
         EL=EL/H1
         EM=EM/H1
         EN=EN/H1
end subroutine ch

Subroutine
Coordinatematrix(CX,CY,CZ,DL,DM,DN,EL,EM,EN,TT)
implicit none
real*8, intent(in) :: CX, CY,CZ,DL,DM,DN,EL,EM,EN
real*8, dimension(3,3) :: T
real*8, dimension(3,3) :: TT
         T=0.0
         TT=0.0
         T(1,1)=CX
         T(2,1)=CY
         T(3,1)=CZ
         T(1,2)=DL
         T(2,2)=DM
         T(3,2)=DN
         T(1,3)=EL
         T(2,3)=EM
         T(3,3)=EN
         TT=Transpose(T)

End subroutine

Subroutine Pointrotate(aa,bb,cc,T)
implicit none
Real*8, dimension(3) :: A(3),B(3)
Real*8, dimension(3,3) :: T
Real*8 :: aa,bb,cc
A(1)=aa
A(2)=bb
A(3)=cc
call matmul(3,3,1,T,A,B)
aa=B(2)
bb=B(3)
cc=B(1)
End Subroutine

subroutine matmul(L,M,N,A,B,C)
implicit none
integer L,M,N,I,J,K
         REAL*8 A(L,M),B(M,N),C(L,N)
         do I=1,N
                 do J=1,L
                          C(J,I)=0D0
                          do K=1,M

         C(J,I)=C(J,I)+A(J,K)*B(K,I)
                          end do
                 end do
         end do
end subroutine matmul

Subroutine omnidirection(i,j,M,C_Grid,pGeven,p)
```

```fortran
implicit none
 Integer, intent(in) :: I,J,M
 Integer :: C, R,CC,RR,Level,CCL(10000),RRL(10000),L
 Integer :: C_Grid(500,500)
 Real*8 :: pGeven(500,500),p(500,500)
        level=1
        CCL(Level)=I
        RRL(Level)=J
        C=I
        R=J
        do
   if(Level.gt.1)then
          Level=Level-1
          C=CCL(Level)
          R=RRL(Level)
       endif
       L=0
        do
        if(L.eq.1)exit
             do
             L=0
             if(C.gt.1)then
               if(R.gt.1)then
                    CC=C-1
                    RR=R-1
            if(C_Grid(CC,RR).lt.1)then
if(pGeven(CC,RR).gt.0.5.or.p(CC,RR).gt.0.5)then
                    C_Grid(CC,RR)=M
                    C=CC
                    R=RR
                    Level=Level+1
                    CCL(Level)=C
                    RRL(Level)=R
                    exit
                    endif
                    endif
               endif
                    CC=C-1
                    RR=R
            if(C_Grid(CC,RR).lt.1)then
if(pGeven(CC,RR).gt.0.5.or.p(CC,RR).gt.0.5)then
                    C_Grid(CC,RR)=M
                    C=CC
                    R=RR
                    Level=Level+1
                    CCL(Level)=C
                RRL(Level)=R
                    exit
                    endif
                    endif
                    CC=C-1
                    RR=R+1
            if(C_Grid(CC,RR).lt.1)then
if(pGeven(CC,RR).gt.0.5.or.p(CC,RR).gt.0.5)then
                    C_Grid(CC,RR)=M
                    C=CC
                    R=RR
                    Level=Level+1
                    CCL(Level)=C
                    RRL(Level)=R
                    exit
                    endif
                    endif
               endif
                if(R.gt.1)then
                    CC=C
                    RR=R-1
                if(C_Grid(CC,RR).lt.1)then
if(pGeven(CC,RR).gt.0.5.or.p(CC,RR).gt.0.5)then
                    C_Grid(CC,RR)=M
                    C=CC
                    R=RR
                    Level=Level+1
                    CCL(Level)=C
                    RRL(Level)=R
                    exit
                    endif
                    endif
                endif
                    CC=C
                    RR=R+1
            if(C_Grid(CC,RR).lt.1)then
if(pGeven(CC,RR).gt.0.5.or.p(CC,RR).gt.0.5)then
                    C_Grid(CC,RR)=M
                    C=CC
                    R=RR
                    Level=Level+1
                    CCL(Level)=C
                    RRL(Level)=R
                    exit
                    endif
                    endif
                if(R.gt.1)then
                    CC=C+1
                    RR=R-1
            if(C_Grid(CC,RR).lt.1)then
if(pGeven(CC,RR).gt.0.5.or.p(CC,RR).gt.0.5)then
                    C_Grid(CC,RR)=M
                    C=CC
                    R=RR
                    Level=Level+1
                    CCL(Level)=C
                    RRL(Level)=R
                    exit
                    endif
                    endif
                    endif
                    CC=C+1
                    RR=R
            if(C_Grid(CC,RR).lt.1)then
if(pGeven(CC,RR).gt.0.5.or.p(CC,RR).gt.0.5)then
                    C_Grid(CC,RR)=M
                    C=CC
                    R=RR
                    Level=Level+1
                    CCL(Level)=C
                    RRL(Level)=R
                    exit
                    endif
                    endif
                    CC=C+1
                    RR=R+1
            if(C_Grid(CC,RR).lt.1)then
if(pGeven(CC,RR).gt.0.5.or.p(CC,RR).gt.0.5)then
                    C_Grid(CC,RR)=M
                    C=CC
                    R=RR
                    Level=Level+1
                    CCL(Level)=C
                    RRL(Level)=R
                    exit
                    endif
                    endif
                    L=1
                    exit
                end do
                if(level.gt.10000)then
                    write(*,*)'level',level
                    pause
```

```
                    endif
                  end do
               if(C.eq.I.and.R.eq.J.and.level.eq.1)then
                    exit
                  endif
          end do

end subroutine omnidirection
subroutine matre1(M,A,B)
implicit none
integer M,I,J,K
        REAL*8 A(M,M),B(M,M),L
  do I=1,M
                do J=1,M
                        B(I,J)=0D0
                        if (I.EQ.J) B(I,J)=1D0
                end do
        end do
  do I=2,M
                IF(ABS(A(I-1,I-1)).LT.1D-10) THEN
                WRITE(*,*)'warning: the value of the
digonal term is too small'
                WRITE(*,*)'*** I-1=',I-1,'    A(I-1,I-
1)=',A(I-1,I-1)
                ENDIF
                do J=I,M
                        L=A(J,I-1)/A(I-1,I-1)
                        A(J,I-1)=0D0
                        do K=I,M
                                A(J,K)=A(J,K)-
A(I-1,K)*L
                        end do
                        do K=1,M
                                B(J,K)=B(J,K)-
B(I-1,K)*L
                        end do
                end do
        end do
        do I=M,1,-1
                do J=1,M
                        do K=I+1,M
                                B(I,J)=B(I,J)-
A(I,K)*B(K,J)
                        end do
                B(I,J)=B(I,J)/A(I,I)
                end do
        end do
end subroutine matre1
```

APPENDIX F: CLEARANCE MEASUREMENT PROGRAM

```
Program main

Write (*,*) 'Please enter the bridge number'
read (*,*) Bridgenumber
write (*,*) 'Please enter the section name you creat of the
analysis part'
Read (*,*) Sectionname
write (*,*) 'Please enter adjust start row number'
Read (*,*)Ad
write(6,*) 'Bridge number=', Bridgenumber
write(6,*) 'Section name=', Sectionname
write(6,*) 'Start adjust row number=', Ad
read (1,*) Start_C, Start_R

I=1
K=1
NR=0
read(1,*)Column, Row, DX(Column,Row-
Ad),DY(Column,Row-Ad),DZ(Column,Row-Ad)
Start_R=Start_R-Ad
End_R=Start_R

do
  j=2
  StartR(Column)=Row-Ad
  if(Start_R.gt.StartR(Column))Start_R=StartR(Column)
  if(Column.lt.Start_C)then
          i=i+Start_C-Column
    Start_C=Column
  endif
  do
    read(1,*)Column, Row, DX(Column,Row-
Ad),DY(Column,Row-Ad),DZ(Column,Row-Ad)
          if((Row-Ad).lt.0.or.(Row-Ad).gt.6000)then
            write(*,*)'exceed',Row-Ad,    Column, Row
            pause
          endif
  if(Column.gt.(i+Start_C-1))then
          EndR(i+Start_C-1)=j+StartR(i+Start_C-1)-2

                  if(j.Gt.NR)NR=j
                  exit
          else
          endif
          do
            if((Row-Ad).gt.(StartR(Column)+j-1))then
                  j=j+Row-Ad-(StartR(Column)+j-1)

                  else
                          exit
          endif
  enddo
          j=j+1
  end do

  if(Column.gt.4400)then
    If(StartR(i+Start_C-1)+j-
2.gt.End_R)End_R=StartR(i+Start_C-1)+j-2
          EndR(i+Start_C-1)=StartR(i+Start_C-1)+j-1
          exit
  else
    i=i+1
          End_C=Column
```

```
    If(StartR(i+Start_C-1)+j-
2.gt.End_R)End_R=StartR(i+Start_C-1)+j-2

  endif
end do
I=1
NR=0
gd=0.0
NG=0
read(2,*) GStart_C, GStart_R
GStart_R=GStart_R-Ad
read(2,*)Column, Row, GX(Column,Row-
Ad),GY(Column,Row-Ad),GZ(Column,Row-Ad)
GEnd_R=GStart_R

do
  j=2
  GStartR(Column)=Row-Ad

if(GStart_R.gt.GStartR(Column))GStart_R=GStartR(Column
)
  if(Column.lt.GStart_C)then
          i=i+GStart_C-Column
    GStart_C=Column
  endif

  do
    read(2,*)Column, Row, GX(Column,Row-
Ad),GY(Column,Row-Ad),GZ(Column,Row-Ad)
          gd=gd+abs(GZ(Column,Row-Ad))
          NG=NG+1
          if(Column.gt.(i+GStart_C-1))then

  GEndR(i+GStart_C-1)=j+GStartR(i+GStart_C-1)-2
                  if(j.Gt.NR)NR=j

                          exit
          else
          endif
          do
            if((Row-Ad).gt.(GStartR(Column)+j-1))then
              j=j+Row-Ad-(GStartR(Column)+j-1)
                          else
                                  exit
          endif
  enddo
          j=j+1
  end do
  if(Column.gt.4400)then
    If(GStartR(i+GStart_C-1)+j-
2.gt.GEnd_R)GEnd_R=GStartR(i+Start_C-1)+j-2
    GEndR(i+GStart_C-1)=GStartR(i+GStart_C-1)+j-1
          exit
  else
    i=i+1
          GEnd_C=Column
          If(GStartR(i+GStart_C-1)+j-
2.gt.GEnd_R)GEnd_R=GStartR(i+GStart_C-1)+j-2
  endif
end do
gd=gd/NG
Do i=1,GEnd_C-GStart_C+1
 Do j=GStartR(GStart_C+i-1),GEndr(GStart_C+i-1)

  Empty_check=0
```

```
      M=1
      do
       if((abs(GX(GStart_C+i-1,j))+abs(GY(GStart_C+i-
1,j))+abs(GZ(GStart_C+i-1,j))).gt.0.0001)then
         if(abs(abs(GZ(GStart_C+i-1,j))-gd).lt.0.5)then

             do ii=End_C-Start_C+1,1,-1
                a=(GX(GStart_C+i-1,j)-DX(Start_C+ii-
1,j))**2+(GY(GStart_C+i-1,j)-DY(Start_C+ii-1,j))**2
                          a=sqrt(a)
                          b=sqrt(DX(Start_C+ii-
1,j)**2+DY(Start_C+ii-1,j)**2+DZ(Start_C+ii-1,j)**2)

             Accuracy=2.0*3.1416*320.0*b/(360.0*4304.0)

                      if(a.lt.Accuracy)then
                       M=ii
                       Empty_check=1
                       exit
               endif
              end do
             else
              gdl=0.0
              NGl=0.0
              if((abs(GX(GStart_C+i-
4,j))+abs(GY(GStart_C+i-4,j))+abs(GZ(GStart_C+i-
4,j))).gt.0.0001)then
                     gdl=gdl+abs(GZ(GStart_C+i-4,j))
                            NGl=NGl+1
                 endif
                 if((abs(GX(GStart_C+i-4,j-
3))+abs(GY(GStart_C+i-4,j-3))+abs(GZ(GStart_C+i-4,j-
3))).gt.0.0001)then
                          gdl=gdl+abs(GZ(GStart_C+i-4,j-4))
                                 NGl=NGl+1
                 endif
                 if((abs(GX(GStart_C+i-
4,j+3))+abs(GY(GStart_C+i-4,j+3))+abs(GZ(GStart_C+i-
4,j+3))).gt.0.0001)then
                           gdl=gdl+abs(GZ(GStart_C+i-4,j+3))
                                  NGl=NGl+1
                 endif
                 if((abs(GX(GStart_C+i-1,j-
3))+abs(GY(GStart_C+i-1,j-3))+abs(GZ(GStart_C+i-1,j-
3))).gt.0.0001)then
                           gdl=gdl+abs(GZ(GStart_C+i-1,j-3))
                     NGl=NGl+1
                 endif
                 if((abs(GX(GStart_C+i-
1,j+3))+abs(GY(GStart_C+i-1,j+3))+abs(GZ(GStart_C+i-
1,j+3))).gt.0.0001)then
                           gdl=gdl+abs(GZ(GStart_C+i-1,j+3))
                                  NGl=NGl+1
                 endif
                 if((abs(GX(GStart_C+i+2,j))+abs(GY(GStart_C+i
+2,j))+abs(GZ(GStart_C+i+2,j))).gt.0.0001)then
                           gdl=gdl+abs(GZ(GStart_C+i+2,j))
                                  NGl=NGl+1
                 endif
                 if((abs(GX(GStart_C+i+2,j-
3))+abs(GY(GStart_C+i+2,j-3))+abs(GZ(GStart_C+i+2,j-
3))).gt.0.0001)then
                           gdl=gdl+abs(GZ(GStart_C+i+2,j-3))
                                  NGl=NGl+1
                 endif
                 if((abs(GX(GStart_C+i+2,j+3))+abs(GY(GStart_
C+i+2,j+3))+abs(GZ(GStart_C+i+2,j+3))).gt.0.0001)then
                           gdl=gdl+abs(GZ(GStart_C+i+2,j+3))
                                  NGl=NGl+1
                 endif
```

```
                    if(NGl.gt.0)then
if(abs(abs(GZ(GStart_C+i-1,j))-gdl/NGl).lt.0.5)then
             do ii=End_C-Start_C+1,1,-1
                a=(GX(GStart_C+i-1,j)-DX(Start_C+ii-
1,j))**2+(GY(GStart_C+i-1,j)-DY(Start_C+ii-1,j))**2
                a=sqrt(a)
                b=sqrt(DX(Start_C+ii-1,j)**2+DY(Start_C+ii-
1,j)**2+DZ(Start_C+ii-1,j)**2)

Accuracy=10.0*3.1416*320.0*b/(360.0*4304.0)
              if(a.lt.Accuracy)then
               M=ii
               Empty_check=1
               exit
              endif
             end do
        endif
             else
              do ii=End_C-Start_C+1,1,-1
                a=(GX(GStart_C+i-1,j)-DX(Start_C+ii-
1,j))**2+(GY(GStart_C+i-1,j)-DY(Start_C+ii-1,j))**2
                a=sqrt(a)
                b=sqrt(DX(Start_C+ii-1,j)**2+DY(Start_C+ii-
1,j)**2+DZ(Start_C+ii-1,j)**2)

Accuracy=10.0*3.1416*320.0*b/(360.0*4304.0)
              if(a.lt.Accuracy)then
                  M=ii
                  Empty_check=1
                       exit
                  endif
                 end do
                endif
          endif
         endif
        exit
      end do
       if(Empty_check.eq.1)then
             if((abs(GX(GStart_C+i-
1,j))+abs(GY(GStart_C+i-1,j))+abs(GZ(GStart_C+i-
1,j))).gt.0.0001)then
                Dis=DZ(Start_C+M-1,j)-GZ(GStart_C+i-1,j)
                CL(GStart_C+i-1,j)=Dis
         write(3,81)GStart_C+i-1,j,Start_C+M-1,GX(GStart_C+i-
1,j),GY(GStart_C+i-1,j),GZ(GStart_C+i-1,j),Dis
        endif
       endif
      end do
     end do
80      format(D19.6,D19.6,D19.6)
81      format(i6,i6,D19.6,D19.6,D19.6,D19.6)
82      format(i6,i6,D19.6,D19.6,D19.6,D19.6,D19.6)
end
```

APPENDIX G: DISPLACEMENT MEASUREMENT PROGRAM

```
Program main

Write (*,*) 'Please enter the bridge number'
read (*,*) Bridgenumber
write (*,*) 'Please enter the section name you creat of the
analysis part'
Read (*,*) Sectionname
write (*,*) 'Please enter adjust start row number'
Read (*,*)Ad

do i=1,4
    read(7,*)SC(i),SR(i),SX(i),SY(i),SZ(i)
end do
FX=0.0
FY=0.0
FZ=0.0
FZ1=0.0
write(6,*) 'Bridge number=', Bridgenumber
write(6,*) 'Section name=', Sectionname
write(6,*) 'Start adjust row number=', Ad
read (1,*) Start_C, Start_R
I=1
K=1
NR=0
read(1,*)Column, Row, DX(Column,Row-
Ad),DY(Column,Row-Ad),DZ(Column,Row-Ad)
Start_R=Start_R-Ad
End_R=Start_R

do
  j=2
  StartR(Column)=Row-Ad
  if(Start_R.gt.StartR(Column))Start_R=StartR(Column)
  if(Column.lt.Start_C)then
            i=i+Start_C-Column
    Start_C=Column
  endif
  do
   read(1,*)Column, Row, X,Y,Z
            if(Row-ad.le.4500)then
            if(Row-ad.gt.0)then
              DX(Column,Row-Ad)=X
              DY(Column,Row-Ad)=Y
              DZ(Column,Row-Ad)=Z
              if(Column.gt.(i+Start_C-1))then
              EndR(i+Start_C-1)=j+StartR(i+Start_C-1)-2
              if(j.Gt.NR)NR=j
                    exit
            else
            endif
            do
             if((Row-Ad).gt.(StartR(Column)+j-1))then

                    j=j+Row-Ad-(StartR(Column)+j-1)

                    else
                    exit
    endif
  enddo
            j=j+1
  endif
            endif
  end do

if(Column.gt.4400)then
```

```
    If(StartR(i+Start_C-1)+j-
2.gt.End_R)End_R=StartR(i+Start_C-1)+j-2
            EndR(i+Start_C-1)=StartR(i+Start_C-1)+j-1
            exit
  else
  i=i+1
  End_C=Column
  If(StartR(i+Start_C-1)+j-
2.gt.End_R)End_R=StartR(i+Start_C-1)+j-2

  endif
end do

I=1
NR=0
gd=0.0
NG=0
read(2,*) GStart_C, GStart_R
GStart_R=GStart_R-Ad
read(2,*)Column,Row,GX(Column,Row-
Ad),GY(Column,Row-Ad),GZ(Column,Row-Ad)
GEnd_R=GStart_R
do
 j=2
 GStartR(Column)=Row-Ad

if(GStart_R.gt.GStartR(Column))GStart_R=GStartR(Column
)
 if(Column.lt.GStart_C)then
  i=i+GStart_C-Column
  GStart_C=Column
 endif
 do
  read(2,*)Column, Row, X,Y,Z
  if(Row-ad.le.4500)then
  if(Row-ad.gt.0)then
  gX(Column,Row-Ad)=X
  gY(Column,Row-Ad)=Y
  gZ(Column,Row-Ad)=Z
  gd=gd+abs(GZ(Column,Row-Ad))
  NG=NG+1
  if(Column.gt.(i+GStart_C-1))then
   GEndR(i+GStart_C-1)=j+GStartR(i+GStart_C-1)-2
   if(j.Gt.NR)NR=j
   exit
  else
  endif
  do
   if((Row-Ad).gt.(GStartR(Column)+j-1))then
            Gx(Column,Row-Ad)=0.0
            Gy(Column,Row-Ad)=0.0
            Gz(Column,Row-Ad)=0.0
   j=j+Row-Ad-(GStartR(Column)+j-1)
  else
            exit
  endif
  enddo
  j=j+1
 endif
 endif
 end do

if(Column.gt.4400)then
 If(GStartR(i+GStart_C-1)+j-
2.gt.GEnd_R)GEnd_R=GStartR(i+Start_C-1)+j-2
```

```
GEndR(i+Start_C-1)=GStartR(i+GStart_C-1)+j-1
 exit
else
 i=i+1
 GEnd_C=Column
 If(GStartR(i+GStart_C-1)+j-
2.gt.GEnd_R)GEnd_R=GStartR(i+GStart_C-1)+j-2

endif
end do
a=(SX(1)-SX(2))**2+(SY(1)-SY(2))**2
SX(5)=(SY(2)-SY(1))*(SX(1)*SY(2)-SY(1)*SX(2))/a
SY(5)=-(SX(2)-SX(1))*(SX(1)*SY(2)-SY(1)*SX(2))/a
a=DATAN(sqrt(SX(5)**2+SY(5)**2)/SZ(1))
ac=0.0006286
SC(5)=a/ac
a=DACOS(sqrt(SX(5)**2+SY(5)**2)/(SX(1)**2+SY(1)**2)
)
ar=2.0*3.14159/9627.0
SR(5)=SR(1)+(a/ar)
FStart_C=SC(5)
FEnd_C=max(SC(3),SC(4))
SX(6)=SX(1)
SY(6)=SY(1)
SZ(6)=SZ(1)
SC(6)=SC(1)
SR(6)=SR(1)
if(((SX(6)*SY(6)).gt.0.0.and.(SX(6)/abs(SX(6))).gt.0.0).or.((
SX(6)*SY(6)).lt.0.0.and.(SY(6)/abs(SY(6))).gt.0.0))then
  s1=DACOS(SX(6)/sqrt(SX(6)**2+SY(6)**2))
else
  s1=2.0*3.14159-DACOS(SX(6)/sqrt(SX(6)**2+SY(6)**2))
endif
gd=gd/NG
 if(ad.ge.sr(1)-1)write(*,*)'error'
Do i=1,FEnd_C-FStart_C+1
 if(SC(1).lt.SC(2))then
   if(FStart_C+i-1.lt.SC(1))then
           FStartR(FStart_C+i-1)=SR(1)-(SR(1)-
SR(5))*(SC(1)-FStart_C-i+1)/(SC(1)-SC(5))-ad
           FEndr(FStart_C+i-1)=SR(5)+(SR(2)-
SR(5))*(FStart_C+i-1-SC(5))/(SC(2)-SC(5))-ad
    else
     FStartR(FStart_C+i-1)=SR(1)+(SR(3)-SR(1))*(SC(1)-
FStart_C-i+1)/(SC(1)-SC(3))-ad
           if(FStart_C-i+1.ge.sc(4))then
             FEndr(FStart_C+i-1)=SR(4)-ad
           else
             FEndr(FStart_C+i-1)=max(SR(4),SR(2))-ad
           endif
  endif
else

  if(FStart_C+i-1.lt.SC(2))then
           FStartR(FStart_C+i-1)=SR(1)+(SR(2)-
SR(1))*(SC(1)-FStart_C-i+1)/(SC(1)-SC(2))-ad
           FEndr(FStart_C+i-1)=SR(4)+(SR(2)-
SR(4))*(SC(4)-FStart_C-i+1)/(SC(4)-SC(2))-ad
    else
     FStartR(FStart_C+i-1)=SR(1)+(SR(3)-SR(1))*(SC(1)-
FStart_C-i+1)/(SC(1)-SC(3))-ad
           if(FStart_C-i+1.ge.sc(4))then
             FEndr(FStart_C+i-1)=SR(4)+(SR(2)-
SR(4))*(SC(4)-FStart_C-i+1)/(SC(4)-SC(2))-ad
           else
             FEndr(FStart_C+i-1)=max(SR(4),sr(2))-ad
           endif
          endif
endif
if(i+FStart_C-1.ge.max(start_C,GStart_C))then

 if(FEndr(FStart_C+i-1).ge.FStartr(FStart_C+i-
1).and.(FStartr(FStart_C+i-1).le.max(SR(3)-ad,SR(4)-
ad)))then
          CD=0
          cdg=0
          cnd=0
          cndg=0
          ND1=0
          N1=1
 Do j=FStartR(FStart_C+i-1),FEndr(FStart_C+i-1)

  a=SZ(6)*Dtan(ac*(FStart_C+i-1))
  X=Dcos(s1-(j-SR(6)+Ad)*ar)
  Y=Dsin(s1-(j-SR(6)+Ad)*ar)
          FX(FStart_C+i-1,j)=a*X
          FY(FStart_C+i-1,j)=a*Y
  Empty_check=0
  MD=1
 c=sqrt(FX(FStart_C+i-1,j)**2+FY(FStart_C+i-1,j)**2)
        do
         do ii=End_C-Start_C+1,1,-1
          b=sqrt(DX(Start_C+ii-
1,j+ND1)**2+DY(Start_C+ii-1,j+ND1)**2+DZ(Start_C+ii-
1,j+ND1)**2)
           if(b.gt.0.0)then
             a=(FX(FStart_C+i-1,j)-DX(Start_C+ii-
1,j+ND1))**2+(FY(FStart_C+i-1,j)-DY(Start_C+ii-
1,j+ND1))**2

             a=sqrt(a)

     Accuracy=0.5*sqrt((3.1416*320.0*b**2/(360.0*4
300.0*DZ(Start_C+ii-1,j+ND1)))**2+(c*ar)**2)
              if(a.lt.Accuracy)then
                MD=ii
                ND=j+ND1


                Empty_check=1
                exit
              endif
              a=sqrt(DX(Start_C+ii-
1,j+ND1)**2+DY(Start_C+ii-1,j+ND1)**2)

           if((c.gt.a+10.0*Accuracy).and.(a.gt.0.0))then
                exit
              endif
            endif
end do
        if(empty_check.eq.0)then
         do ii=End_C-Start_C+1,1,-1
          b=sqrt(DX(Start_C+ii-
1,j+1+ND1)**2+DY(Start_C+ii-
1,j+1+ND1)**2+DZ(Start_C+ii-1,j+1+ND1)**2)
            if(b.gt.0.0)then
               a=(FX(FStart_C+i-1,j)-DX(Start_C+ii-
1,j+1+ND1))**2+(FY(FStart_C+i-1,j)-DY(Start_C+ii-
1,j+1+ND1))**2

              a=sqrt(a)


     Accuracy=0.5*sqrt((3.1416*320.0*b**2/(360.0*4
304.0*DZ(Start_C+ii-1,j+1+ND1)))**2+(c*ar)**2)
              if(a.lt.Accuracy)then
                MD=ii
                ND=j+1+ND1


                Empty_check=1
                exit
              endif
```

```fortran
                    a=sqrt(DX(Start_C+ii-
1,j+1+ND1)**2+DY(Start_C+ii-1,j+1+ND1)**2)

                    if(c.gt.a+10.0*Accuracy.and.(a.gt.0.0))then
                            exit
                          endif
                endif
   end do
endif
 if(empty_check.eq.0)then
          do ii=End_C-Start_C+1,1,-1
          b=sqrt(DX(Start_C+ii-1,j-
1+ND1)**2+DY(Start_C+ii-1,j-1+ND1)**2+DZ(Start_C+ii-
1,j-1+ND1)**2)
            if(b.gt.0.0)then
   a=(FX(FStart_C+i-1,j)-DX(Start_C+ii-1,j-
1+ND1))**2+(FY(FStart_C+i-1,j)-DY(Start_C+ii-1,j-
1+ND1))**2
              a=sqrt(a)
              Accuracy=0.5*sqrt((3.1416*320.0*b**2/(360.0*4
304.0*DZ(Start_C+ii-1,j-1+ND1)))**2+(c*ar)**2)
              if(a.lt.Accuracy)then
               MD=ii
               ND=j-1+ND1

               Empty_check=1
               exit
   endif
              a=sqrt(DX(Start_C+ii-1,j-
1+ND1)**2+DY(Start_C+ii-1,j-1+ND1)**2)
              if(c.gt.a+10.0*Accuracy.and.(a.gt.0.0))then
                exit
                endif
   endif
   end do
endif
 if(cd.eq.0.and.empty_check.eq.0)then
  do ii=End_C-Start_C+1,1,-1
          b=sqrt(DX(Start_C+ii-
1,j+2+ND1)**2+DY(Start_C+ii-
1,j+2+ND1)**2+DZ(Start_C+ii-1,j+2+ND1)**2)
   if(b.gt.0.0)then
              a=(FX(FStart_C+i-1,j)-DX(Start_C+ii-
1,j+2+ND1))**2+(FY(FStart_C+i-1,j)-DY(Start_C+ii-
1,j+2+ND1))**2
              a=sqrt(a)

Accuracy=0.5*sqrt((3.1416*320.0*b**2/(360.0*4304.0*DZ(
Start_C+ii-1,j+2+ND1)))**2+(c*ar)**2)
              if(a.lt.Accuracy)then
               MD=ii
               ND=j+2+ND1

               Empty_check=1
               CD=1
               cnd=j
               exit
             endif
              a=sqrt(DX(Start_C+ii-
1,j+2+ND1)**2+DY(Start_C+ii-1,j+2+ND1)**2)
              if(c.gt.a+10.0*Accuracy)then
                      exit
                endif
                endif
                end do
   if(empty_check.eq.0)then
          do ii=End_C-Start_C+1,1,-1
          b=sqrt(DX(Start_C+ii-1,j-
2+ND1)**2+DY(Start_C+ii-1,j-2+ND1)**2+DZ(Start_C+ii-
1,j-2+ND1)**2)
```

```fortran
          if(b.gt.0.0)then
          a=(FX(FStart_C+i-1,j)-DX(Start_C+ii-1,j-
2+ND1))**2+(FY(FStart_C+i-1,j)-DY(Start_C+ii-1,j-
2+ND1))**2
          a=sqrt(a)

Accuracy=0.5*sqrt((3.1416*320.0*b**2/(360.0*4304.0*DZ(
Start_C+ii-1,j-2+ND1)))**2+(c*ar)**2)
              if(a.lt.Accuracy)then
               MD=ii
               ND=j-2+ND1

               Empty_check=1
               CD=1
               cnd=j
               exit
              endif
              a=sqrt(DX(Start_C+ii-1,j-
2+ND1)**2+DY(Start_C+ii-1,j-2+ND1)**2)
              if(c.gt.(a+10.0*Accuracy))then
                      exit
                  endif
          endif
          end do
   endif
          endif
          exit
end do

          if(cd.gt.0.and.abs(cnd-j).gt.5)then
            CD=0
          endif
          if(Empty_check.eq.1)then
             if((abs(dX(Start_C+MD-
1,ND))+abs(dY(Start_C+MD-1,ND))+abs(dZ(Start_C+MD-
1,ND))).gt.0.0001)then
              FZ(FStart_C+i-1,j)=DZ(Start_C+MD-1,ND)

             if(cd.gt.0)then
              cnd=cnd+1
             endif
            endif
             Empty_check=0
    M=1
          do ii=GEnd_C-GStart_C+1,1,-1
          b=sqrt(GX(GStart_C+ii-
1,j+N1)**2+GY(GStart_C+ii-1,j+N1)**2+GZ(GStart_C+ii-
1,j+N1)**2)
             if(b.gt.0.0)then
   a=(FX(FStart_C+i-1,j)-GX(GStart_C+ii-
1,j+N1))**2+(FY(FStart_C+i-1,j)-GY(GStart_C+ii-
1,j+N1))**2
                a=sqrt(a)
             Accuracy=0.5*sqrt((ac*(b**2)/GZ(GStart_C+ii-
1,j+N1))**2+(c*ar)**2)
                if(a.lt.Accuracy)then
                 M=ii
                 N=j+N1
                 Empty_check=1
                 exit
                endif
                a=sqrt(GX(GStart_C+ii-
1,j+N1)**2+GY(GStart_C+ii-1,j+N1)**2)
                if(c.gt.a+10.0*Accuracy)then
                  exit
                endif
          endif
          end do
          if(empty_check.eq.0)then
           do ii=GEnd_C-GStart_C+1,1,-1
```

```fortran
          b=sqrt(GX(GStart_C+ii-
1,j+1+N1)**2+GY(GStart_C+ii-
1,j+1+N1)**2+GZ(GStart_C+ii-1,j+1+N1)**2)
               if(b.gt.0.0)then
                    a=(FX(FStart_C+i-1,j)-
GX(GStart_C+ii-1,j+1+N1))**2+(FY(FStart_C+i-1,j)-
GY(GStart_C+ii-1,j+1+N1))**2
                      a=sqrt(a)


          Accuracy=0.5*sqrt((ac*(b**2)/GZ(GStart_C+ii-
1,j+1+N1))**2+(c*ar)**2)
                    if(a.lt.Accuracy)then
                     M=ii
                     N=j+1+N1
                     Empty_check=1
                     exit
                    endif
                    a=sqrt(GX(GStart_C+ii-
1,j+1+N1)**2+GY(GStart_C+ii-1,j+1+N1)**2)
                    if(c.gt.a+10.0*Accuracy)then
                     exit
                    endif
               endif
      end do
    endif
   if(empty_check.eq.0)then
    do ii=GEnd_C-GStart_C+1,1,-1
          b=sqrt(GX(GStart_C+ii-1,j-
1+N1)**2+GY(GStart_C+ii-1,j-1+N1)**2+GZ(GStart_C+ii-
1,j-1+N1)**2)
               if(b.gt.0.0)then
                 a=(FX(FStart_C+i-1,j)-GX(GStart_C+ii-1,j-
1+N1))**2+(FY(FStart_C+i-1,j)-GY(GStart_C+ii-1,j-
1+N1))**2
                 a=sqrt(a)
                 Accuracy=0.5*sqrt((ac*b**2/GZ(GStart_C+ii-
1,j-1+N1))**2+(c*ar)**2)
                 if(a.lt.Accuracy)then
                  M=ii
                  N=j-1+N1
                  Empty_check=1
                  exit
                 endif
                 a=sqrt(GX(GStart_C+ii-1,j-
1+N1)**2+GY(GStart_C+ii-1,j-1+N1)**2)
                 if(c.gt.a+10.0*Accuracy)then
                        exit
                 endif
               endif
      end do
    endif
    if(cdg.eq.0.and.empty_check.eq.0)then
          do ii=GEnd_C-GStart_C+1,1,-1
          b=sqrt(GX(GStart_C+ii-
1,j+2+N1)**2+GY(GStart_C+ii-
1,j+2+N1)**2+GZ(GStart_C+ii-1,j+2+N1)**2)
               if(b.gt.0.0)then
                 a=(FX(FStart_C+i-1,j)-GX(GStart_C+ii-
1,j+2+N1))**2+(FY(FStart_C+i-1,j)-GY(GStart_C+ii-
1,j+2+N1))**2
                 a=sqrt(a)
                 Accuracy=0.5*sqrt((ac*b**2/GZ(GStart_C+ii-
1,j+2+N1))**2+(c*ar)**2)
                 if(a.lt.Accuracy)then
                   M=ii
                   N=j+2+N1
                   Empty_check=1
                   cdg=1
                   cndg=j
```

```fortran
             exit
            endif
            a=sqrt(GX(GStart_C+ii-
1,j+2+N1)**2+GY(GStart_C+ii-1,j+2+N1)**2)
               if(c.gt.a+10.0*Accuracy)then
                     exit
               endif
            endif
      end do
   if(empty_check.eq.0)then
          do ii=GEnd_C-GStart_C+1,1,-1
          b=sqrt(GX(GStart_C+ii-1,j-
2+N1)**2+GY(GStart_C+ii-1,j-2+N1)**2+GZ(GStart_C+ii-
1,j-2+N1)**2)
          if(b.gt.0.0)then
          a=(FX(FStart_C+i-1,j)-GX(GStart_C+ii-1,j-
2+N1))**2+(FY(FStart_C+i-1,j)-GY(GStart_C+ii-1,j-
2+N1))**2
          a=sqrt(a)
          Accuracy=0.5*sqrt((ac*b**2/GZ(GStart_C+ii-
1,j-2+N1))**2+(c*ar)**2)
          if(a.lt.Accuracy)then
           M=ii
           N=j-2+N1
           Empty_check=1
     cdg=1
           cndg=j
           exit
          endif
          a=sqrt(GX(GStart_C+ii-1,j-
2+N1)**2+GY(GStart_C+ii-1,j-2+N1)**2)
          if(c.gt.a+10.0*Accuracy)then
     exit
          endif
     endif
    end do
   endif


   endif
   if(cdg.gt.0.and.abs(cndg-j).gt.5)then
    CDg=0
   endif

   if(Empty_check.eq.1)then
    if(((abs(GX(GStart_C+M-1,N))+abs(GY(GStart_C+M-
1,N))+abs(GZ(GStart_C+M-
1,N))).gt.0.0001).and.((abs(FX(FStart_C+i-
1,j))+abs(FY(FStart_C+i-1,j))+abs(FZ(FStart_C+i-
1,j))).gt.0.0001))then
          Dis=FZ(FStart_C+i-1,j)-GZ(GStart_C+M-1,N)
          CL(FStart_C+i-1,j)=Dis
          FZ1(FStart_C+i-1,j)=GZ(GStart_C+M-1,N)
          if(cdg.gt.0)then
           cndg=cndg+1
          endif
          write(4,83)FStart_C+i-1,j+Ad,FX(FStart_C+i-
1,j),FY(FStart_C+i-1,j),FZ(FStart_C+i-1,j),CL(FStart_C+i-
1,j)
    endif
   endif
  endif
 end do
 endif
 endif
 end do
 interval=2
 Do i=1,FEnd_C-FStart_C+1
  if(i+FStart_C-1.ge.max(start_C,GStart_C))then
```

```
  if(FEndr(FStart_C+i-1).ge.FStartr(FStart_C+i-
1).and.(FStartr(FStart_C+i-1).le.max(SR(3)-ad,SR(4)-
ad)))then
  Do j=FStartR(FStart_C+i-1),FEndr(FStart_C+i-1)
  if((abs(Fz(FStart_C+i-1,j)).gt.0).and.(abs(Fz1(FStart_C+i-
1,j)).gt.0.0).and.abs(CL(FStart_C+i-1,j)).lt.0.5)then
  if(abs(CL(FStart_C+i+interval-
1,j)).lt.0.5.and.abs(CL(FStart_C+i-interval-
1,j)).lt.0.5.and.abs(CL(FStart_C+i-
1,j+interval)).lt.0.5.and.abs(CL(FStart_C+i-1,j-
interval)).lt.0.5)then
  if((abs(FZ(FStart_C+i+interval-
1,j)).gt.0.0).and.(abs(FZ(FStart_C+i-interval-
1,j)).gt.0.0).and.(abs(FZ1(FStart_C+i+interval-
1,j)).gt.0.0).and.(abs(FZ1(FStart_C+i-interval-
1,j)).gt.0.0))then
    strainc(FStart_C+i-1,j)=4*(CL(FStart_C+i+interval-1,j)-
2*CL(FStart_C+i-1,j)+CL(FStart_C+i-interval-
1,j))/((FX(FStart_C+i+interval-1,j)-FX(FStart_C+i-interval-
1,j))**2+(FY(FStart_C+i+interval-1,j)-FY(FStart_C+i-
interval-1,j))**2)
   endif
   if((abs(FZ(FStart_C+i-
1,j+interval)).gt.0.0).and.(abs(FZ(FStart_C+i-1,j-
interval)).gt.0.0).and.(abs(FZ1(FStart_C+i-
1,j+interval)).gt.0.0).and.(abs(FZ1(FStart_C+i-1,j-
interval)).gt.0.0))then
    strainr(FStart_C+i-1,j)=4*(CL(FStart_C+i-1,j+interval)-
2*CL(FStart_C+i-1,j)+CL(FStart_C+i-1,j-
interval))/((FX(FStart_C+i-1,j+interval)-FX(FStart_C+i-1,J-
interval))**2+(FY(FStart_C+i-1,j+interval)-FY(FStart_C+i-
1,j-interval))**2)
   endif
   write(3,81)FStart_C+i-1,j+Ad,FX(FStart_C+i-
1,j),FY(FStart_C+i-1,j),FZ(FStart_C+i-1,j),CL(FStart_C+i-
1,j),strainc(FStart_C+i-1,j),strainr(FStart_C+i-
1,j),sqrt(strainc(FStart_C+i-1,j)**2+strainr(FStart_C+i-
1,j)**2)
  endif
  endif
  end do
 endif
 endif
end do
81
format(i6,i6,D19.6,D19.6,D19.6,D19.6,D19.6,D19.6,D19.6)
83      format(i6,i6,D19.6,D19.6,D19.6,D19.6)
end
```